ไฮโดรจิเนชันเชิงเร่งปฏิกิริยาของคาร์บอนไดออกไซด์สำหรับการสังเคราะห์ไฮโดรคาร์บอน

นายณัฐกร บริบูรณ์

วิทยานิพนธ์นี้เป็นส่วนหนึ่งของการศึกษาตามหลักสูตรปริญญาวิทยาศาสตรดุษฎีบัณฑิต
สาขาวิชาเคมีเทคนิค ภาควิชาเคมีเทคนิค
คณะวิทยาศาสตร์ จุฬาลงกรณ์มหาวิทยาลัย
ปีการศึกษา 2560

CATALYTIC HYDROGENATION OF CARBON DIOXIDE FOR HYDROCARBON SYNTHESIS

Mr. Nuttakorn Boreriboon

A Dissertation Submitted in Partial Fulfillment of the Requirements
for the Degree of Doctor of Philosophy Program in Chemical Technology
Department of Chemical Technology
Faculty of Science
Chulalongkorn University
Academic Year 2017

Thesis Title	CATALYTIC HYDROGENATION OF CARBON DIOXIDE FOR HYDROCARBON SYNTHESIS
By	
Field of Study	Chemical Technology
Thesis Advisor	Professor Pattarapan Prasassarakich, Ph.D.
Thesis Co-Advisor	Professor Chunshan Song, Ph.D.

Accepted by the Faculty of Science, Chulalongkorn University in Partial Fulfillment of the Requirements for the Doctoral Degree

.....Dean of the Faculty of Science

(Professor Polkit Sangvanich, Ph.D.)

THESIS COMMITTEE

.....Chairman

(Associate Professor Prasert Reubroycharoen, Ph.D.)

.....Thesis Advisor

(Professor Pattarapan Prasassarakich, Ph.D.)

.....Thesis Co-Advisor

(Professor Chunshan Song, Ph.D.)

.....Examiner

(Associate Professor Chawalit Ngamcharussrivichai, Ph.D.)

.....Examiner

(Associate Professor Napida Hinchiranan, Ph.D.)

.....External Examiner

(Boonyawan Yoosuk, Ph.D.)

ณัฐกร บริบูรณ์ : ไฮโดรจิเนชันเชิงเร่งปฏิกิริยาของคาร์บอนไดออกไซด์สำหรับการสังเคราะห์ไฮโดรคาร์บอน (CATALYTIC HYDROGENATION OF CARBON DIOXIDE FOR HYDROCARBON SYNTHESIS) อ.ที่ปรึกษาวิทยานิพนธ์หลัก: ศ. ดร.ภัทรพรรณ ประศาสน์สารกิจ, อ.ที่ปรึกษาวิทยานิพนธ์ร่วม: ศ. ดร.ชุนชาน ซอง, 145 หน้า.

ไฮโดรจิเนชันเชิงเร่งปฏิกิริยาสามารถเปลี่ยน CO_2 ให้กลายเป็นเชื้อเพลิงไฮโดรคาร์บอน การพัฒนา ตัวเร่งปฏิกิริยาสำหรับไฮโดรจิเนชันของ CO_2 กำลังได้รับความสนใจเนื่องจากตัวเร่งปฏิกิริยาจำเป็นต้องมี ความจำเพาะเจาะจงต่อการผลิตไฮโดรคาร์บอนสายยาว ก่อนการนำไปใช้งานในระดับอุตสาหกรรมได้ งานวิจัยนี้เป็นการสังเคราะห์ตัวเร่งปฏิกิริยาโลหะเดี่ยวและโลหะคู่ Fe-M (M = Co และ Cu) บนตัวรองรับไทเทเนี และทดสอบสำหรับไฮโดรจิเนชันของ CO_2 573 เคลวิน และ 1.1 เมกะพาสคัล เมื่อเปรียบเทียบตัวเร่งปฏิกิริยา โลหะเดี่ยว (Fe, Co และ Cu/TiO_2) มีเพียงตัวเร่งปฏิกิริยา Fe/TiO_2 เท่านั้นที่แสดงการเลือกเกิดไฮโดรคาร์บอนสายยาวได้ ในขณะที่ ตัวเร่งปฏิกิริยา Co/TiO_2 และ Cu/TiO_2 แสดงการเลือกเกิดเฉพาะ CH_4 และ CO อย่างสูงตามลำดับ การเติม โลหะชนิดที่สอง (Co และ Cu) ในปริมาณเพียงเล็กน้อย (M/M+Fe=0.10 โดยอะตอม) บนตัวเร่งปฏิกิริยา Fe แสดงการส่งเสริมร้อยละเปลี่ยน CO_2 และผลได้ space-time yield ของผลิตภัณฑ์ไฮโดรคาร์บอน จากการวิเคราะห์ด้วย temperature-programmed desorption (TPD) และ diffuse reflectance infrared Fourier transform spectroscopy (DRIFTS) แสดงให้เห็นว่าการมีอยู่ของตัวส่งเสริม K สามารถลดการดูด ซับของ H_2 อย่างมีนัยสำคัญซึ่งยับยั้งการเกิด CH_4 ในทางตรงกันข้ามการเติม La สามารถส่งเสริมการดูดซับ ชนิดแรงปานกลางของ CO_2 สปีชีส์ (ส่วนใหญ่ในรูปของ monodentate carbonate สปีชีส์) ซึ่งนำไปสู่การ เลือกเกิด C_5-C_7 ที่มากขึ้น การใช้ตัวส่งเสริม La และ K ร่วมกันสามารถปรับ การปกคลุมของ H และ C บน พื้นผิวของตัวเร่งปฏิกิริยาให้เหมาะสมได้ ซึ่งมีบทบาทสำคัญในการเปลี่ยนการแจกแจงผลิตภัณฑ์จากไฮโดรจิเนชันของ CO_2 ดังนั้นการเติม La และ K ร่วมกันในฐานะตัวส่งเสริมสามารถปรับปรุงแอคทิวิตีและร้อยละการ เลือกเกิดของผลิตภัณฑ์ไฮโดรคาร์บอนสายยาว ซึ่งบ่งบอกได้ว่าตัวเร่งปฏิกิริยาโลหะคู่ฐานเหล็กที่มีตัวส่งเสริม เหมาะสมสำหรับกระบวนการผลิตไฮโดรคาร์บอนจากไฮโดรจิเนชันของ CO_2

ภาควิชา เคมีเทคนิค ลายมือชื่อนิสิต .....

สาขาวิชา เคมีเทคนิค ลายมือชื่อ อ.ที่ปรึกษาหลัก .....

ปีการศึกษา 2560 ลายมือชื่อ อ.ที่ปรึกษาร่วม .....

5772814423 : MAJOR CHEMICAL TECHNOLOGY
KEYWORDS: CARBON DIOXIDE HYDROGENATION / IRON-BASED CATALYST / BIMETALLIC CATALYST / POTASSIUM PROMOTION / LANTHANUM PROMOTION / HIGHER HYDROCARBONS / ADSORPTION PROPERTIES

NUTTAKORN BORERIBOON: CATALYTIC HYDROGENATION OF CARBON DIOXIDE FOR HYDROCARBON SYNTHESIS. ADVISOR: PROF. PATTARAPAN PRASASSARAKICH, Ph.D., CO-ADVISOR: PROF. CHUNSHAN SONG, Ph.D., 145 pp.

Catalytic hydrogenation can turn CO_2 into hydrocarbon fuel. The development of the catalysts for CO_2 hydrogenation has become important since the catalysts are critical for selective production of more higher hydrocarbons for practical application. In this work, the titania supported monometallic and bimetallic Fe-M (M = Co and Cu) catalysts were synthesized and tested for CO_2 hydrogenation at 573 K and 1.1 MPa. Among the monometallic catalysts (Fe, Co and Cu/TiO_2), only Fe/TiO_2 catalyst exhibited some selectivity to higher hydrocarbons, while Co/TiO_2 and Cu/TiO_2 catalysts were highly selective only to CH_4 and CO, respectively. The addition of a small amount of a second metal M (M= Co, Cu) to Fe at M/(M + Fe) = 0.10 atom atom^{-1} showed the synergetic promotion on the CO_2 conversion and the space-time yields (STY) of hydrocarbon products. Characterization by temperature-programmed desorption (TPD) and diffuse reflectance infrared Fourier transform spectroscopy (DRIFTS) showed that the presence of K promoter significantly decreased the adsorption of H_2, which suppressed the CH_4 formation. On the other hand, La addition could promote the moderately adsorbed CO_2 species (mainly monodentate carbonate species), which led to the enhanced C_5-C_7 selectivity. The simultaneous use of La and K promoters can tailor the H and C coverage on the catalyst surface, which plays an important role in altering product distribution in CO_2 hydrogenation. Thus, incorporation of K and La as promoter can further improve the catalyst activity and product selectivity to higher hydrocarbons, indicating that the promoted Fe-based bimetallic catalysts are promising for CO_2 hydrogenation to higher hydrocarbons.

Department:	Chemical Technology	Student's Signature	.....
Field of Study:	Chemical Technology	Advisor's Signature	.....
Academic Year:	2017	Co-Advisor's Signature	.....

ACKNOWLEDGEMENTS

After an intensive period of four years. It has been a period of intense learning for the author, not only in the scientific research area but also on his personal level. Doing this doctoral dissertation has gained a significant impact on him. The author would like to reflect on the people who have supported and helped him throughout this period.

The author would like to express heartfelt gratitude and sincere appreciation to his advisor, Prof. Dr.Pattarapan Prasassarakich and co-advisor, Prof. Dr.Chunshan Song for the encouraging guidance, supervision, helpful discussion and support throughout this research. The author also would like to acknowledge Assoc. Prof. Dr.Prasert Reubroycharoen, Assoc. Prof. Dr.Chawalit Ngamcharussrivichai, Assoc. Prof. Dr.Napida Hinchiranan and Dr. Boonyawan Yoosuk for serving as the dissertation chairman and members of the thesis committee, respectively.

The author gratefully acknowledges the funding support from the Thailand Research Fund (through the Royal Golden Jubilee Project) and the Pennsylvania State University. Many thanks also go to EMS Energy Institute, Department of Energy and Mineral Engineering, Pennsylvania State University and Department of Chemical Technology, Faculty of Science, Chulalongkorn University for providing research facilities throughout his research work.

The author is deeply grateful to Dr.Xiao Jiang and Wenjia Wang who gave much valuable advice and taught him many important things about the research work. Special thanks are also extended to members of the Clean Fuels and Catalysis Program in the Energy Institute of the Pennsylvania State University and his friends in Department of Chemical Technology for friendship, support and encouragement. We were not only able to support each other by deliberating over our problems and findings but also happily by talking other things than just our research work.

Finally, the author would like to express his sincere gratitude to his family for their love, endless support and encouragement throughout the tenure of his Ph.D. program.

CONTENTS

Page

Page

Page

Page

LIST OF TABLES

Page

Page

LIST OF FIGURES

Page

Page

Page

Page

Page

Page

LIST OF ABBREVIATIONS

α	:	Chain Growth Probability
ASF	:	Anderson-Schulz-Flory
BET	:	Brunauer-Emmett-Teller
BJH	:	Barrett-Joyner-Halenda
DME	:	Dimethyl Ether
DRIFTS	:	Diffuse Reflectance Infrared Fourier Transform Spectroscopy
EIA	:	Environmental Impact Assessment
FTIR	:	Fourier Transform Infrared Spectroscopy
FTS	:	Fischer-Trospch Synthesis
GHG	:	Greenhouse Gas
GHSV	:	Gas Hourly Space Velocity
$\Delta G_{298\ K}$	:	Gibb Free Energy
$\Delta H_{298\ K}$	:	Heat of Reaction
MS	:	Mass Spectrometry
NIST	:	National Institute of Standard and Technology
ppm	:	Parts-Per-Million
PFR	:	Plug Flow Reactor
RWGS	:	Reverse Water-Gas Shift
STY	:	Space-Time Yield
TOS	:	Time-On-Stream
TPD	:	Temperature-Programmed Desorption
TPR	:	Temperature-Programmed Reduction
WGS	:	Water-Gas Shift
XRD	:	X-Ray Diffraction

CHAPTER I

INTRODUCTION

1.1 Motivation

The atmospheric CO_2 concentration has been steadily increased from only 310 ppm since 1950 (industrial revolution) and surpassed 400 ppm for the first time in 2013 as shown in Fig. 1.1 [1]. This recent relentless rise in CO_2 indicates a relationship with the burning of carbon-rich fossil fuels such as coal, natural gas and oil, which currently represent 78 % of the world's energy source (EIA, 2017 [2]). There is no doubt that fossil-fuels are still relatively inexpensive energy sources and will continue to play a significant role at least in the next decades [3]. It should be noted that the atmospheric CO_2 has positive roles in the ecological system because it is a carbon source for food and energy production, namely photosynthesis and fossil fuels. However, the increase in carbon dioxide emission is one of the major environmental issues since a direct link between the rise in global temperatures and CO_2 emission level has been reported [4, 5]. The increase of greenhouse-gas (GHG) is mainly due to the rising emissions of CO_2 which represents 80% of the total emission of GHG [6].

Nowadays, scientists and environmental groups are aiming to find methods for reducing CO_2 emission from industrial, transportation and social activities. Many counties have paid much attention to low-carbon economic development; the low-carbon economy is a general term of low-carbon industry, low-carbon technology and low-carbon life [6]. Technological innovations are one of the most feasible ways of reducing the GHG effect. A possible technology to mitigate the CO_2 emissions involves the capturing CO_2 from flue gas and atmospheric air first, followed by the conversion

of CO_2 to synthesize the petrochemicals and petrol fuels. The CO_2 utilization has become more important recently because a major advance in energy-efficient CO_2 conversion could reduce both the dependence on fossil fuel and the greenhouse-gas emissions [7-10]. The hydrogenation using hydrogen produced with renewable energy can turn CO_2 into the oxygenated and hydrocarbon products [11].

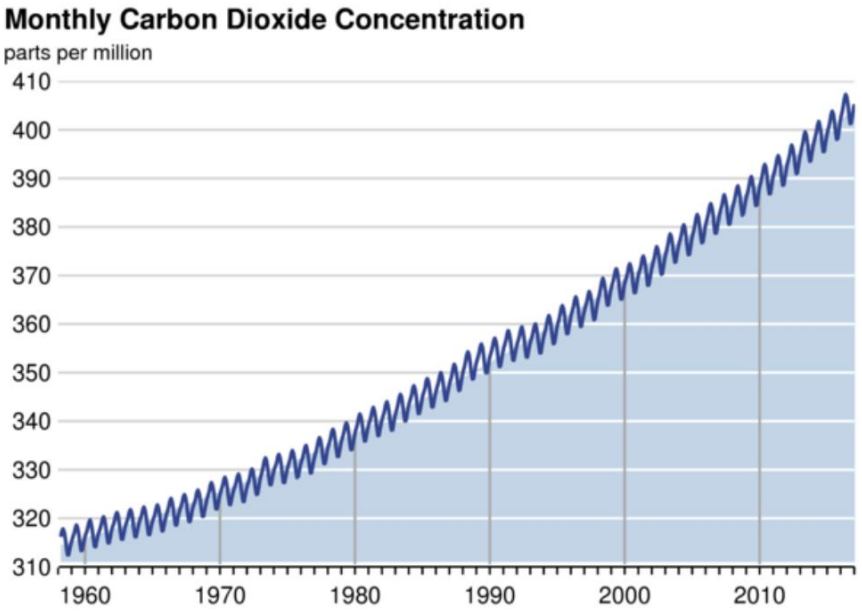

Figure 1.1 Monthly CO_2 concentration at Mauna Loa Observatory, Hawaii. Measurements by the Scripps CO_2 program are supported by the U.S. Department of Energy (DOE) and by Earth Networks [1].

1.2 Challenges for CO_2 utilization

CO_2 is not only a GHG but also be an important carbon source for synthesized chemical feedstocks, materials and fuels, which should be a sustainable way in the long term when renewable energy such as solar energy could be used for the chemical processing. Using renewable energy in an endothermic chemical process can reduce

the need for using heat from fossil fuels combustion. It should be noted that the fossil fuel-based electricity generators in the US have an average efficiency of only 35% and the efficiency for automobiles are less than 20% [12]. The issues of major concern for renewable energy are availability, energy density, efficiency and capital cost. Development for improved energy efficiency and switching from fossil fuels toward renewable sources could have a significant impact on CO_2 reduction and utilization [13].

The energy requirements of CO_2 chemical conversion (include source and cost of H_2 and/or other co-reactants) is the primary challenge for CO_2 utilization because CO_2 represents as a low-value product, the energy-consuming conversion is viewed as unfavorable and against the economics. This is principally due to the high stability of CO_2; thus, high energy substance (such as Hydrogen) or electroreductive processes are required to turn CO_2 into other chemical feedstocks [9, 14, 15]. Not only the energetic issues but the costs of CO_2 capture, separation, purification and transportation to user site also be the challenges and the barriers for CO_2 utilization and conversion. Hydrogen is a high energy reagent that can be used for CO_2 transformation. The plausible products of CO_2 hydrogenation are shown in Fig. 1.2. The products from CO_2 hydrogenation such as dimethyl ether (DME), methanol and hydrocarbons are excellent for fuels and also good for transportation and storage [13]. Moreover, alcohols and formic acid are raw materials for many chemical industries. It should be noted that hydrogen sources for CO_2 hydrogenation could be produced using renewable energy including water splitting by using electrolysis (by solar, wind, nuclear or other renewable sources), photocatalytic, photoelectrochemical, or enzymatic biological processes [16, 17].

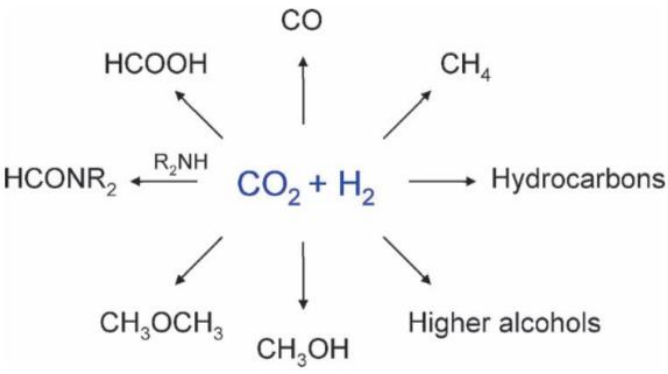

Figure 1.2 Plausible products from CO_2 hydrogenation [13].

1.3 Catalytic hydrogenation of CO_2

CO_2 hydrogenation has been more intensively explored due to fundamental of catalysis, surface science, nanoscience and environmental science. Both homogeneous and heterogeneous catalysts have been used to catalyze the hydrogenation of CO_2 [18-20]. Homogeneous catalysts show acceptable activity and selectivity however the separation and recovery are complicated. On the other hand, using heterogeneous catalysts have advantages in stability, handling, separation, recovery and reactor design, which prefers for commercial and large-scale production [9, 14, 19, 21-23]. The understanding of catalytic activity, reactor innovation and reaction mechanism over various types of catalysts for CO_2 hydrogenation is still being explored with an emphasis on practical aspects.

(i) Synthesis of CO *via* reverse water-gas shift (RWGS) reaction

Many researchers proposed that the reverse water-gas shift reaction (RWGS) is a key reaction of catalytic CO_2 hydrogenation [11, 24-26]. The RWGS reaction is a mildly endothermic and reversible reaction as shown in Eq. (1.1).

$$CO_2 + H_2 \rightleftharpoons CO + H_2O \quad ;\Delta H_{298\,K} = 41.2 \text{ kJ/mol} \quad ;\Delta G_{298\,K} = 28.6 \text{ kJ/mol} \tag{1.1}$$

Catalysts that active in the water gas shift (WGS) reaction are also used in the RWGS reaction [27]. Copper-based catalysts are the most favorable for catalytic RWGS process [22, 28-30]. RWGS reaction is an endothermic thus high temperature would enhance the CO formation. However, the Cu-based catalyst has poor thermal stability and using high temperature would cause the sintering of copper nanoparticles unless modified by adding a thermal stabilizer. The addition of a small amount of iron can improve the catalytic activity and stability of Cu/SiO_2 catalyst at high temperature [31, 32]. Moreover, using potassium (K) as a promoter on copper-based catalysts can give better catalytic activity. Potassium could create new active sites located at the interface between K and Cu increasing the formate (HCOO) species formation. The primary role of K_2O is to provide active sites for formate decomposition and CO_2 adsorption [33]. Cerium-based catalysts are also showed excellent catalytic performance in term of activity and selectivity for the RWGS reaction [34-36]. However, deactivation of ceria-supported catalysts is a crucial issue due to the carbon deposition on the ceria [37].

The equilibrium of RWGS reaction can be driven to the right side by (i) increasing the CO_2 concentration or H_2 concentration and (ii) removing water vapor from the reactor (using membrane permeoselective to water). The reaction mechanism of RWGS is still debated. Two main mechanisms have been proposed [22, 38]; (i) The “redox” mechanism, CO_2 is first dissociatively adsorbed on reduced metal sites (in this case is Cu^0) and releases CO. Then the oxidized metal sites

(Cu_2O) are reduced with H_2 back to reduced metal sites releasing water as shown in Fig. 1.3 [39, 40]. (ii) The associative "formate" mechanism, CO could be formed from the decomposition of an intermediate formate species from hydrogen associated with CO_2 as proposed in Fig. 1.4 [33, 41-43].

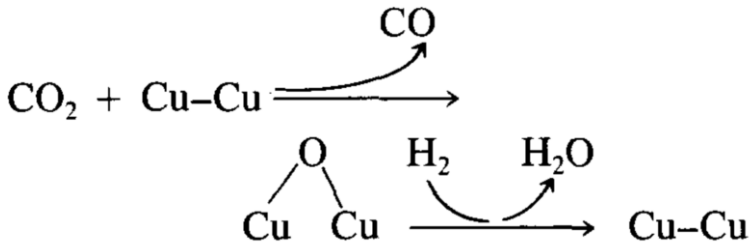

Figure 1.3 Proposed redox mechanism of RWGS reaction over Cu-based catalyst [39].

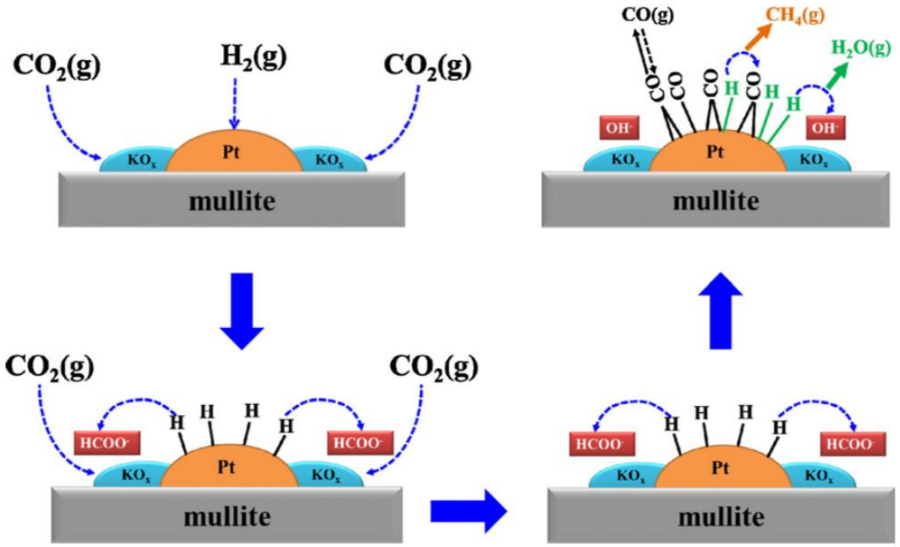

Figure 1.4 Schematic representation of the plausible associative formate mechanism of RWGS reaction over K-Pt/mullite catalyst [41].

(ii) CO_2 hydrogenation to dimethyl ether

Dimethyl ether (DME) is a viable alternative fuel to diesel oil due to its better combustion performance including high cetane number, low emissions (e.g., NO_x, hydrocarbons and CO), and does not produce soot [44-46]. Figure 1.5 shows road load test data comparing engine emissions using diesel and DME [44]. DME is also considered to be used in DME-fired turbines to generate electricity. In 2010, 50% of the potential demand for DME in Asia is to be used for electricity [47]. General Electric has evaluated the power generation *via* DME-fired turbines. For a 700 MW combined cycle power plant, using DME produced a lower amount of NO_x and CO than using natural gas and liquid naphtha [48, 49]. Moreover, DME can be reformed to hydrogen-rich gas at low temperatures, which can be used as fuel-cell feeds [50-52].

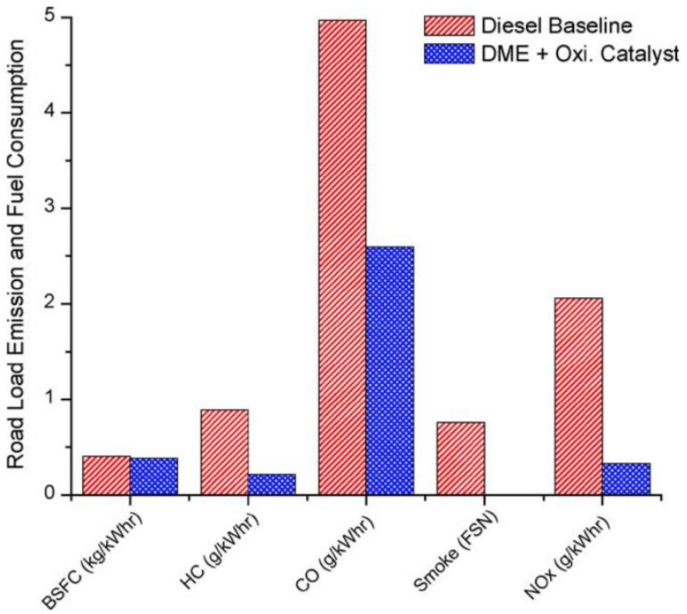

Figure 1.5 Road load test data comparing engine emission using diesel and DME [44].

The direct CO_2 hydrogenation to DME is an exothermic reversible reaction (Eq. (1.2)). In order to obtain DME *via* this direct reaction, the multi-

functional catalyst is necessary, as the reaction proceeds through the methanol synthesis on metal-oxide sites (Eq. (1.3)) and subsequent dehydration to DME on acid sites (Eq. (1.4)) [53-56].

$$2CO_2 + 6H_2 \rightleftharpoons CH_3OCH_3 + 3H_2O \quad ;\Delta H_{298\,K} = -122\ kJ/mol \quad (1.2)$$

$$CO_2 + 3H_2 \rightleftharpoons CH_3OH + H_2O \quad ;\Delta H_{298\,K} = -49\ kJ/mol \quad (1.3)$$

$$2CH_3OH \rightleftharpoons CH_3OCH_3 + H_2O \quad ;\Delta H_{298\,K} = -23\ kJ/mol \quad (1.4)$$

The Cu-based catalyst is commonly used for producing methanol in DME synthesis. The acidic catalysts such as γ-Al_2O_3 and zeolite, typically ZSM-5 and Ferrierite (FER) are used for the subsequent step which is the dehydration of methanol to synthesized DME [57-62]. There is two proposed process for the production of DME *via* CO_2 hydrogenation; (i) a two-step process (methanol synthesis on a metallic catalyst and subsequent methanol dehydration on an acid catalyst) and (ii) a single-step process using a bifunctional catalyst to perform the two steps simultaneously [55, 63-66].

(iii) CO_2 hydrogenation to formic acid and formates

Formic acid is widely used in many fields such as leather, rubber, chemical textile and other industries [67]. Recent studies have shown that formic acid has the potential to be power for fuel cells [68, 69]. Moreover, formic acid has been considered as a hydrogen storage material by combining CO_2 hydrogenation with selective formic acid decomposition [70-72]. Equation 1.5 shows the formic acid formation *via* CO_2 hydrogenation. To shift the reaction equilibrium, the addition of inorganic or organic base to the reaction system is necessary. The

addition of an inorganic base can generate formate which subsequently needs strong acid to convert to formic acid [73].

$$CO_2 + H_2 \rightarrow HCOOH \qquad ;\Delta G_{273\ K} = 32.9\ kJ/mol \qquad (1.5)$$

The CO_2 hydrogenation to formic acid and formate is typically catalyzed by organometallic complexes of transition-metal such as Ru, Rh and Ir (homogeneous catalysts) [3, 19, 74]. The formic acid synthesis *via* CO_2 hydrogenation is carried out in the presence of additives such as amines, KOH, Na_2CO_3 and water or in the supercritical CO_2, which can give high turnover numbers of catalysts [19]. Using supercritical CO_2 in reaction has gained an interest since CO_2 can play a dual role as both reactant and solvent [75]. There have many advantages of using supercritical CO_2 in CO_2 hydrogenation to formic acid including improved mass- and heat- transfer, easy to separation and high solubility of H_2 with supercritical CO_2 [76, 77].

Both Ru and Ir complexes share the similar mechanism (Fig. 1.6), but the only difference in the determining step. The rate-determining step for the CO_2 hydrogenation with the Ru catalysts is the reaction of the aqua complex with H_2. On the other hand, the rate-determining step of Ir catalysts is the reaction between the hydride complex and CO_2 [74, 75].

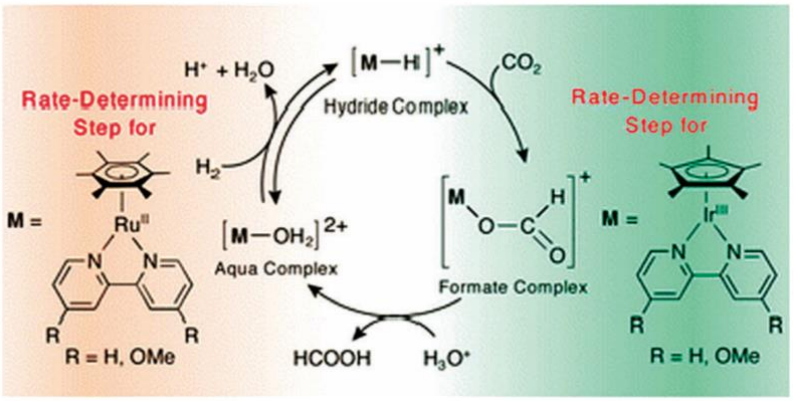

Figure 1.6 Mechanisms of CO_2 hydrogenation to formic acid by Ru(II) and Ir(III) aqua complexes under acidic conditions [74].

(iv) CO_2 hydrogenation to formamides

Formamides are a class of compounds widely used in organic synthesis including the synthesis of heterocycle, pharmaceuticals, biological intermediates and also used as Lewis base organocatalysts in hydrosilylation and other transformation. In addition, the formyl group of formamides is a useful protecting group of the amine functionality in peptide synthesis [78-80]. The use of CO_2 and H_2 as formylation agents instead of CO and phosgene which are toxic compounds, is a step toward green formylation of amines [81]. Similar to the CO_2 hydrogenation to formic acid, supercritical CO_2 has also been applied to the formamides synthesis. The formamides synthesis *via* CO_2 hydrogenation is shown in Eq. 1.6.

$$R_2NH + CO_2 + H_2 \rightarrow HCONR_2 + H_2O \qquad (1.6)$$

Typically, Ru complexes has been used as homogenous catalysts for formylation of amines with CO_2 [19, 82, 83]. The CO_2 hydrogenation to formamides is reported to accompany with a formate salt as intermediate (Fig. 1.7) [84-86]. The

high temperatures or pressures are required for the condensation of formic acid salts with high turnover numbers [82].

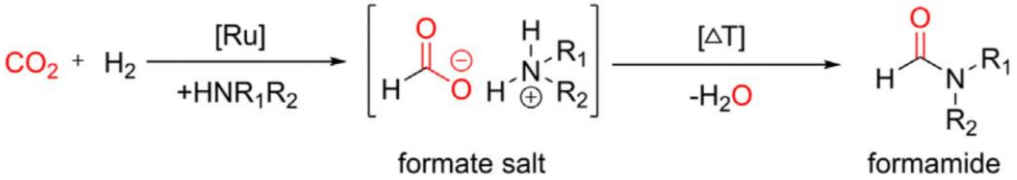

Figure 1.7 Hydrogenation of carbon dioxide to formamides [86].

The synthesis of *N,N*-dimethylformamide (DMF) from CO_2 hydrogenation with dimethylamine has well investigated and the catalysts with very high activities was reported [78, 87]. Kuhlmann *et. al.* recently reported that an *in situ* formed catalyst system for the synthesis of DMF with CO_2 and H_2 showed the promising catalytic properties referring to its good stability and recyclability [86]. The catalyst is based on the Ru(III)Cl_3 hydrate and the bidentate phosphine ligand BISBI (2,2'-bis(diphenylphosphinomethyl)-1,1'-bi-phenyl). The catalyst was immobilized by applying a biphasic solvent system consisting of 2-ethylhexan-1-ol as catalyst solvent and aqueous dimethylamine (DMA) solution as both substrate supply and extraction agent for the DMF product (Fig. 1.8).

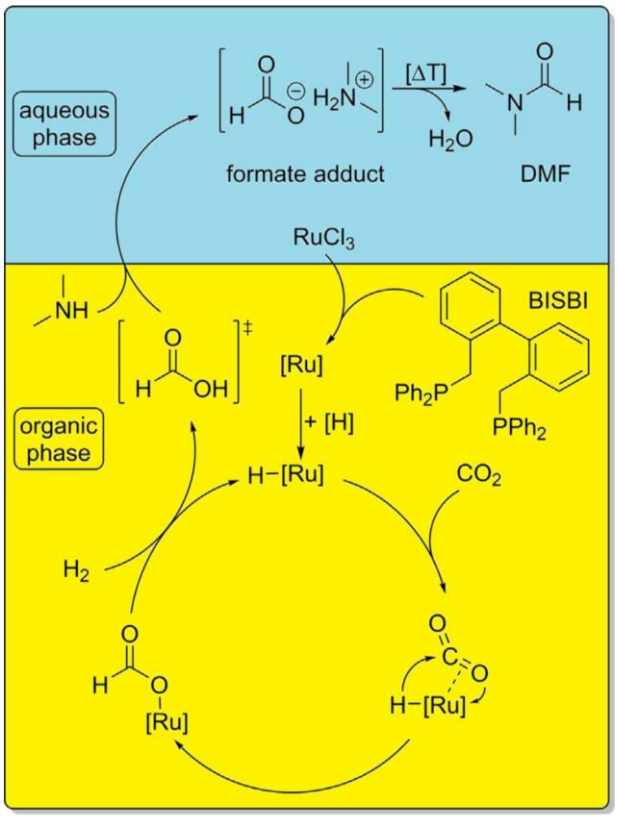

Figure 1.8 Basic setup of the reaction system with in situ product extraction [86].

(v) CO_2 hydrogenation to methanol

Methanol is a general solvent, a chemical feedstock and an alternative fuel. As an alternative chemical feedstock, CO_2 has been used instead of CO and is considered as an effective way for CO_2 utilization in the methanol production [9, 88]. The CO_2 hydrogenation to methanol is shown in Eq. 1.7.

$$CO_2 + 3H_2 \rightarrow CH_3OH + H_2O \qquad ;\Delta H_{273\,K} = -49.5\ kJ/mol \qquad (1.7)$$

From a thermodynamic point of view, an increase in reaction pressure or a decrease in reaction temperature could felicitate the methanol synthesis from CO_2 hydrogenation [9]. Moreover, other by-products are usually formed during the

CO_2 hydrogenation, such as CO, higher alcohols and hydrocarbons [89]. Therefore, a highly selective catalyst is required to avoid the formation of undesired products [9, 11, 90].

The methanol synthesis from CO_2 hydrogenation has been typically preformed with Cu and Pd-based catalysts [91-96]. Methanol synthesis generally occurring at the interface of metal and oxides. In other words, CO_2 is adsorbed on bare oxides and H_2 can dissociate on metal like Cu or Pd species [92, 96]. However, the nature of the active metal phase at interface is still in debate. Based on X-ray diffraction (XRD) results, it suggested that the active copper species are predominantly present as Cu^0 over Cu/ZrO_2 [97]. On the other hand, Cu^+ was proposed to be the active component of $Cu/ZnO/SiO_2$ catalyst, which was determined by static low-energy ion scatter experiments [98]. However, Cu metal and low valence of Cu ($Cu^{\delta+}$ and Cu^+) have also been suggested that it could affect the catalytic activity of Cu-based oxide catalysts [99-102]. Hence, the electronic and geometrical structures of the active site is the fundamental step for a catalyst design with high activity and selectivity of CO_2 hydrogenation [103].

There are two proposed reaction routes for CO_2 hydrogenation to methanol. First is the (i) formate pathway, where the intermediate HCOO formation is usually considered as the rare-determining step [104-106]. On Cu sites, the intermediate is a bidentate formate species, which is the most stable adsorbed species; while on ZnO, a monodentate formate is an intermediate species [107, 108]. The formate pathway suggests that CO may formed as a byproduct due to methanol decomposition [108]. The other pathway involves (ii) the formation of CO through the RWGS (Eq.1.1) and conventional gas-to-methanol conversion (Eq.1.8) [109, 110].

$$CO + 2H_2 \rightarrow CH_3OH \quad (1.8)$$

An *in situ* FTIR spectroscopy was carried out to identify the intermediates during methanol synthesis over Pd/β-Gq_2O_3 catalyst [111]. The mechanism follows the formate pathway proceeding through the formation of H_2COO (dioxomethylene), CH_3O (methoxy), HCOO and CH_3OH as shown in Fig. 1.9. The outstanding activity and selectivity of Pd/β-Gq_2O_3 catalyst are attributed to the atomic hydrogen spillover from Pd surface to the carbonaceous species and the moderate stability of methoxy species on Ga_2O_3. The density functional theory (DFT) calculations on Cu(1 1 1) and Cu_{29} nanoparticles indicated that the superior activity of Cu nanoparticles for the methanol synthesis is associated with active corner sites and structural flexibility, which stabilize the key intermediates (H_2COO, CH_2O and HCOO) and reduce the barrier of the rate-determining steps (HCOO and H_2COO hydrogenation) [112].

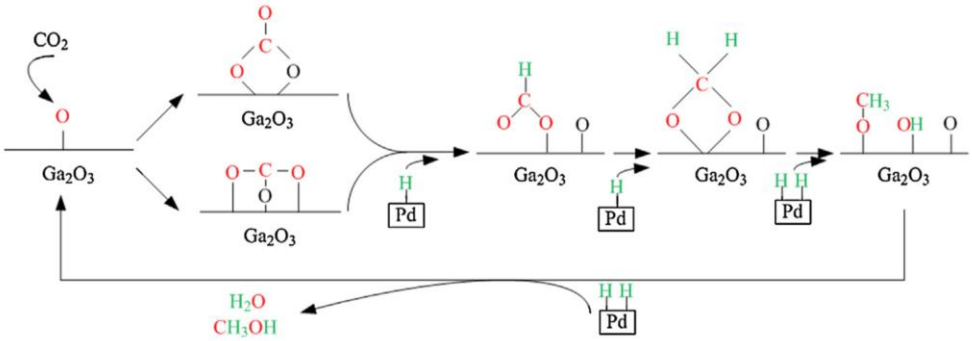

Figure 1.9 Reaction pathways for the methanol synthesis from CO_2/H_2 over Pd/β-Ga_2O_3 catalyst [13].

A simplified mechanism of methanol synthesis *via* CO_2 hydrogenation on catalyst surface is proposed in Fig. 1.10. CO_2 first adsorbed on

the ZrO_2 surface to form a bicarbonate species which is then hydrogenated to produce formate intermediate species. The required H_2 for the formate species formation could be provided by the spillover of adsorbed hydrogen on Cu [11, 13].

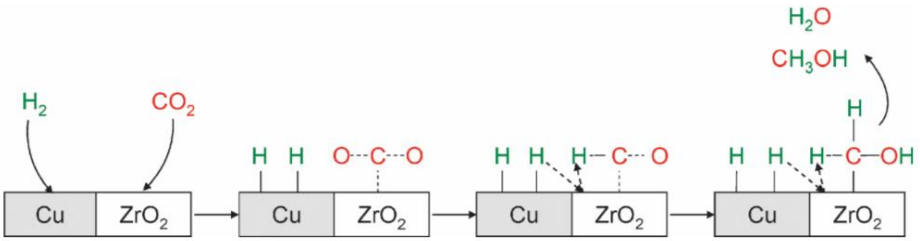

Figure 1.10 Proposed mechanism reaction pathway for the methanol formation over CO_2 hydrogenation with Cu/ZrO_2 catalyst [13].

(vi) CO_2 hydrogenation to higher alcohols

Higher alcohols are more preferable than methanol as product of CO_2 hydrogenation due to the safe transport, excellent compatibility to gasoline and high energy and value. CO_2 hydrogenation to higher alcohols could be a combination of the RWGS reaction and subsequent the formation of higher alcohols from syngas (CO and H_2) as shown in Fig. 1.11 [22]. Hence, a catalyst that is active for both RWGS and higher alcohols formation reaction would be suitable for the higher alcohols synthesis *via* CO_2 hydrogenation, for example, Fe- and Rh-based catalysts [113, 114].

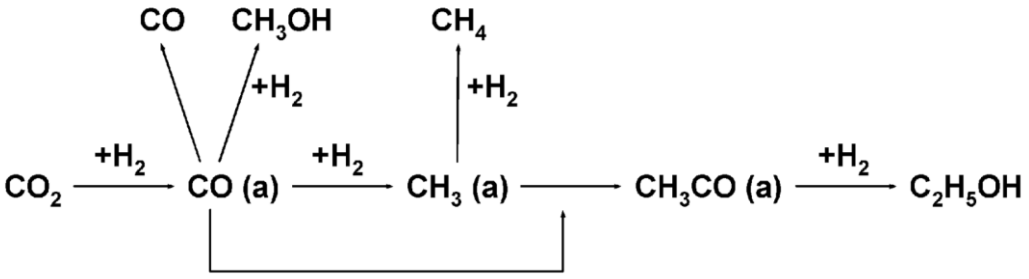

Figure 1.11 Plausible reaction mechanism of CO_2 hydrogenation to ethanol [13].

Furthermore, Tominaga *et al*. introduced a multi-step method for CO_2 hydrogenation and hydroformylation reaction [115]. Hydroformylation with CO_2 proceeds in two steps; (i) CO_2 is first converted into CO by RWGS and further involves in (ii) hydroformylation of alkenes as shown in Fig. 1.12. Ruthenium carbonyls are active for the process since it is capable of catalyzing both steps.

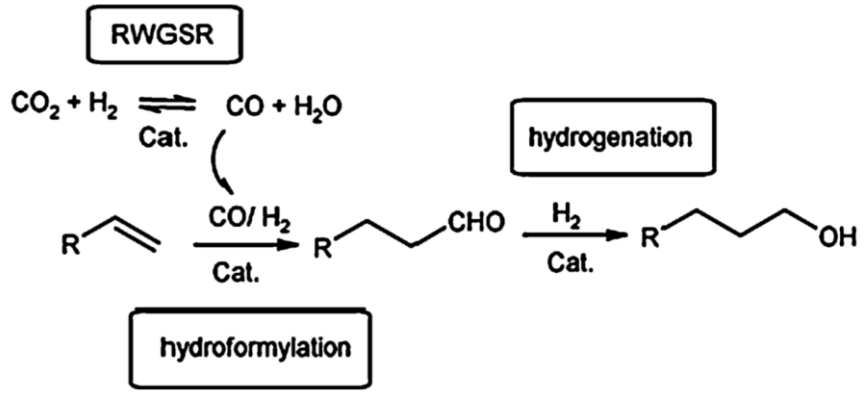

Figure 1.12 Alcohols formation from alkenes by hydroformylation with CO_2 [13].

(vii) CO_2 hydrogenation to hydrocarbons

Carbon dioxide can be hydrogenated to hydrocarbons either by direct or indirect routes (*via* synthesis gas and/or methanol intermediate formation) [116]. The active metals Fe, Ru, Co, Ni and Rh as the conventional catalyst for Fischer-Tropsch synthesis (FTS) could also be employed for CO_2 hydrogenation [117, 118]. The comparative study on the hydrogenation of CO and CO_2 over Co and Fe catalysts, reported that the supported iron-based catalysts showed good performance for the CO_2 hydrogenation to higher hydrocarbons [119]. The synthesis of hydrocarbons *via* CO_2 hydrogenation could be viewed as a modification of FTS, wherein CO_2 is first converted to CO by reverse water-gas shift (RWGS) reaction (Eq. 1.9), then CO or CO-like intermediates are subsequently consumed in the formation

of carbon-carbon bond building unit and hence producing hydrocarbons through FTS (Eq. 1.10). Meanwhile, an additional reaction, namely the direct CO_2 hydrogenation (Eq. 1.11), is also proposed, but it is thought to be difficult due to the high-energy barrier of CO_2 activation [11, 24-26].

$$CO_2 + H_2 \rightleftharpoons CO + H_2O \quad ;\Delta H_{573\,K} = 38 \text{ kJ/mol} \tag{1.9}$$

$$CO + 2H_2 \rightarrow -(CH_2)- + H_2O \quad ;\Delta H_{573\,K} = -166 \text{ kJ/mol} \tag{1.10}$$

$$CO_2 + 3H_2 \rightarrow -(CH_2)- + 2H_2O \quad ;\Delta H_{573\,K} = -128 \text{ kJ/mol} \tag{1.11}$$

The plausible mechanism of CO_2 hydrogenation over iron-based catalyst have been proposed and shown in Fig. 1.13 [120]. CO_2 adsorption on metal surface is the important step and the preliminary step for CO_2 hydrogenation. Firstly, CO_2 is adsorbed on the metal surface and converted to CO by the RWGS reaction. Consequently, CO intermediate is hydrogenated and transform to the monomers.

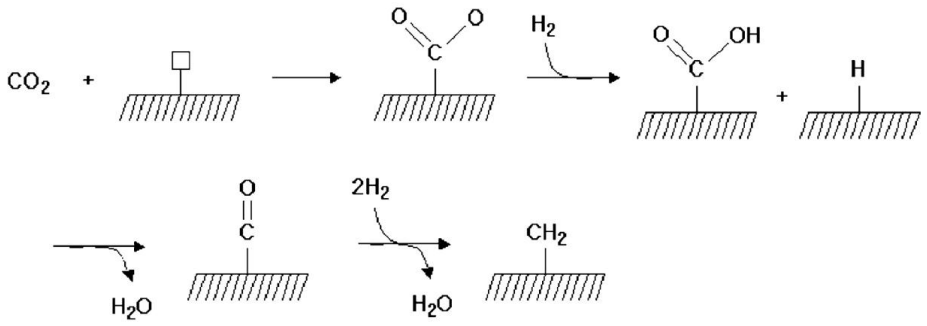

Figure 1.13 Proposed mechanism of CO_2 hydrogenation over Fe-K/γ-Al_2O_3 catalyst [120].

Moreover, according to recent density functional theory (DFT) study by Nie *et al*., they suggested that the CO_2 dissociation to CO* intermediate is preferred on Fe(100) and the kinetically favorable path changes to CO_2 hydrogenation to a HCOO* intermediate when Cu was added to Fe catalyst as shown in Fig. 1.14. CH* intermediate is found to be the most favorable monomeric species for production of CH_4 and C_2H_4 *via* C-C coupling of CH* species and subsequent hydrogenation [121]. Typically, methane is the most product for CO_2 hydrogenation, which is not the desired products. The main propose of the CO_2 hydrogenation is to synthesize light olefins and the long chain hydrocarbons as liquid fuels.

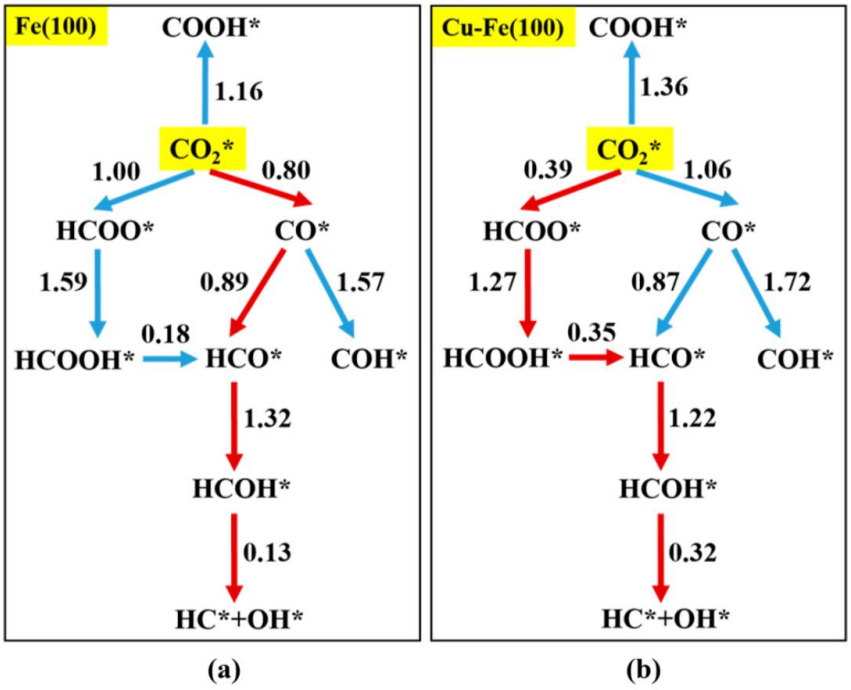

Figure 1.14 Reaction networks examined to identify energetically favorable C_1 species from CO_2 hydrogenation on (a) Fe(100) and (b) the Cu–Fe(100) surface at 4/9 ML Cu coverage. Activation barriers are given in eV (The networks connected with red arrows represent the preferred path for CO_2 conversion to CH*.) [121].

Recently, our research group reported on the bimetallic promotion on the selective CO_2 hydrogenation to methanol using Pd-Cu catalysts [91] and to light hydrocarbons using Fe-based bimetallic catalysts [122]. Moreover, the addition of promoters, such as K and Mn, on Fe-based catalysts significantly promoted the selectivity to olefinic products and suppressed the methane formation [11, 25, 122, 123]. CO_2 hydrogenation to liquid fuels and highly value-added products remains a challenging research topic. For this purpose, La as promoter was introduced in the preparation of Fe-based bimetallic catalysts since La could enhance the selectivity of higher hydrocarbons in FTS [124] and CO_2 hydrogenation [125, 126].

In addition to the active metal, the chemical and textural properties of the support also influence the product selectivity of CO_2 hydrogenation. Although γ-Al_2O_3 is widely used as a support due to its high surface area, TiO_2 is also a good candidate as support, which showed better selectivity to higher hydrocarbon products of CO_2 hydrogenation [125]. It was reported that the oxygen vacancy of TiO_2 could increase bridge-type adsorbed CO_2, which can be dissociated to carbon species, thereby enhancing C-C bonds formation [127, 128].

The chain-growth probability (α) of FTS limits the proportion of desired fuel hydrocarbons (C_5-C_{15}) according to the work by Anderson, Schulz and Flory [129-131]. Form theoretical ASF distribution calculation using Eq. 1.12, it revealed that the product proportion of C_5-C_{15} reached its maximum of 60% at a chain-growth probability of α=0.8 (Fig. 1.15). Therefore, the highest theoretically achievable yield of C_5-C_{15} hydrocarbon products is 60%. From recent studies, the chain-growth probability of α up to 0.5 could be achieved, hence the yield of higher hydrocarbons products could be further improved [122, 132].

$$W_n = (\ln^2 \alpha)\, n\, \alpha^n \qquad (1.12)$$

where W_n is wt.% of hydrocarbons, α is the chain-growth probability and n is the number of C atoms.

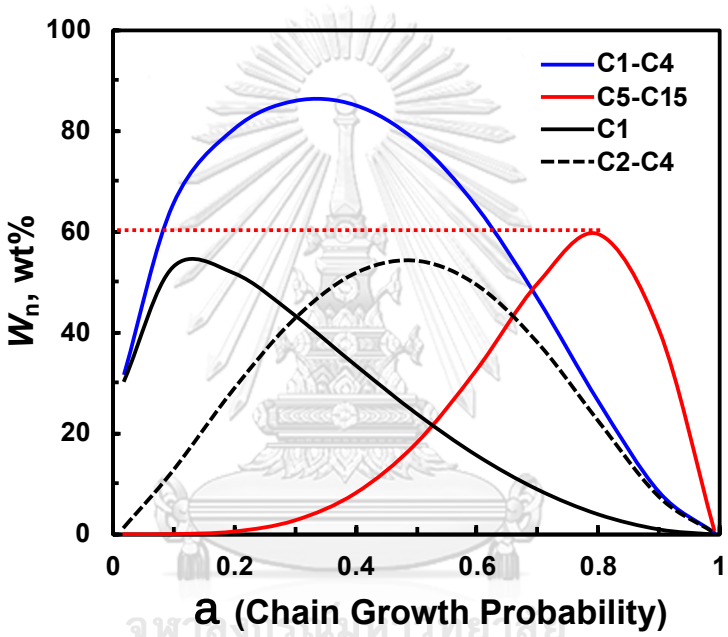

Figure 1.15 Theoretical proportion of C_1, C_1-C_7 and C_5-C_{15} hydrocarbons among all hydrocarbons formed by FTS. Calculation according to ASF distribution equation (Eq. 1.12).

1.4 Objectives and scope of dissertation

The objective of this research is to develop efficient catalysts for CO_2 hydrogenation to higher hydrocarbons especially liquid hydrocarbons (C_{5+}). One approach is to investigate the adsorption properties of CO_2 and H_2 on the TiO_2-supported catalyst surfaces with various active metal compositions. The effects of catalyst formulations on the physical and chemical properties as well as the activity of the catalyst were also studied.

Chapter I of this dissertation provides a review of the global challenges and strategies for CO_2 utilization focusing on the catalytic hydrogenation of CO_2.

The experimental procedures for the catalyst preparation as well as the catalyst evaluation on CO_2 hydrogenation and the various techniques used for the characterization are given in Chapter II.

The catalytic activities and product selectivities of the monometallic including Fe, Co and Cu catalysts for the hydrogenation of CO_2 are reported in Chapter III. The promotion effect of K promoter on the monometallic catalyst is also studied as well as the textural properties of the catalysts.

In Chapter IV, the Fe-based bimetallic catalysts were studied in detail to understand the bimetallic synergistic promotion effect on CO_2 hydrogenation to hydrocarbons. The second metal; Co and Cu were incorporated with Fe catalysts to synthesize the TiO_2 supported Fe-based bimetallic catalysts. The Fe-based bimetallic catalysts (Fe-M/TiO_2; M = Co or Cu) were prepared at various M/(M+Fe) atomic ratio from 0-1 and tested for CO_2 hydrogenation reaction. The effect of K and La promoter on Fe-based bimetallic catalyst is also investigated as well as the physical properties of synthesized catalysts.

To explore the surface chemistry of the Fe-Cu bimetallic catalysts, the temperature-programmed desorption (TPD) and diffuse reflectance Infrared Fourier

transform spectroscopy (DRIFTS) were performed and their results are reported in Chapter V. To clarify the effect of K and La promoter addition on the CO_2 and H_2 adsorption, and their impact on the catalytic activity, the *in situ* TPD and DRIFTS techniques was used to characterize the fresh and spent-catalysts after H_2 reduction and CO_2 hydrogenation, respectively.

In Chapter VI, the kinetics study of catalytic CO_2 hydrogenation to hydrocarbons was investigated. The ASPEN PLUS was employed to simulate the catalytic CO_2 hydrogenation process with the kinetic model from the experiment data, for further study on the reactor performance and process scale-up.

Finally, the conclusions of this dissertation and recommendations for future work are provided in Chapter VII. The results of this research would contribute the understanding and useful guidance to the development of Fe-based bimetallic catalyst for catalytic CO_2 hydrogenation to higher hydrocarbons synthesis.

CHAPTER II

EXPERIMENTAL AND CHARACTERIZATION

2.1 Materials

Titania (AEROXIDE TiO_2 P 25) was supplied by Evonik Corporation and calcined at 723 K for 4 h before being used. $Fe(NO_3)_3{\cdot}9H_2O$ (99.99%), $Co(NO_3)_2{\cdot}6H_2O$ (≥98%), KNO_3 (99.0%) and $La(NO_3)_3{\cdot}6H_2O$ (≥99.99%) were purchased from Sigma-Aldrich Chemical Company. $Cu(NO_3)_2{\cdot}2.5H_2O$ (≥98%) was purchased from Alfa-Aesar Chemical Company. All precursors were used witout further purification. The mixed gas of 24 vol% CO_2/ 72 vol% H_2/ 4 vol% Ar (purity >99.999%), H_2 (99.999%) and He gas (99.999%) were supplied by Praxair Inc.

2.2 Catalyst preparation

Titania (AEROXIDE TiO_2 P 25) was used as support material. The unpromoted supported Fe-based bimetallic catalysts were prepared by a wet impregnation method using an aqueous solution containing $Fe(NO_3)_3{\cdot}9H_2O$, $Co(NO_3)_2{\cdot}6H_2O$ and $Cu(NO_3)_2{\cdot}2.5H_2O$. Concentrations of Fe and co-metal (Co, Cu = M) precursors in the solution were adjusted to obtain desired M/(Fe+M) atomic ratios (0.0-1.0 atom $atom^{-1}$) while maintaining total metal (Fe+M) loading at 15 wt% (support weight basis). Typically, 1 g of support was impregnated with 4 mL of precursor solution. The impregnated sample was dried at 363 K in a rotary evaporator for 4 h and then dried in an oven at 383 K overnight in ambient air, followed by calcination in a furnace in dry air of 100 mL (NTP) min^{-1} at 673 K for 2 h (Fig. 2.1).

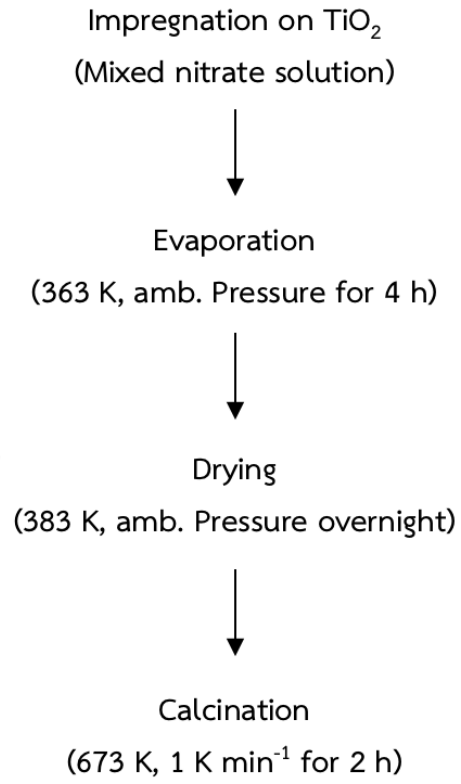

Figure 2.1 Procedures for preparation of TiO_2 supported catalyst.

The K- and La-promoted catalysts were also prepared by a wet impregnation method, wherein the mixed solution of KNO_3 and $La(NO_3)_3{\cdot}6H_2O$ were used as precursors. Then, mixed nitrate precursor solution was impregnated, followed by drying and calcination at the same conditions as the unpromoted catalysts. The prepared catalysts are denoted as "Fe-M(*X*)-K(*Y*)-La(*Z*)/TIO_2", where *X*, *Y* and *Z* represent the atomic ratios of M/(Fe+M), K/Fe and La/Fe, respectively. Total metal loading for monometallic and bimetallic catalysts (M and M+Fe) was fixed at 15 wt%, unless otherwise noted. Corresponding metal loadings of catalysts for different components are summarized in Table 2.1 for clarity.

Table 2.1 Fe, Co, Cu, K and La loadings of Fe-M(X)-K(Y)-La(Z)/TiO_2 catalysts (M = Co and Cu)

Catalyst	Loading, wt% (support weight basis)				
	Fe	Co	Cu	K	La
Unpromoted catalyst					
Fe	15.0	-	-	-	-
Co	-	15.0	-	-	-
Cu	-	-	15.0	-	-
Fe-Co(0.1)	13.4	1.6	-	-	-
Fe-Co(0.17)	12.4	2.6	-	-	-
Fe-Co(0.5)	7.3	7.7	-	-	-
Fe-Cu(0.1)	13.3	-	1.7	-	-
Fe-Cu(0.5)	7.0	-	8.0	-	-
Promoted catalyst					-
Fe-K(0.1)	15.0	-	-	1.1	-
Fe-Co(0.1)-K(0.1)	13.4	1.6	-	0.9	-
Fe-Co(0.1)-K(0.3)	13.4	1.6	-	2.8	-
Fe-Cu(0.1)-K(0.05)	13.4	1.6	-	0.5	-
Fe-Cu(0.1)-K(0.1)	13.3	-	1.7	0.9	-
Fe-Cu(0.1)-K(0.2)	13.3	-	1.7	1.9	-
Fe-Cu(0.1)-K(0.3)	13.3	-	1.7	2.8	-
Fe-Cu(0.1)-K(0.05)-La(0.05)	13.3	-	1.7	0.5	1.7
Fe-Cu(0.1)-K(0.05)-La(0.1)	13.3	-	1.7	0.5	3.3
Fe-Cu(0.1)-K(0.05)-La(0.2)	13.3	-	1.7	0.5	6.6
Fe-Cu(0.1)-K(0.05)-La(0.3)	13.3	-	1.7	0.5	9.9
Fe-Cu(0.1)-K(0.1)-La(0.1)	13.3	-	1.7	0.9	3.3
Fe-Cu(0.1)-K(0.2)-La(0.1)	13.3	-	1.7	1.9	3.3
Fe-Cu(0.1)-K(0.3)-La(0.1)	13.3	-	1.7	2.8	3.3

2.3 Activity test

CO_2 hydrogenation was performed in a high-pressure fixed-bed reactor system (Fig. 2.2). For each activity test, about 0.20 g of the catalyst was mixed with ca. 0.48 g amorphous SiO_2 (Davisil Grade 62, particle size = 75-250 × 10^{-6} m) as a diluent to maintain an aspect ratio of approximately 6.0 and then loaded in a 6 mm I.D. stainless-steel reactor between two glass wool layers. The upper part of the bed was packed with borosilicate glass bead as a pre-heating zone. Prior to the activity test, the prepared catalyst was reduced under a H_2 (purity > 99.995) flow of 50 mL (STP) min^{-1} at 673 K with a ramping rate of 2 K min^{-1} for 2 h and then allowed to cool to the hydrogenation temperature of 573 K. The feed gas, 24 vol% CO_2/ 72 vol% H_2/ 4 vol% Ar (purity > 99.99995 %), was employed to pressurize the system to 1.1 MPa (GHSV = 3600 mL (STP) g^{-1} h^{-1}) and regulated using mass flow controllers and a backpressure regulator.

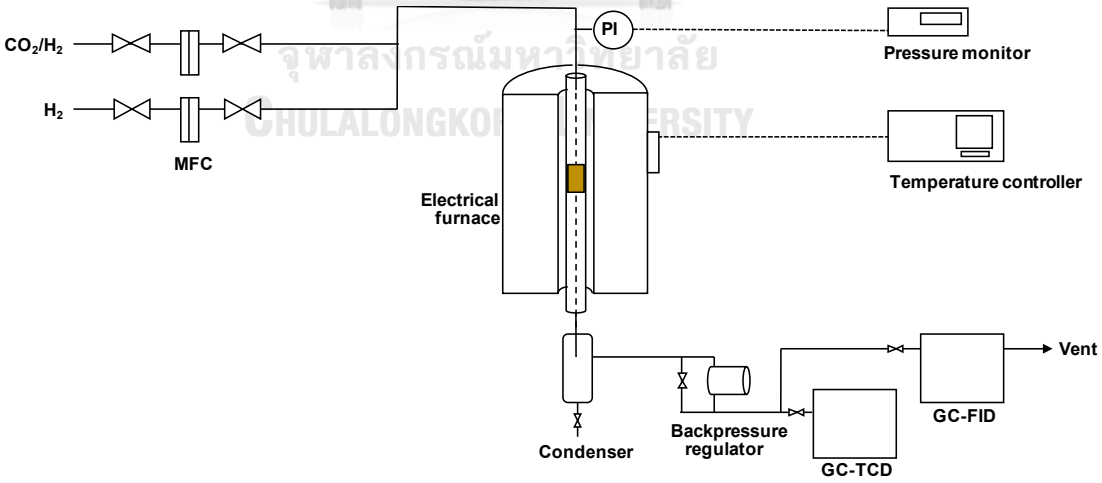

Figure 2.2 Schematic illustration of a fixed-bed reactor system for CO_2 hydrogenation.

2.4 CO_2 hydrogenation product analysis

For analysis of Ar, CO, CH_4 and CO_2, an online Agilent 3000 micro Gas Chromatography equipped with molecular sieve-type column and Plot-Q column was used. The gas-phase hydrocarbon products (C_1-C_7) were analyzed using an online SRI 8610C GC equipped with flame ionization detector (GC-FID) (Porapak Q column). CO_2 conversion and gas-phase product space-time yields (STY) were evaluated by the values obtained at 16-18 h on-stream. The condition and temperature program for both GC are described in Appendix A. Activity data reported here were based upon at least two runs for each catalyst, and average deviations of CO_2 conversion and product formation rate are 0.9% and 0.02 μmol g^{-1} s^{-1}, respectively.

For analysis of liquid hydrocarbon products, the liquid products from CO_2 hydrogenation were collected in an ice trapped condenser connected to the reactor. The gas chromatography-mass spectrometry (GC/MS) (Agilent, 7890) with a capillary column RTX-PAH (60 m x 0.25 mm I.D. x 0.25 μm film thickness) and a split mode injector (ratio 20:1) was used with ultra-high purity helium as a carrier gas. The condition and temperature program for GC/MS are described in Appendix B.

2.5 Catalyst passivation

After CO_2 hydrogenation at 573 K and 1.1 MPa for 15-16 h, the catalyst was cooled down to 298 K under 24 vol% CO_2/ 72 vol% H_2/ 4 vol% Ar and subsequently passivated using 0.95 vol % O_2/He (purity > 99.999%) at a flow rate of 30 mL min^{-1} until an area of O_2 peak (effluent of O_2) observed by Micro GC equipped with TCD became constant. Then, the catalyst was collected from the reactor for further characterizations, hereafter simply denoted as “spent catalyst”.

2.6 Adsorption/Desorption of N_2

The catalyst surface area (SA), pore volume (PV) and average pore diameter (D_p) were determined from N_2 sorption isotherms at 77 K using fully automated TriStar II (Micromeritics) surface area and porosity analyzer. Before analysis, all samples (ca. 0.20-0.25 g) were degassed under N_2 at 363 K for 1 h and 473 K for 12 h. From isotherms, Brunauer-Emmett-Teller (BET) method was used to determine the surface area, while Barrett-Joyner-Halenda (BJH) model was used for calculation of pore volume and average pore diameter of the catalysts.

2.7 X-ray diffraction

XRD patterns of calcined catalysts were obtained using a PANalytical Empyrean X-ray Diffractometer with Cu Kα (λ= 0.154059 nm) radiation, fixed slit incidence (0.25° divergence, 0.5° anti-scatter, specimen length of 10 mm) and diffracted optics (0.25° anti-scatter, 0.02 mm nickel filter). Data obtained at 45 kV and 40 mA from 20-90 (2θ) using a PIXcel detector with a PSD length of 3.35° (2θ), and 255 active channels. From the relative XRD diffraction intensities corresponding to anatase (101) and rutile (110) reflections [133], the mass fraction of rutile and anatase was calculated using Eqs. 2.1 and 2.2 [134, 135].

$$\text{Anatase (\%)} = [0.79I_A / (I_R + 0.79I_A)] \times 100 \quad (2.1)$$

$$\text{Rutile (\%)} = [1/[(I_R + 0.79I_A)/I_R]] \times 100 \quad (2.2)$$

where I_A and I_R are the peak intensities of (101) and (110) reflections for anatase and rutile, respectively.

The XRD peaks of crystal plane (101) and (200) in anatase was selected to determine the lattice parameter of TiO_2 supported catalysts according to Eqs. 2.3 and 2.4 [136].

Bragg's law: $d_{(hkl)} = \lambda / 2 \sin\theta$ (2.3)

$$d^{-2}_{(hkl)} = h^2a^{-2} + k^2b^{-2} + l^2c^{-2} \quad (2.4)$$

where $d_{(hkl)}$ is the distance between crystal planes of (*hkl*), λ is the X-ray wavelength, θ is the diffraction angle of crystal plane (*hkl*), *hkl* is the crystal plane index, and *a*, *b* and *c* are lattice parameters ($a = b \neq c$) of anatase.

2.8 Temperature-programmed reduction

2.8.1 Calcined catalyst

Temperature-programmed reduction (TPR) experiments were performed at ambient pressure in a Micromeritics AutoChem 2910 using hydrogen as a reducing agent. About 0.10 g of sample was charged in a U-shaped quartz tube reactor and held by quartz wool. Prior to the reduction program, the sample was heated *in situ* to 393 K (10 K min^{-1}) under Ar (purity > 99.999%) flow (25 mL min^{-1}) for 1 h to remove adsorbed species on the sample surface. The sample was then cooled down to 323 K, followed by switching to 4.93 vol% H_2/Ar at 20 mL min^{-1}. After the baseline was stable, the temperature program started by a ramping rate of 10 K min^{-1} up to 1173 K and held at this temperature for 30 min. The effluent gas was cooled down by a slush bath consisting of isopropanol and liquid N_2 located between a reactor and detector to trap the water formed during the reduction process. The gas was then analyzed using a thermal conductivity detector (TCD).

2.8.2 Pre-reduced catalyst

0.1 g of catalyst was loaded to the U-shaped quartz tube reactor and pre-reduced *in situ* at 673 K (5 K min^{-1}) under H_2 (purity > 99.999%) flow (50 mL min^{-1}) for 2 h. After pre-reduction step, the catalyst was cooled down to 423 K under flowing 20 mL min^{-1} Ar (purity > 99.999%) for 30 min to remove H_2 gas that might be remained

in the system. The gas was then switched to 4.93 vol% H_2/Ar at 20 mL min^{-1} and followed the same procedures used for calcined catalysts in section 2.8.1.

2.9 Temperature-programmed desorption

2.9.1 CO_2-TPD

Prior to the CO_2- and H_2-temperature programed desorption (TPD), about 150 mg of catalyst was loaded in a U-shaped quartz tube reactor and pre-reduced *in situ* in a H_2 flow (purity > 99.999%, 50 mL min^{-1}) at 673 K (5 K min^{-1}) for 2 h. For CO_2-TPD, the catalyst was then purged with He (purity > 99.999%, 30 mL min^{-1}) at 573 K for 30 min to remove the remaining H_2 in the reactor tube. The catalyst was subsequently dosed with 12 vol% CO_2/He (at 573 K) at a flow rate of 30 mL min^{-1} for 1 h, followed by cooling down to room temperature. The catalyst was then purged with 30 mL min^{-1} He (purity > 99.999%) to remove any trace of CO_2 gas until CO_2 signal (observed from Mass Spectrometer) became constant. The TPD experiment was started by heating at a ramp of 10 K min^{-1} to 1173 K under 30 mL min^{-1} He (purity > 99.999%) flow. The desorbed gas was analyzed using a Dycor Dymaxion Mass Spectrometer DM200M (AMETEK) (Fig. 2.3).

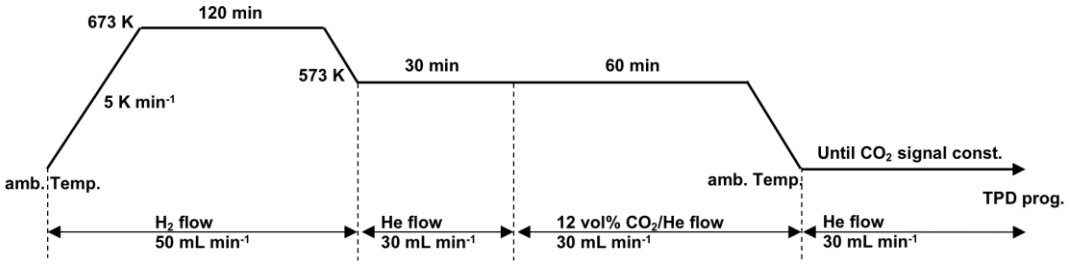

Figure 2.3 Schematic illustration of CO_2-TPD over Fe-Cu-K-La/TiO_2 catalyst.

2.9.2 H_2-TPD

For H_2-TPD, the pre-reduced catalyst was cooled down to 200 K in H_2 using a slush bath of isopropanol-liquid N_2 mixture to prevent the desorption of weakly-adsorbed hydrogen from the catalyst surface. Then, the catalyst was purged with He (purity > 99.999%, 30 mL min^{-1}) until the H_2 signal became constant (Fig. 2.4). The temperature program was started at around 280 K. The H_2-TPD experiment was performed by following the same procedures used for CO_2-TPD.

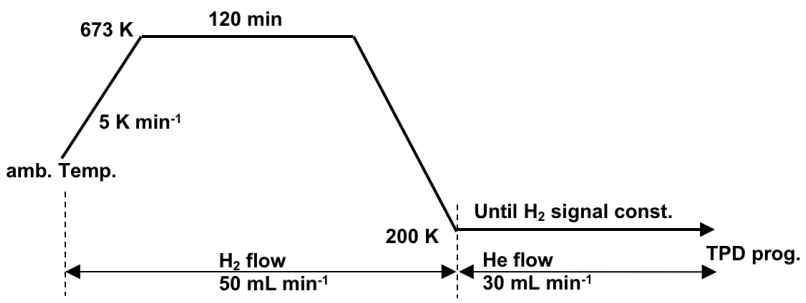

Figure 2.4 Schematic illustration of H_2-TPD over Fe-Cu-K-La/TiO_2 catalyst.

2.10 *In situ* diffuse reflectance infrared Fourier transform spectroscopy (DRIFTS)

The adsorption states of CO_2 on the reduced catalysts were studied by *in situ* diffuse reflectance infrared Fourier transform spectroscopy (DRIFTS) using a Thermo Nicolet NEXUS 470 equipped with a diffuse reflectance cell (Spectra Tech) and a mercury cadmium telluride (MCT-A) detector cooled by liquid N2 and a KBr beam splitters. The infrared cell with a ZnSe window was employed at high temperatures. The cell was directly connected to a gas flow system equipped with rotameter and a

set of valves to switch and control the gas flow rate. The temperature of the catalyst was monitored by a K-type thermocouple placed 2 mm underneath the crucible surface.

Before the experiment, about 50 mg of the calcined catalyst was gently mixed and ground with 50 mg of KBr powder uniformly. The mixed powder was charged into the sample cell and then pre-reduced *in situ* at 523 K (10 K min^{-1}) under H_2 flow for 1 h, followed by flushing with N_2 at this temperature for 30 min. The background was collected at this temperature after the system was stabilized for 30 min. The *in situ* DRIFT spectra of the adsorbed CO_2 were recorded at the same temperature in a 12 vol% CO_2/Ar flow and the time-on-stream (TOS) of 3, 10, 20, 60 and 120 min. The total flow of all gases through the sample cell was kept constant at 50 mL min^{-1}.

The surface species formed during CO_2 hydrogenation on the spent catalysts were also studied by DRIFTS. About 50 mg of the spent catalyst was gently mixed and grinded with 50 mg of KBr powder. The mixed powder was then charged into the sample holder and was purged in N_2 (purity > 99.999%) at 298 K for 1 h to remove any moisture and gases, before recording the DRIFT spectrum. After that, the sample was pre-reduced *in situ* at 523 K (10 K min^{-1}) under H_2 flow (purity > 99.999%) for 2 h, and then cooled down to 310 K under a H_2 flow. The DRIFT spectrum was then recorded after flushing the sample with N_2 for 30 min. These spectra were transformed to Kubelka-Munk functions using a KBr background spectrum measured under a N_2 flow at ambient temperature.

2.11 Transmission electron microscopy (TEM)

Morphologies and particle sizes were evaluated by transmission electron microscopy (TEM; JEM-2500SE) with an accelerating voltage of 200 kV. The samples were prepared by dispersion of prepared catalyst in ethanol under ultrasonication for

15 min. Then, the suspension was dropped onto a 150 mesh Cu TEM grid and the solvent was left to evaporate for overnight prior to the investigation. The EDS analysis was analyzed by using a nominal electron beam size of 1 nm.

CHAPTER III

COMPARATIVE STUDY OF Fe-BASED CATALYSTS FOR CO_2 HYDROGENATION TO HIGHER HYDROCARBONS

3.1 Introduction

Recently, CO_2 has become an attractive renewable carbon source as a nontoxic C_1 building block for fuels. One processes to transform CO_2 to hydrocarbon fuels as hydrogenation is of interest because hydrogen is a high-energy substance which can be used as the reagent for CO_2 conversion. The conventional active metals for Fischer-Tropsch synthesis (FTS) such as Fe, Co, Ni, Ru and Rh have been applied as a catalyst for CO_2 hydrogenation to higher hydrocarbons [26, 117, 137, 138]. However, CH_4 was the dominant product from CO_2 hydrogenation over these conventional catalysts. Therefore, the developing of the catalysts for CO_2 hydrogenation has become of great interest since these catalysts need to selectively produce more higher hydrocarbons before use in industrial scale. The Fe-based catalyst has been reported as a promising catalyst for CO_2 hydrogenation to hydrocarbons due to its high activity, low cost, and flexible operation conditions, as well as reasonable hydrocarbon products distribution [118, 139]. To further improve the higher hydrocarbons selectivity, the addition of promoters is required. The addition of K and Mn promoters on Fe-based catalysts have been reported that it significantly promoted the selectivity to olefinic products and suppressed the methane formation [11, 25, 122, 123].

In this chapter, a comparative study on the CO_2 hydrogenation to higher hydrocarbons over monometallic catalyst including Fe, Cu and Co metal. γ-Al_2O_3 and

TiO_2 supported catalysts were synthesized and evaluated for CO_2 hydrogenation to higher hydrocarbons. The activities and selectivities of these monometallic catalysts were investigated as well by the effect of K addition.

3.2 Equilibrium conversion of CO_2 hydrogenation to higher hydrocarbons

Form thermodynamic point of view for CO_2 hydrogenation, the equilibrium CO_2 conversion and product yields are dependent on temperature and pressure. In this study, the equilibrium CO_2 conversion of CO_2 hydrogenation to higher hydrocarbons could be estimated using Aspen HYSYS 7.1 and the system flow diagram are shown in Fig. 3.1. For calculating the equilibrium CO_2 conversion, the equations (3.1) – (3.12) are input reactions in the reactor as lines (a), (b) and (c), CH_4 is the most thermodynamically stable product and C_2H_4 – C_5H_{10} were chosen as relatively stable higher hydrocarbon products. Figure 3.2a-b showed the calculated CO_2 conversion at various temperatures (Fig. 3.2a) and various pressure (Fig. 3.2b) at constant mixed feed gas molar ratio of H_2/CO_2 of 3. The results from ASPEN HYSYS 7.1 are presented in Table C-1 (temperature) and C-2 (pressure) of Appendix C.

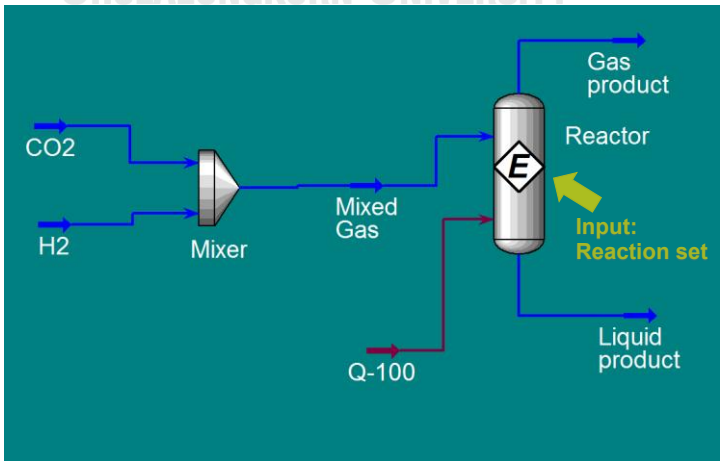

Figure 3.1 The flow diagram using in Aspen HYSYS 7.1.

Line (a): Reverse water-gas shift (RWGS)

$$CO_2 + H_2 \longleftrightarrow CO + H_2O \quad (3.1)$$

Line (b): CO_2 hydrogenation to CO and hydrocarbons

$$CO_2 + H_2 \longleftrightarrow CO + H_2O \quad (3.2)$$

$$CO + 3H_2 \longleftrightarrow CH_4 + H_2O \quad (3.3)$$

$$CO + 2H_2 \longleftrightarrow 1/2C_2H_4 + H_2O \quad (3.4)$$

$$CO + 2H_2 \longleftrightarrow 1/3C_3H_6 + H_2O \quad (3.5)$$

$$CO + 2H_2 \longleftrightarrow 1/4C_4H_8 + H_2O \quad (3.6)$$

$$CO + 2H_2 \longleftrightarrow 1/5C_5H_{10} + H_2O \quad (3.7)$$

Line (c): Direct CO_2 hydrogenation to hydrocarbons

$$CO_2 + 4H_2 \longleftrightarrow CH_4 + 2H_2O \quad (3.8)$$

$$CO_2 + 3H_2 \longleftrightarrow 1/2C_2H_4 + 2H_2O \quad (3.9)$$

$$CO_2 + 3H_2 \longleftrightarrow 1/3C_3H_6 + 2H_2O \quad (3.10)$$

$$CO_2 + 3H_2 \longleftrightarrow 1/4C_4H_8 + 2H_2O \quad (3.11)$$

$$CO_2 + 3H_2 \longleftrightarrow 1/5C_5H_{10} + 2H_2O \quad (3.12)$$

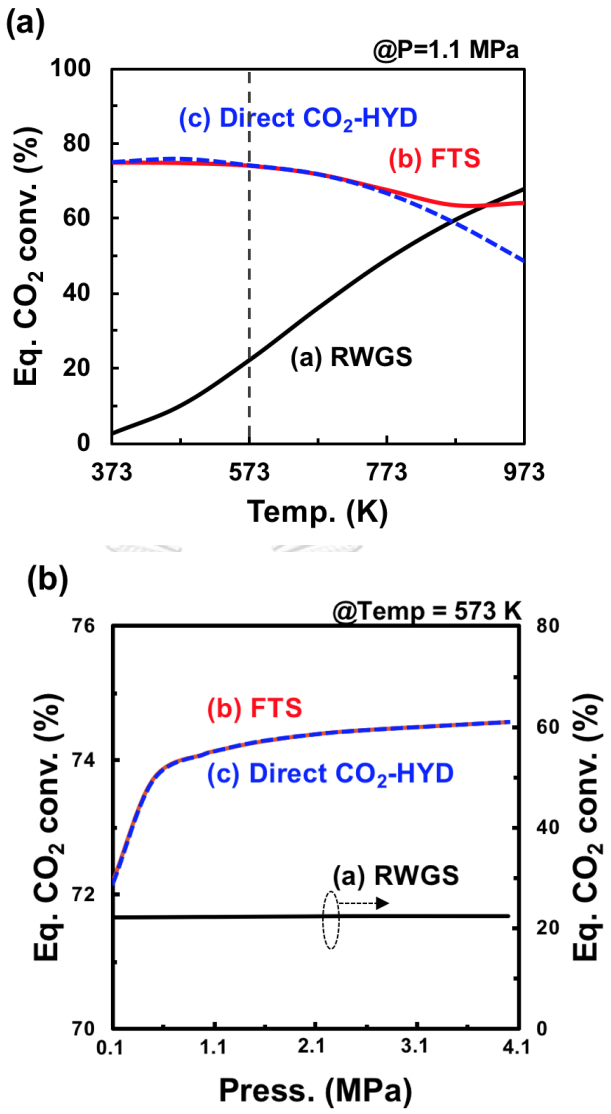

Figure 3.2 Equilibrium CO_2 conversion for a molar ratio of H_2/CO = 2:3 as a function of reaction (a) temperature and (b) pressure.

According to the calculation, temperature is more pronounced effect than pressure on the equilibrium CO_2 conversion. At high temperature, RWGS (line a) is more favorable than CO_2 hydrogenation to hydrocarbons (line b and c). From thermodynamic point of view, at low temperature, the CO_2 conversion by RWGS reaction is limited due to its endothermic reaction. The exothermic FTS reaction is not

thermodynamically limited in the temperature regime below 673 K and thus, it is possible to achieve higher CO_2 conversion for the overall reaction because of the consecutive reaction of CO formed by the RWGS reaction. Therefore, the catalysts have to be developed that both RWGS and FTS reaction could be catalyzed. In addition, the reaction rate of FTS should be equal or higher than that of the RWGS to overcome the thermodynamic limitation of the RWGS reaction [125]. For the pressure effect, the equilibrium CO_2 conversion of line b and c (CO_2 hydrogenation to hydrocarbons) are slightly increased with increasing pressure, while the RWGS is not dependent on pressure. The optimal condition for CO_2 hydrogenation to hydrocarbons is 300 ^{o}C (573 K) and 1.1 MPa and this condition was also chosen as a reaction condition for research work on CO_2 hydrogenation to hydrocarbons [140-142].

3.3 Support comparison

The chemical and textural properties of the support could influence the catalyst activity. Commonly, γ-Al_2O_3 is widely used as a support material due to its high surface area and acid properties. A previous study on CO_2 hydrogenation reported that using TiO_2 as support, it can give better selectivity to higher hydrocarbon [125]. It suggested that the oxygen vacancy of TiO_2 could increase bridge-type adsorbed CO_2, which can be dissociated to carbon species, thereby enhancing C-C bonds formation [127, 128].

Table 3.1 Activities and selectivities of supported monometallic catalysts for CO_2 hydrogenation [a]

Catalyst [b]	CO_2 conv. (%)	Prod. selec. (C-mol%)			STY (μmol g^{-1} s^{-1})			O/P [e]	α [f]
		CH_4	C_{2+} [c]	CO	CH_4	C_2-C_7 [d]	CO		
Fe/Al_2O_3 [g]	19.7	33	46	21	0.87	0.28	0.51	0.00	0.39
Fe/TiO_2 (P25) [h]	16.1	34	42	25	0.59	0.23	0.43	0.02	0.39
Fe/TiO_2 [i]	inactive	-	-	-	-	-	-	-	-
Co/TiO_2 (P25)	54.5	87	12	1	5.22	0.04	0.06	0.02	0.01
Cu/TiO_2 (P25)	9.7	1	9	90	0.01	0.01	0.97	0.00	0.00
Fe-K(0.1)/TiO_2 (P25)	18.0	11	40	49	0.22	0.18	0.91	0.50	0.54
Fe-K(0.3)/TiO_2 (P25)	17.1	4	40	56	0.06	0.08	1.02	6.60	0.60

[a] Reaction conditions: 573 K, 1.1 MPa, GHSV = 3600 mL (STP) g^{-1} h^{-1}, [b] Total metal loading (Co/Cu+Fe) = 15 wt% based on support, [c] Including small amounts of alcohols, [d] Only vapor phase, [e] Olefin to paraffin (O/P) ratio of C_2-C_4 hydrocarbons

[f] Chain growth probability of C_2–C_7 hydrocarbons determined by Anderson-Schulz-Flory (ASF) distribution equation

[g] γ-Al_2O_3 (PURALOX TH 100/150, Sasol), [h] TiO_2 (AEROXIDE P25, Evonik), [I] TiO_2 (Catalyst support, Alfa Aesar)

The effect of support material over Fe monometallic catalyst on CO_2 and selectivity are presented in Table 3.1. The γ-Al_2O_3 (PURALOX TH 100/150), TiO_2 (catalyst support, Alfa Aesar) and TiO_2 (AEROXIDE P 25, Evonik) were chosen as support material for Fe monometallic catalyst. Fe/γ-Al_2O_3 catalyst gave slightly higher CO_2 conversion and C_{2+} selectivity while gave significantly higher STY of CH_4 compare with TiO_2 (P 25) support. However, when using TiO_2 from Alfa Aesar as a support, it did not show any activity although the BET surface area (Table 3.2) of this TiO_2 is significant higher than TiO_2 (P 25). It should be noted that the TiO_2 (Alfa Aesar) synthesized *via* wet process (using sulfur-containing precursor), still contained small amount of sulfur, unlike TiO_2 (AEROXIDE P 25, Evonik) which was synthesized *via* dry process. When using TiO_2 (Alfa Aesar) as support of Fe catalyst, the inactive phenomena possibly occur because the sulfur can cause the poisoning on Fe catalyst [143]. This suggested that the activity of the Fe monometallic catalysts could depend on the metal-support interaction and surface chemical properties, rather than the textural properties of support materials.

3.4 Monometallic catalysts

The CO_2 hydrogenation over TiO_2-supported monometallic catalysts (Fe, Co and Cu) was performed in a fixed-bed flow reactor system at 573 K and 1.1 MPa. The steady-state activity data was obtained after 6-8 h on stream for all catalysts as shown in Fig. 3.3. The steady-state activities and selectivities at 16-18 h on stream of monometallic catalysts were chosen for evaluating the catalytic activity, which are presented in Table 3.1. Among from monometallic catalysts tested here, only Fe/TiO_2 catalyst produced a significant amount of C_{2+} hydrocarbons (selectivity = 41 mol%) as well as high chain growth probability (α=0.39). Riedel *et al.* [119] suggested that the iron-carbide could be an active phase for the FTS leading to C_{2+} hydrocarbon formation

over Fe-based catalysts, and this carbide species was a prerequisite for carbon-carbon bond formation. Co/TiO_2 showed a much higher CO_2 conversion (55%) than Fe catalyst (16%), but CH_4 was the dominant product due to the high hydrogenation ability of Co. Such ability of Co/Al_2O_3 catalyst was reported by Satthawong *et al.* [17]. On the other hand, Cu/TiO_2 exhibited a low activity compared with Fe and Co catalysts and CO was the primary product as expected because Cu is well-known as an active metal for reverse water-gas shift (RWGS) [33, 144, 145]. Based on the activity of metal carbides for CO_2 hydrogenation, a transition metal (Fe, Co or Ni) carbide can cleave the C-O bonds, thereby leading to hydrocarbon formation in the subsequent hydrogenation, whereas Cu carbide does not break these bonds [146]. It should be noted that the active phases of the TiO_2-supported monometallic catalysts remain to be clarified.

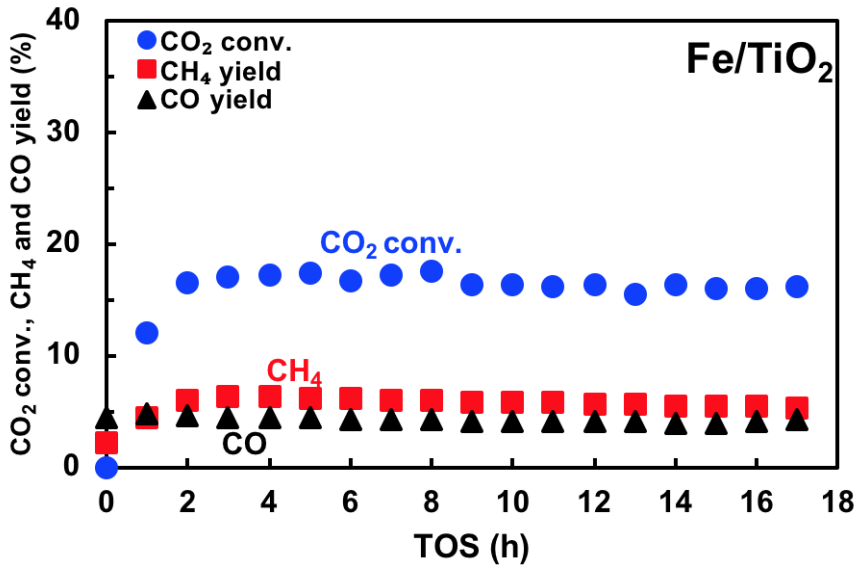

Figure 3.3 Catalytic stability of Fe/TiO_2 at time on stream (TOS). Reaction conditions: 573 K, 1.1 MPa, GHSV = 3600 mL (STP) g^{-1} h^{-1}.

3.5 K-promoted monometallic catalysts

To further improve CO_2 hydrogenation performance of heterogeneous catalysts for CO_2 hydrogenation to hydrocarbons. The addition of electronic or structural promoters have been investigated, K as a promoter of Fe-based catalysts can promote the selectivity to olefin, long chain hydrocarbons, and also suppress the methane formation [11, 25, 122, 147]. The effect of K promoter addition (K/Fe= 0.1 atom $atom^{-1}$) to Fe monometallic catalysts is tabulated in Table.3.1. The results indicated that K significantly suppressed CH_4 STY, while CO STY was increased. This suggested that K could suppress the methanation reaction. Moreover, when the amount of K/Fe atomic ratio was further increased to 0.3, the CH_4 STY was further suppressed and led to higher chain growth probability (α) and olefin to paraffin (O/P) ratio. Such dependence reported by Choi *et al.* suggested that the addition of K could decrease H_2 chemisorption capacity, while it enhanced CO_2 adsorption on catalyst surface [148]. For clarity, the chromatograms of gas-phase hydrocarbon product with α and O/P are shown in Fig. 3.4. Hence, K promoter acts a different role compared to that by the active metal including Fe, Co and Cu, which enhanced the hydrogen coverage. To clarify the role of K on the catalyst surface, the characterization of adsorbed species will be investigated.

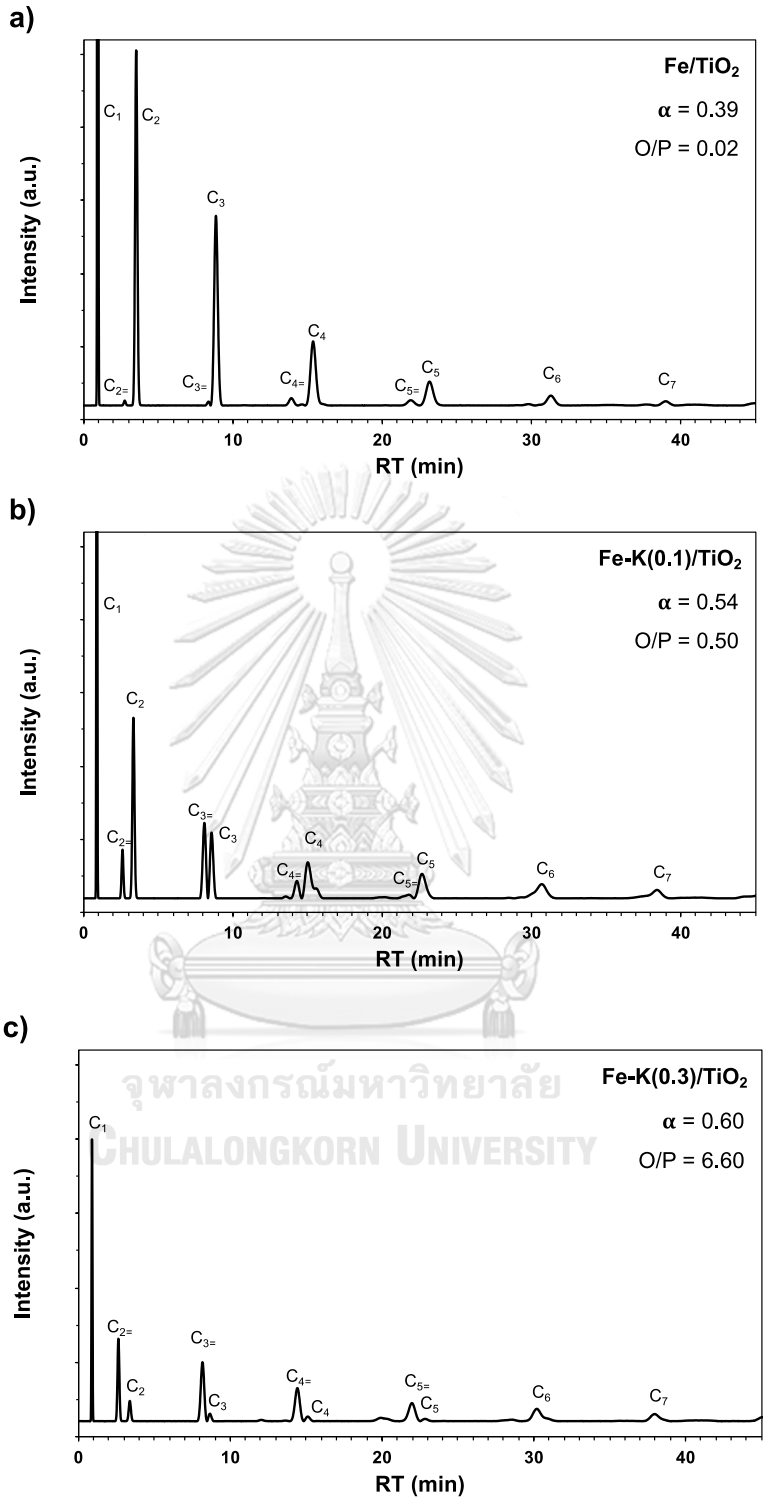

Figure 3.4 GC-FID chromatograms of gas-phase hydrocarbons from CO_2 hydrogenation over Fe-K(X)/TiO_2 with different K/Fe atomic ratio. (a) X=0, (b) X=0.1 and (c) X=0.3.

3.6 Textural properties of monometallic catalysts

A correlation of physical properties to the catalytic activity of the monometallic catalysts has been investigated using the N_2 adsorption-desorption analyses. The textural properties of support materials and all monometallic catalysts are summarized in Table. 3.2. According to the catalytic activity results of TiO_2-supported monometallic catalysts in Table 3.1, it suggested that there is no relation between textural properties of the catalysts and CO_2 conversion. The BET surface area (SA) of the calcined Fe/TiO_2 catalysts was close to that of the bare TiO_2 (P 25) support (44 m^2 g^{-1}), while SA of the monometallic Co/TiO_2 and Cu/TiO_2 catalysts was lower (36 and 35 m^2 g^{-1}, respectively). Upon loading the metal oxides, the pore volume (PV) and average pore diameter (D_p) were about 34% and 18% lower, respectively compared with bare TiO_2 (P 25), suggesting that the small metal oxide particles could fill in the pores of TiO_2 support.

Table 3.2 Physical properties of TiO_2 supported monometallic catalysts.

Catalyst [a]	SA[b] (m^2 g^{-1})	PV[c] (cm^3 g^{-1})	D_p[d] (nm)
Al_2O_3[e]	139	1.03	24
TiO_2 (Alfa)[f]	112	0.34	11
TiO_2 (P25)[g]	44	0.42	35
Fe/TiO_2 (P25)	44	0.29	27
Co/TiO_2 (P25)	36	0.26	28
Cu/TiO_2 (P25)	35	0.28	30

[a] Total metal loading = 15 wt% based on support, [b] BET surface area

[c] BJH desorption cumulative pore volume, [d] BJH desorption average pore diameter

[e] γ-Al_2O_3 (PURALOX TH 100/150, Sasol, [f] TiO_2 (Catalyst support, Alfa Aesar).

[g] TiO_2 (AEROXIDE P25, Evonik)

CHAPTER IV

Fe-BASED BIMETALLIC CATALYSTS SUPPORTED ON TiO_2 FOR SELECTIVE CO_2 HYDROGENATION TO HYDROCARBONS

4.1 Introduction

Recently, the bimetallic promotion on the selective CO_2 hydrogenation to methanol using Pd-Cu catalysts [91] and to light hydrocarbons using Fe-based bimetallic catalysts [122, 123] have been reported. CO_2 hydrogenation to liquid fuels and highly value-added products remains a challenging research topic. For this purpose of promoter addition, such as K and La, on Fe-based catalysts, K significantly promoted the selectivity to olefinic products and suppressed the methane formation [11, 25, 122, 123] and La could enhance the selectivity of higher hydrocarbons in FTS [124] and CO_2 hydrogenation [125, 126]. In this work, a comparative study on the CO_2 hydrogenation activities and product selectivities of the titania-supported Fe-based bimetallic catalysts was carried out. The addition of a small amount of second metal (Co and Cu) on Fe showed the synergetic promotion on the CO_2 conversion and the space-time yields (STY) of hydrocarbon products. The incorporation of K and La as promoters can further improve the activity and product selectivity to higher hydrocarbons, indicating that the promoted Fe-based bimetallic catalysts are promising for CO_2 hydrogenation to higher hydrocarbons.

The aims of this work are to study the CO_2 hydrogenation to higher hydrocarbons (C_{5+}) over Fe-based bimetallic catalysts and to explore the synergetic effect of bimetallic catalysts. TiO_2-supported Fe-based bimetallic catalysts were synthesized and evaluated for CO_2 hydrogenation activity, wherein Co and Cu were

selected as the second metals. The effect of promoters, K and La, was investigated as well by a comparative study with the unpromoted catalysts.

4.2 Characterization of TiO_2 supported Fe-based catalysts

4.2.1 Physical properties

The physical properties and crystalline structure parameters of calcined catalysts are summarized in Table 4.1. The BET surface area (SA) of the calcined Fe and Fe-Co (X = 0.1) catalysts (43-44 $m^2 g^{-1}$) was close to that of the bare TiO_2 support (44 $m^2 g^{-1}$), while SA of the Co-rich and Cu-rich Fe-M(0.5) catalysts was lower (36 and 37 $m^2 g^{-1}$, respectively). Upon loading the metal oxides, the pore volume (PV) and average pore diameter (D_p) were about 35% and 23% lower, respectively, suggesting that small metal oxide particles were dispersed inside the pores of TiO_2 support.

4.2.2 X-ray diffraction patterns

Figure. 4.1a presents the X-ray diffraction patterns of the calcined mono- and bimetallic catalysts, as well as the bare support as benchmark. The calcined Fe-Cu(0.1)/TiO_2 and Fe-Co(0.1)/TiO_2 showed the similar XRD patterns with the monometallic Fe catalyst, and the diffraction peaks of polycrystalline α-Fe_2O_3 [PDF #00-001-1053] were observed centered at 33.14, 35.56 and 49.35°. Only Cu and Co-rich bimetallic catalysts, Fe-Cu(0.5)/TiO_2 and Fe-Co(0.5)/TiO_2, showed the peaks of Cu and Co metal oxide, wherein the calcined Fe-Cu(0.5)/TiO_2 exhibited diffraction peaks at 35.55 and 38.60° corresponding to polycrystalline CuO [PDF #00-005-0661], while the calcined Fe-Co(0.5)/TiO_2 catalyst displayed diffractions at 31.29, 36.86, and 65.28° corresponding to polycrystalline Co_3O_4 [PDF #00-042-1467]. As depicted in Fig. 4.1b, the magnified range (60-68°) clearly illustrates the existence of polycrystalline Co oxide. The crystallite size was determined by Scherrer equation and tabulated in Table 4.1. The polycrystalline Co oxide crystallite size of Fe-Co(0.5)/TiO_2 (19.4 nm) was larger

than that of the catalysts with lower Co loading. Besides, the SA of Fe-Co(0.5)/TiO_2 was lower than that of Fe-Co(0.1)/TiO_2, suggesting that Co oxide particles are larger in the former. The average size of the α-Fe_2O_3 phase in the calcined Fe-Co(0.5)/TiO_2 was 19.2 nm which was larger than those of Fe alone and Fe-rich bimetallic (i.e., Fe-Co(*X*) and Fe-Cu(*X*), $X \leq 0.1$) catalysts (e.g., 13.9-14.9 nm).

Table 4.1 Physical properties and crystalline structure of TiO_2 supported catalysts

Catalyst [a]	SA ($m^2 g^{-1}$)	PV ($cm^3 g^{-1}$)	D_p (nm)	Crystalline phase comp.[c] (wt%)		Lattice parameter [d] (Å)		Cell vol. [d] ($Å^3$)	Crystallite size [e] (nm)		
				Anatase	Rutile	a = b	c		Fe_2O_3	Co_3O_4	CuO
TiO_2 [b]	44	0.42	35	85	15	3.784	9.384	134.4	-	-	-
Fe/TiO_2	44	0.29	27	83	17	3.789	9.622	138.1	14.9	-	-
$Fe\text{-}Co(0.1)/TiO_2$	43	0.29	27	83	17	3.787	9.585	137.5	13.9	N/A	-
$Fe\text{-}Co(0.5)/TiO_2$	36	0.27	28	82	18	3.786	9.558	137.0	19.2	19.4	-
Co/TiO_2	36	0.26	28	83	17	3.786	9.564	137.1	-	22.7	-
$Fe\text{-}Cu(0.1)/TiO_2$	37	0.29	32	83	17	3.786	9.502	136.2	13.9	-	N/A
$Fe\text{-}Cu(0.5)/TiO_2$	37	0.29	31	83	17	3.786	9.559	137.0	13.2	-	18.1
Cu/TiO_2	35	0.28	30	83	17	3.784	9.528	136.4	-	-	32.7

[a] Total metal loading (Co/Cu+Fe) = 15 wt% based on support.

[b] AEROXIDE TiO_2 P 25, Evonik calcined at 723 K for 4 h.

[c] Determined from the relative XRD diffractions corresponding to anatase (101) and rutile (110) reflections.

[d] Estimated from the Bragg's law of anatase reflections.

[e] Estimated from the Scherrer equation of corrected 2θ position.

From Table 4.1, the mass fractions of anatase and rutile for all catalysts were similar to those of the bare TiO_2, indicating that the TiO_2 phase exists regardless of the catalyst preparation. The lattice parameter (*a*, *b*, and *c*) and cell volume of anatase unit cell generally increased with increasing metal loading on the TiO_2 support compared with the bare support. It is known that the ionic radius of Fe^{3+}, Co^{3+}, Co^{2+}, and Cu^{2+} (0.645, 0.610, 0.745 and 0.650 Å, respectively) are larger than that of Ti^{4+} (0.605 Å) [149]. Thus, the changes of the anatase unit cell implies that the loaded metals were incorporated into the anatase crystalline structure, thereof leading to the unit cell distortion.

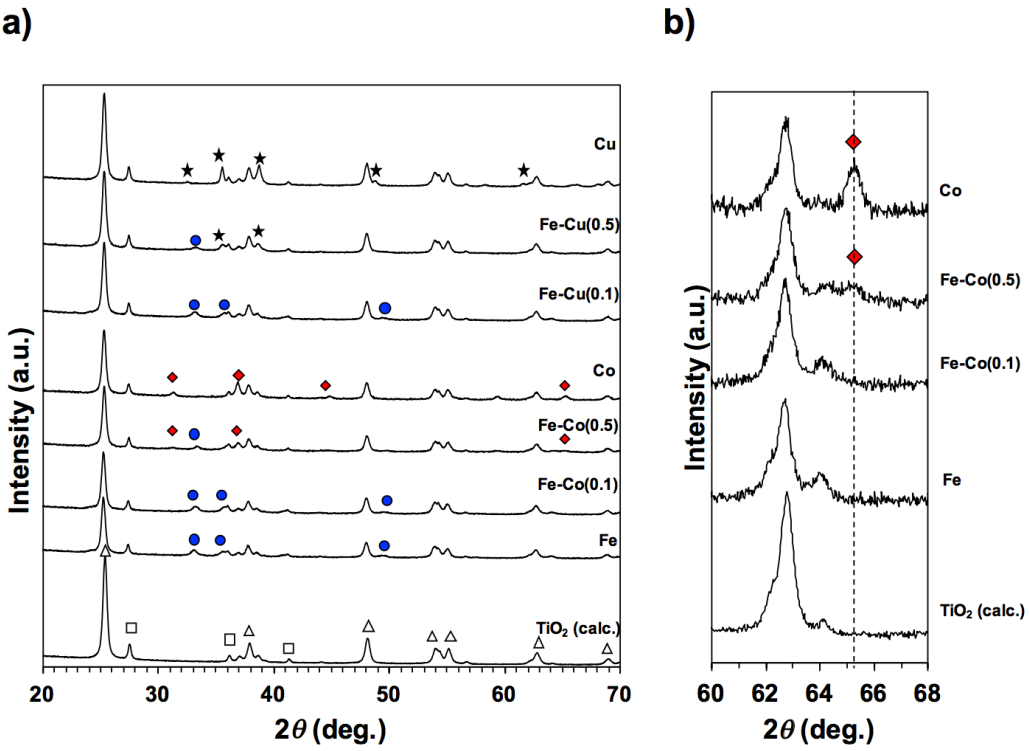

Figure 4.1 XRD patterns of TiO_2 support (P25, Evonik), TiO_2-supported monometallic, Fe-Co and Fe-Cu bimetallic catalysts in the 2θ ranges (a) between 20 and 70° and (b) between 60 and 68°, ΔTiO_2 (anatase), □ TiO_2 (rutile), ● α-Fe_2O_3, ◆ Co_3O_4 and ★ CuO.

4.3 Reducibility of supported metal oxides

The TPR profiles of the calcined Fe-Co/TiO_2 and Fe-Cu/TiO_2 catalysts with various M/(M+Fe) atomic ratios, along with the degree of reduction (DR) of the supported metal oxides are illustrated in Fig. 4.2. The DR of the supported metal oxides was defined as the ratio of the measured H_2 consumption from TPR experiment to the theoretical H_2 consumption. The measured H_2 consumption was determined by integrating the whole TPR profile, while the theoretical H_2 consumption was calculated from the amount of H_2 required for the reduction of the supported Fe and Co oxides to their metallic states according to the stoichiometry of the Eq. 5.1 and 5.2. The calibration of the H_2 consumption was done by the reduction of Ag_2O powder.

$$Fe_2O_3 + 3H_2 \longleftrightarrow 2Fe^0 + 3H_2O \quad (5.1)$$

$$Co_3O_4 + 4H_2 \longleftrightarrow 3Co^0 + 4H_2O \quad (5.2)$$

$$CuO + H_2 \longleftrightarrow Cu^0 + H_2O \quad (5.3)$$

A calcined TiO_2 support material was also tested, and barely showed any major reduction peak. For the Fe/TiO_2 catalyst, a broad peak with several shoulders was observed at 659, 728, and 886 K, attributing to a stepwise reduction of Fe_2O_3 to Fe^0 through Fe_3O_4 and FeO [150-152]. The Co/TiO_2 catalyst exhibited two peaks at 621 and 792 K relating to two different oxidation states, Co_3O_4 and CoO, of the cobalt [150, 151, 153]. The TPR profile of Fe/TiO_2 was significantly changed by Co addition. The peaks at 638 and 793 K were clearly observed and accompanied by a significant enhancement of the peak intensities, demonstrating a considerable improvement in total degree of reduction in the Fe-Co bimetallic catalysts from only 25% (Fe/TiO_2) to 93% (Fe-Co(0.5)/TiO_2). Noticeably, only Fe-Co(0.5)/TiO_2 catalyst showed a single broad peak centering at 925 K, suggesting the formation of Fe-rich Fe-Co alloy phase. Such similar peak was also reported by Duvenhage and Coville [151], suggesting the

formation of stable and hardly reduced Fe-rich phase in the synthesized bimetallic catalyst. However, the peak of stable and hardly reduced did not appear for Fe-Cu(0.5)/TiO_2 catalyst as shown in Appendix F. Moreover, If the Fe/TiO_2 and Co/TiO_2 catalysts were prepared by physical mixing, the calculated DR for Fe-Co(0.1)/TiO_2 would be 30%, which was equal to the measured DR. However, the measured DR of Fe-Co(0.5)/TiO_2 catalyst was 93% which was much higher than those calculated DR (58%) suggesting that the supported metal oxides possibly become more reducible by the alloy formation of Fe-Co spinels [153]. The *in situ* H_2-TPR analysis of pre-reduced catalysts was also carried out for all Fe-containing catalysts, and the resultant profiles are shown as well in Fig. 4.2 (red line). Apparently, H_2-reduction peak was not observed for pre-reduced catalysts, implying that the Fe-based bimetallic catalysts could be reduced almost completely under this pretreatment condition.

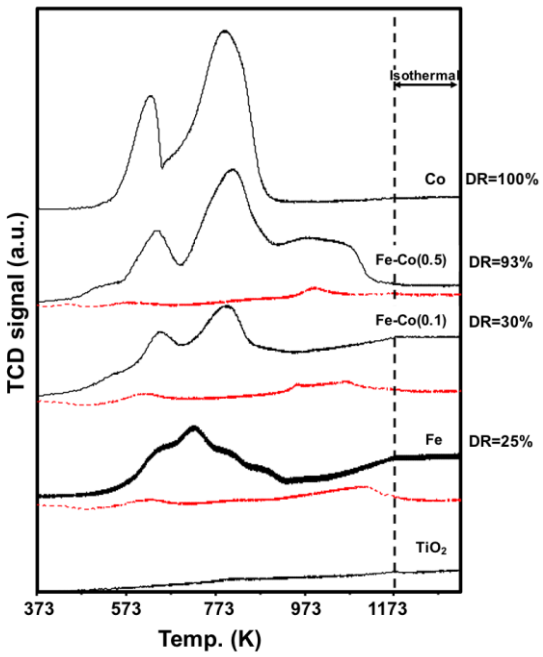

Figure 4.2 Effect of combining Fe and Co on the H_2-TPR profiles of the calcined Fe-Co(X)/TiO_2 catalysts, (_____) calcined catalysts and (- - - - - -) pre-reduced catalysts.

4.4 CO_2 hydrogenation over Fe-based bimetallic catalysts

To enhance CO_2 hydrogenation activities for higher hydrocarbon production, Satthawong *et al.* and Wang *et al*. [17, 154] reported on the corporation of Co and Cu as a second metal to γ-Al_2O_3-supported Fe-based catalysts that found the synergetic promotion effect on CO_2 conversion and product selectivity of Fe-based bimetallic catalysts was observed. In this work, the TiO_2-supported Fe-based bimetallic catalysts (Fe-M; M = Co or Cu) with 15 wt% total metal loading (Fe + M, support weight basis) were tested and the results are shown in Table 4.2.

Figure. 4.3 showed the synergistic promotion effect of second metal addition to Fe-based catalysts with using both TiO_2 (present work) and γ-Al_2O_3 (previous works. [17, 154]) as support materials. Combining Fe with the second metal (Co or Cu) on TiO_2 can significantly improve the CO_2 conversion (from 16% to 33%) and enhance the space-time yields (STY) of higher hydrocarbons. It can be noted that the synergistic promotion of Fe and other metal combination can increase the C_{2+} hydrocarbons formation. However, comparing the promotion effect of Co and Cu over the Fe-based bimetallic catalyst, the Fe-Co exhibited much higher promotion effect on the activity than Fe-Cu due to the stronger hydrogenation ability of Co resulting in higher CH_4 and C_{2+} hydrocarbons formation. According to Satthawong *et al.* [122], tailoring the adsorbed hydrogen surface properties of catalyst is essential for enhancing the higher hydrocarbon formation. Hence, combining the second metal with Fe possibly changed the adsorption properties of catalyst surface and led to the synergistic promotion on the activity of Fe-based bimetallic catalysts.

To verify this idea, the Fe-M/TiO_2 bimetallic catalyst with difference M/(M+Fe) atomic ratios were tested and the CO_2 hydrogenation results are compared in Fig. 4.4. The product selectivities of both Fe-Co/TiO_2 and Fe-Cu/TiO_2 catalysts changed with

Table 4.2 Activities and selectivities of TiO_2 supported Fe-based bimetallic catalysts for CO_2 hydrogenation [a]

Catalyst [b]	CO_2 conv. (%)	Prod. selec. (C-mol%)				STY (μmol g^{-1} s^{-1})				O/P [e]	α [f]
		CH_4	C_2-C_4	C_{5+} [c]	CO	CH_4	C_2-C_4	C_5-C_7 [d]	CO		
Fe	16.1	34	13	28	25	0.59	0.21	0.016	0.43	0.02	0.39
Fe-Co(0.1)	33.3	51	11	32	6	1.43	0.38	0.012	0.26	0.00	0.30
Fe-Co(0.5)	18.4	72	20	3	5	1.56	0.17	0.005	0.09	0.03	0.26
Fe-Cu(0.1)	19.5	27	11	39	23	0.60	0.23	0.023	0.46	0.10	0.41
Fe-Cu(0.5)	19.7	21	26	15	38	0.47	0.23	0.022	0.76	0.02	0.43
Fe-Co(0.1)-K(0.1)	23.9	23	11	35	31	0.56	0.29	0.026	0.78	0.20	0.44
Fe-Co(0.1)-K(0.3)	21.2	9	6	31	54	0.16	0.13	0.020	1.25	4.06	0.50
Fe-Cu(0.1)-K(0.1)	19.9	12	8	31	49	0.27	0.17	0.028	0.98	0.38	0.52
Fe-Cu(0.1)-K(0.3)	20.8	5	3	30	62	0.10	0.08	0.019	1.35	4.91	0.57
Fe-Cu(0.1)-La(0.1)	22.5	25	12	38	25	0.61	0.28	0.033	0.61	0.05	0.44
Fe-Cu(0.1)-K(0.1)-La(0.1)	23.1	13	9	45	33	0.31	0.21	0.043	0.76	0.52	0.56
Fe-Co(0.1)-K(0.1)-La(0.1)	21.9	18	10	30	42	0.40	0.23	0.031	0.98	0.35	0.49

[a] Reaction conditions: 573 K, 1.1 MPa, GHSV = 3600 mL (STP) g^{-1} h^{-1}, [b] Total metal loading (Co/Cu+Fe) = 15 wt% based on support,

[c] Including small amounts of alcohols, [d] Only vapor phase, [e] Olefin to paraffin (O/P) ratio of C_2-C_4 hydrocarbons,

[f] Chain growth probability of C_2–C_7 hydrocarbons determined by Anderson-Schulz-Flory (ASF) distribution equation.

the varying bimetallic composition and both catalysts gave the highest C_{2+} hydrocarbons selectivity at M/(M+Fe) atomic ratio of 0.1 (43 and 50%, respectively) which was also higher than the monometallic Fe catalyst (41%). A further Co addition promoted CH_4 formation to a dominant product due to the stronger hydrogenation ability of Co (Fig. 4.4a). Surprisingly, the Fe-Co(0.5) catalyst showed only 18% of CO_2 conversion, which was lower than other Fe-Co bimetallic catalysts . However, such negative effect was not observed for Al_2O_3-supported Fe-Co(0.5) catalyst (Fig. 4.3). According to the lattice parameters (Table 4.1), the Fe and Co were possibly present in the form of Fe-rich alloy in Fe-Co(0.5) as evidenced from the distortion of crystallite structure, resulting in a smaller cell volume of Fe-Co(0.5) in comparison to that of Fe-Co(0.1).

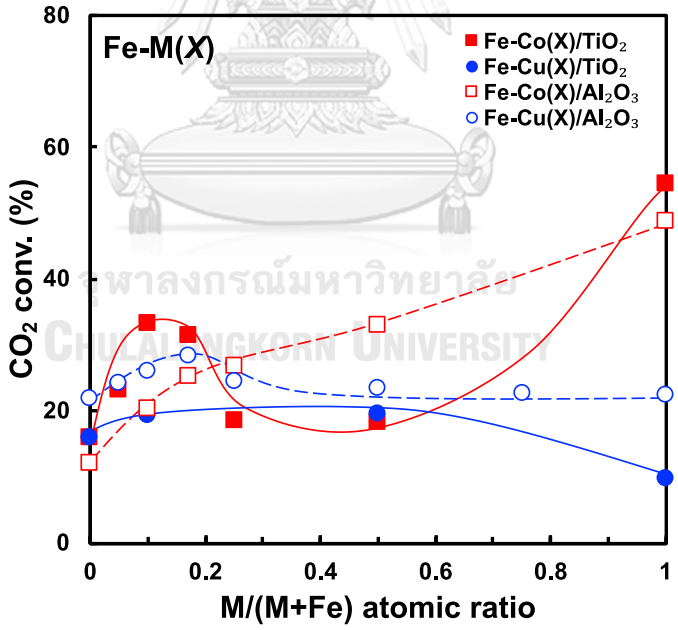

Figure 4.3 Effect of (red square) Co/(Co+Fe) atomic ratio and (blue circle) Cu/(Cu+Fe) atomic ratio on CO_2 conversion over Fe-M(X)/TiO_2 catalysts (present work) and Fe-M(X)/Al_2O_3 (from ref. [17, 154]). Reaction conditions: 573 K, 1.1 MPa, GHSV = 3600 mL (STP) g^{-1} h^{-1}.

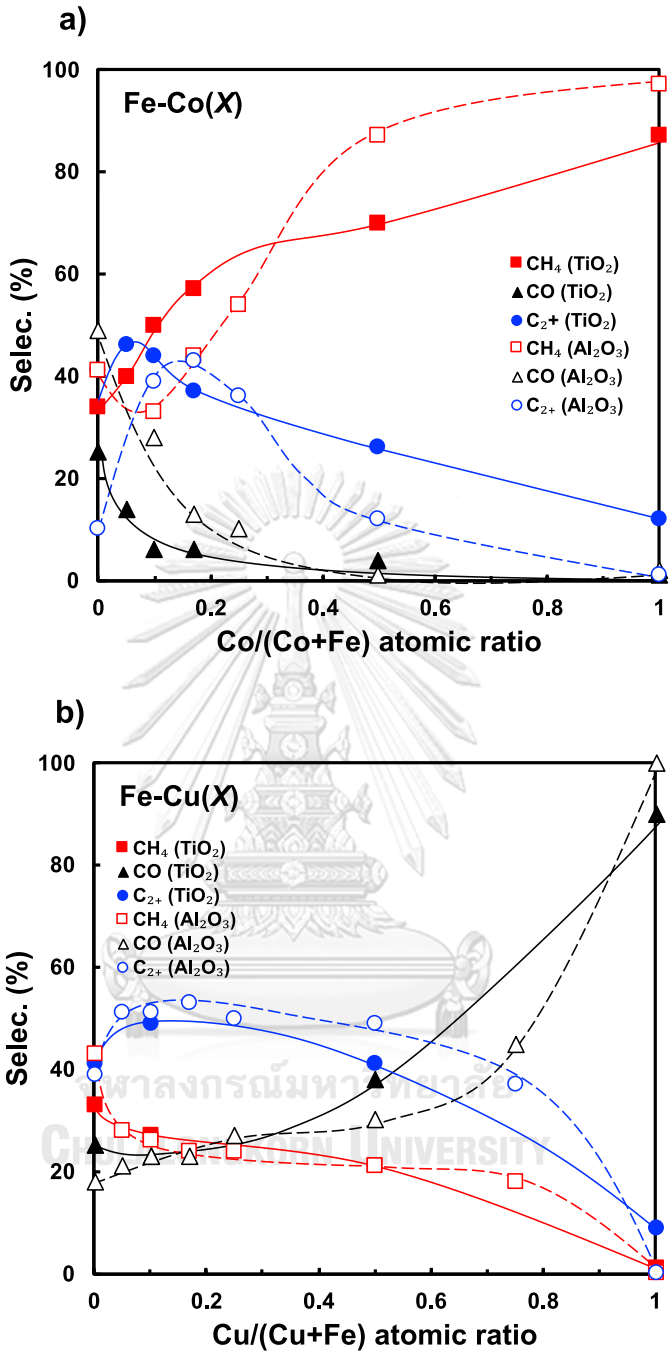

Figure 4.4 Effect of (a) Co/(Co+Fe) atomic ratio and (b) Cu/(Cu+Fe) atomic ratio on CH_4, C_{2+} hydrocarbons, and CO product selectivities over Fe-M(X)/TiO_2 (present work) and Fe-M(X)/Al_2O_3 (from ref. [17, 154]) catalysts. Reaction conditions: 573 K, 1.1 MPa, GHSV = 3600 mL (STP) g^{-1} h^{-1}.

As aforementioned, the H_2-TPR profile of Fe-Co(0.5)/TiO_2 catalyst exhibited a reduction peak at 925 K (Fig. 4.2), relevant to alloy phase which was difficult to be reduced. However, this catalyst was reduced almost completely under the pre-treatment condition. Thus, the low activity of Fe-Co(0.5)/TiO_2 was possibly ascribed to the Fe-rich alloy phase which was not quite active compared with the catalysts at other bimetallic composition.

On the other hand, adding more Cu into Fe evidently enhanced the RWGS reaction which exhibited a favorable production towards CO (Fig. 4.4b). However, at the same M/(M+Fe) atomic ratio of 0.1, the Fe-Cu(0.1) catalyst gave C_5-C_7 hydrocarbons STY almost 1-fold higher than Fe-Co(0.1)/TiO_2 catalyst (Table 4.2). Such high increase in C_5-C_7 suggests that more CO in the system possibly enhanced the chance of chain-growth reaction *via* FTS.

From Fig. 4.3 and 4.4 regarding to the support materials, although the surface area of γ-Al_2O_3 (139 m^2 g^{-1}) is much higher than that of TiO_2 (44 m^2 g^{-1}) support, both support materials exhibited the similar promotion effect on both CO_2 conversion and product selectivity of supported Fe-based bimetallic catalysts. The γ-Al_2O_3 supported Fe-based bimetallic catalysts (Fe-Co/Al_2O_3 and Fe-Cu/Al_2O_3) gave highest C_{2+} hydrocarbons selectivity at M/(M+Fe) atomic ratio of 0.17 (44 and 53%, respectively). On the other hand, TiO_2 supported Fe-based bimetallic catalysts (Fe-Co/TiO_2 and Fe-Cu/TiO_2) have highest C_{2+} selectivity at 0.10 atomic ratio (43 and 50%, respectively). However, at high Fe-Co atomic ratio of 0.5, TiO_2 supported catalysts could maintain higher C_{2+} hydrocarbons selectivity (23%) than γ-Al_2O_3 supported catalysts (12%). This could possibly explain by the difference of γ-Al_2O_3 and TiO_2 support properties. The first reason is that the $CoAl_2O_4$ spinel structure is easily formed on Co/Al_2O_3 rather than TiO_2 support. The other reason is that the acid sites on Al_2O_3-supported catalysts may facilitate carbon deposition [155]. However, the properties of support, Al_2O_3 and TiO_2,

has less influence than the combining transition metal as active phase or active site(s) of the catalysts for the catalytic CO_2 hydrogenation.

The addition of a small amount of second metal (Co or Cu) to Fe catalyst could, upon reduction, induce the formation of alloy which modify the adsorption and activation of CO_2 and H_2 , alter the reaction pathways and thus change the selectivity to higher hydrocarbons [122]. The DFT studies by Xiaowa Nie *et al.* [121, 156] indicate that doping second metal such as Cu to Fe can alter the surface properties of the catalyst, alter the relative kinetic barriers of different reaction pathways and lower the kinetic barrier of the rate-determining step; thus bimetallic Fe-Cu enhances CO_2 conversion by reducing the kinetic barriers, and alters the selectivity preference to more valuable C_2 products from CH_4 on mono-metallic Fe surface. The alloy effect may include changes in surface structure and binding energies for CO_2 and H_2 and the reaction intermediates, thus the alloy effect could involve both electronic and geometric factors on surface.

4.5 CO_2 hydrogenation over K promoted Fe-based bimetallic catalyst

Time-on-stream (TOS) performance of promoted Fe-based bimetallic catalysts for CO_2 conversion and product selectivity are illustrated in Fig. 4.5 as examples. From the initial increase in CO_2 conversion with time on stream for Fe-Co(0.1)-K(0.1)/TiO_2 in the first 4 h, it appears the *in situ* activation is required for this catalyst which includes but is not limited to reduction of oxides of Fe and Co. On the other hand, the *in situ* activation is not really needed for the Fe-Cu(0.1)-K(0.1)-La(0.1)/TiO_2 catalyst. Fe-M/TiO_2 showed relatively stable CO_2 conversion and selectivities after 6-8 h on stream. Although CO_2 conversion with the catalysts slightly decreased with TOS, the decreasing rates were less than 0.3% per hour at 16-18 h on stream.

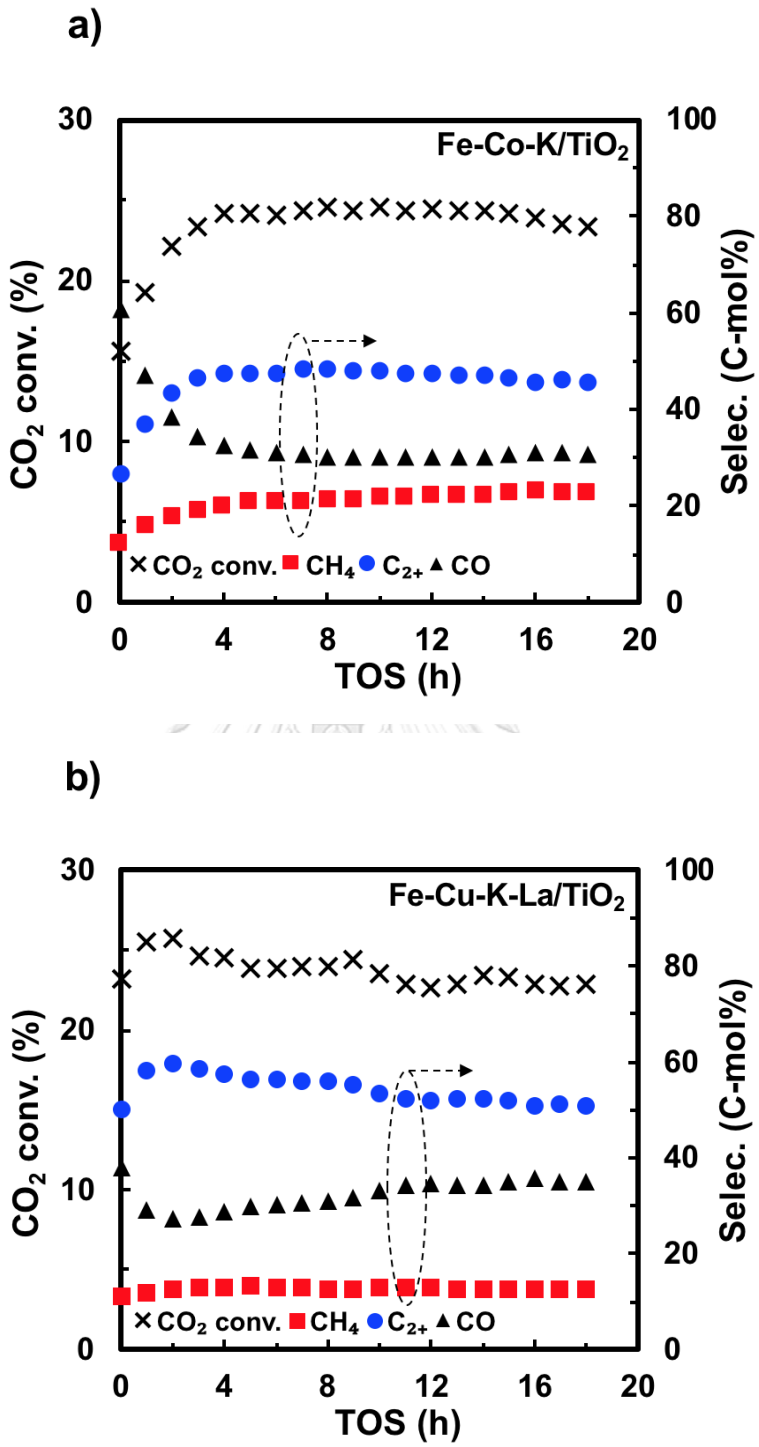

Figure 4.5 Catalytic stability of (a) Fe-Co(0.1)-K(0.1)/TiO_2 and (b) Fe-Cu(0.1)-K(0.1)-La(0.1)/TiO_2 at time on stream (TOS). Reaction conditions: 573 K, 1.1 MPa, GHSV = 3600 mL (STP) g^{-1} h^{-1}.

The performance of Fe-M(0.1)/TiO_2 catalysts at various K/Fe atomic ratios was also studied, and the corresponding results are shown in Fig. 4.6a (Fe-Co(0.1)-K(*Y*)/TiO_2) and Fig. 4.6b (Fe-Cu(0.1)-K(*Y*)/TiO_2). For comparison, all Fe-based catalysts were incorporated with K, and the K/Fe atomic ratio was initially fixed at 0.1 and 0.3 (Table 4.2). The addition of K to the metal with an atomic ratio of 0.1 can suppress the CH_4 formation and promote the C_{5+} hydrocarbons STY. Both K promoted Fe-Co/TiO_2 and Fe-Cu/TiO_2 catalysts exhibited the similar trends on STY of CH_4 and C_2-C_7 hydrocarbons and olefin to paraffin ratio of C_2-C_4 products (O/P). The K addition increased the light olefin content (O/P of C_2-C_4 hydrocarbons) and improved the chain growth probability of hydrocarbons as evidenced from the increased α value. For clarity, the chromatograms of gas-phase hydrocarbon product over Fe-Cu-K(*X*)/TiO_2 catalysts with α and O/P value are shown in Appendix G. This dependence suggests that, the presence of K can suppress the methanation and olefin hydrogenation. On the other hand, a further increase of K/Fe up to 0.3 on both catalysts reduced the activity towards the hydrocarbons formation (decrease in CH_4, C_2-C_4 and C_5-C_7 STY) and gave more CO (Table 4.2). Such decreased performance suggests that K could covered the active metal of the catalyst on TiO_2 support. The chemisorption property towards CO_2 and H_2 over K-promoted Fe catalysts has been reported that the K addition could reduce the H_2 adsorption capacity of Fe-based catalyst while enhancing CO_2 adsorption [119, 123, 147]. The K addition plays a different role compared to that of the second metal added to Fe. K promoter is expected to enhance CO_2 chemisorption and suppress H_2 coverage on surface.

Although, the K-promoted catalysts gave a slightly lower CO_2 conversion than unpromoted ones, the promoted catalyst exhibited high selectivity towards higher hydrocarbons especially C_{5+} and lower methane selectivity. From the value-added

product point of view, the lowest methane selectivity is desired for liquid-fuel production *via* CO_2 hydrogenation [125].

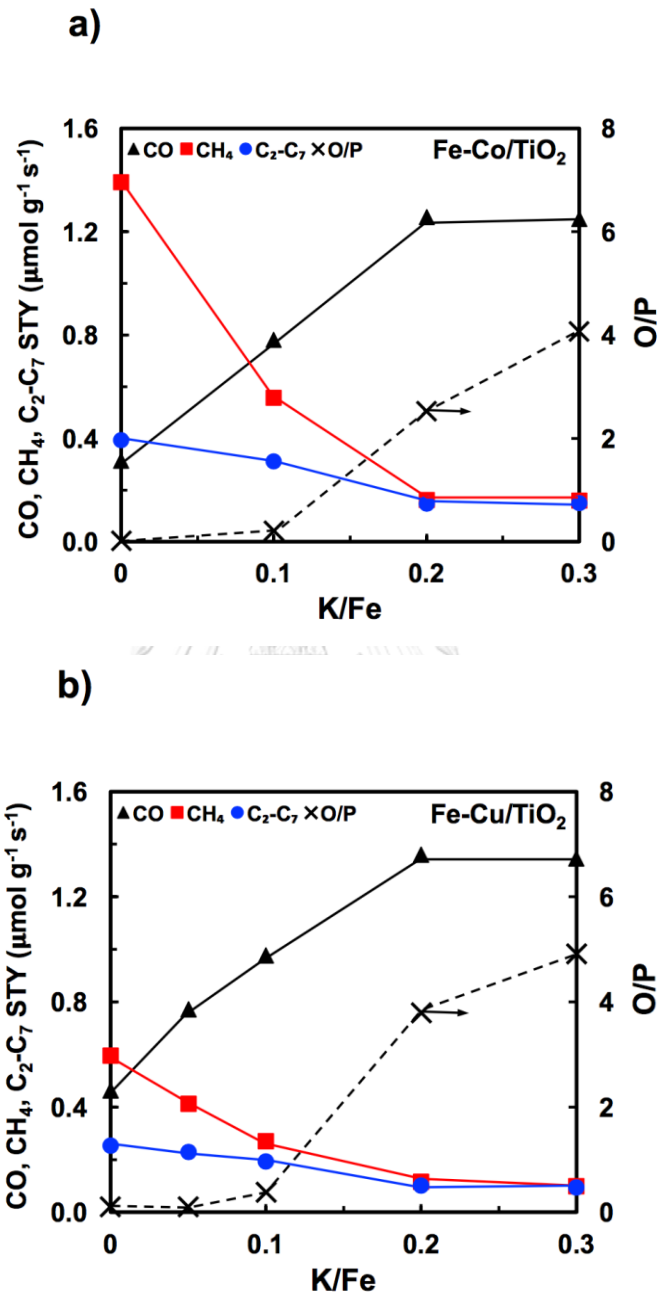

Figure 4.6 STY of CH_4 and C_2-C_7 products, and olefin to paraffin ratio (O/P) of C_2-C_4 products over (a) Fe-Co(0.1)-K(Y)/TiO_2 and (b) Fe-Cu(0.1)-K(Y)/TiO_2 catalysts at various K/Fe atomic ratios. Reaction conditions: 573 K, 1.1 MPa, GHSV = 3600 mL (STP) g^{-1} h^{-1}.

4.6 CO_2 hydrogenation over La promoted Fe-based bimetallic catalyst

The performance of TiO_2-supported Fe bimetallic catalysts with La addition was also investigated. For comparison, the M/(M+Fe) and K/Fe atomic ratio of all bimetallic catalysts were kept constant at 0.1 atom atom^{-1} as well as the La/Fe atomic ratio as presented in Table 4.2. Among the K-promoted bimetallic catalysts, the La-loaded Fe-Cu catalyst showed the maximum values of both C_{5+} selectivity (45%) and C_5-C_7 STY (0.043 μmol g^{-1} s^{-1}). In comparison to both K-promoted and unpromoted Fe-Cu bimetallic catalysts, when La was added, the C_5-C_7 STY was improved to 0.033 and 0.043 μmol $g^{-1}s^{-1}$, respectively, which were almost 2-fold higher than those on corresponding catalysts with no La addition (0.023 and 0.028 μmol $g^{-1}s^{-1}$, respectively). However, this promoting effect of La was not observed on Fe-Co-K-La/TiO_2 catalyst. Due to the positive effect of La on the higher hydrocarbons synthesis, a series of La-loaded Fe-Cu(0.1)-K(0.05) catalysts were tested, and the corresponding activity performance was depicted in Fig. 4.7.

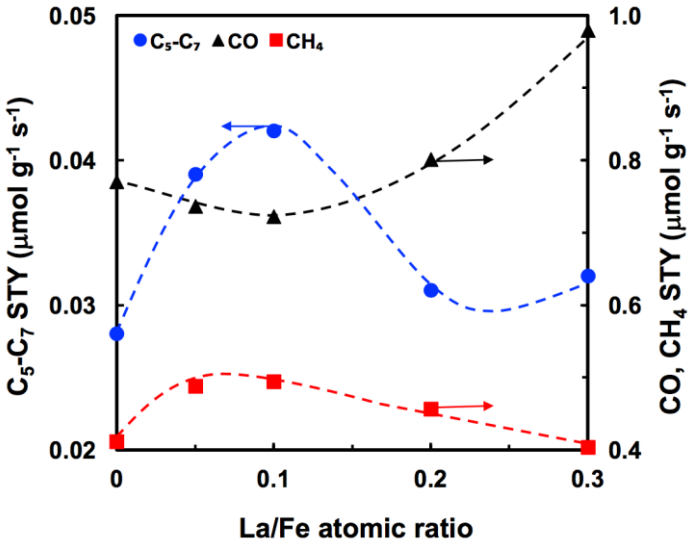

Figure 4.7 STY of C_5-C_7, CH_4 and CO products over Fe-Co(0.1)-K(0.05)-La(Z)/TiO_2 catalysts at various La/Fe atomic ratios. Reaction conditions: 573 K, 1.1 MPa, GHSV=3600 mL (STP) g^{-1} h^{-1}.

The La addition clearly showed a volcano-shape trend on the C_5-C_7 formation along with the varied La/Fe atomic ratio, and the maximum C_5-C_7 STY was achieved at La/Fe of 0.1 atom atom^{-1}. However, the CO formation revealed a reverse trend and reached the minimum CO STY at La/Fe=0.1 atom atom^{-1}. Such opposite behavior suggested that CO was likely to contribute to the synthesis of higher hydrocarbons *via* CO-FTS route and/or the CO_2 was likely to directly convert to C_{5+} higher hydrocarbons at low La/Fe atomic ratio (La/Fe$\leq$0.1 atom atom^{-1}) (see Fig. 4.8), while it hardly showed any influence of La/Fe atomic ratio on the CH_4 synthesis since the La-loaded catalyst exhibited almost identical STY and selectivity of CH_4 as the non-La addition catalyst (see Table 4.2). This similar improvement on C_{5+} yield and selectivity when adding La on Fe-K/La-Al_2O_3 catalyst was also reported by Nam *et al.* [126], suggesting that La could enhance the *in situ* iron-carbide species during the CO_2 hydrogenation reaction. Among the varied composition of La-loaded Fe-Cu-K/TiO_2 catalyst, the Fe-Cu(0.1)-K(0.1)-La(0.1) exhibited the highest STY and C_5-C_7 selectivity with a low amount of CH_4. Thus, such performance makes Fe-Cu(0.1)-K(0.1)-La(0.1)/TiO_2 catalyst a promising catalyst for CO_2 hydrogenation to liquid-fuels.

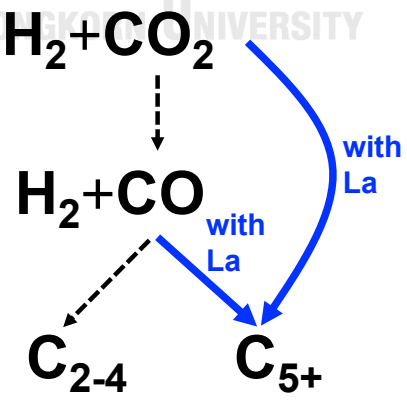

Figure 4.8 Schematic illustration of proposed reaction route of Fe-Cu-K/TiO_2 catalyst with La addition.

4.7 Liquid hydrocarbon products

The obtained liquid products from CO_2 hydrogenation was also analyzed using the Gas Chromatography-Mass Spectrometry (GC/MS). Figures 4.9 illustrates the total ion chromatograms of liquid products from CO_2 hydrogenation over Fe-Cu(0.1)-K(0.1)-La(0.1)/TiO_2 catalyst. The hexadecane ($C_{16}H_{34}$) was used for extracting the hydrocarbon products from the liquid products from CO_2 hydrogenation, therefore the mass spectrometer filament was turned off at retention time of hexadecane in order to protect the instrument.

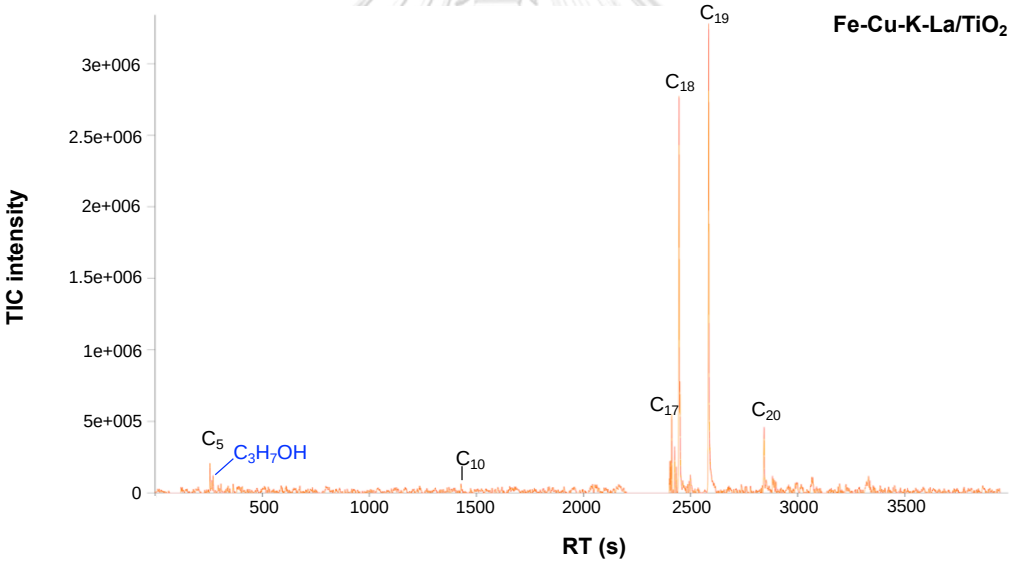

Figure 4.9 GC/MS total ion chromatogram of liquid products from CO_2 hydrogenation over Fe-Cu(0.1)-K(0.1)-La(0.1)/TiO_2 catalyst.

According to the chromatogram (Fig. 4.9), the linear hydrocarbon products mainly from octadecane ($C_{18}H_{38}$) to icosane ($C_{20}H_{42}$) were observed in the liquid product. Moreover, small amount of alcohols (mainly iso-propyl alcohol) was also observed in the liquid products from CO_2 hydrogenation.

CHAPTER V

HIGHER HYDROCARBONS SYNTHESIS FROM CO_2 HYDROGENATION OVER K- AND La-PROMOTED Fe-Cu/TiO_2 CATALYSTS

5.1 Introduction

Developing selective and active catalyst is crucial for CO_2 hydrogenation to higher hydrocarbons especially C_{5+} products. The synergetic effect of the titania-supported Fe-based bimetallic catalysts for the CO_2 hydrogenation is being explored in this ongoing work. To further enhance the selectivity of the desired hydrocarbon products, the promoters can be added to tune the surface property and optimize the product distribution. Potassium as promoter of iron-based catalysts could increase the selectivity to olefin and suppress the methane formation [11, 25, 122, 123]. In addition, the addition of La as promoter could also enhance the selectivity of higher hydrocarbons in FTS [124] and CO_2 hydrogenation [125, 126].

In the present study, the TiO_2-supported Fe-Cu bimetallic catalysts promoted by K and La were prepared and tested for CO_2 hydrogenation to higher hydrocarbon products. These catalysts were characterized by temperature-programmed desorption (TPD) and diffuse reflectance infrared Fourier transform (DRIFTS) to elucidate the influence of K and La promoters on adsorption properties of CO_2 and H_2 on the Fe-Cu/TiO_2 catalyst and their correlation with the product distribution.

The incorporation of K and La promoters could improve both CO_2 hydrogenation activity and selectivity to higher hydrocarbons of Fe-based catalyst. Characterization by TPD and DRIFTS showed that the presence of K promoter significantly decreased the adsorption of H_2, which suppressed the CH_4 formation. On

the other hand, La addition could promote the moderately adsorbed CO_2 species (mainly monodentate carbonate species), resulting the enhanced C_5-C_7 selectivity. The simultaneous addition of La and K promoters would tailor the H and C coverage on the catalyst surface, which plays an important role in altering product distribution in CO_2 hydrogenation.

5.2 CO_2 hydrogenation over Fe-Cu-K-La/TiO_2 catalyst

CO_2 hydrogenation over TiO_2 supported Fe-Cu bimetallic catalysts with and without K-La promoter was performed in a fixed-bed reactor system at 573 K and 1.1 MPa. The steady-state activity and selectivity of catalysts (K/Fe atomic ratio of 0-0.3) were obtained at 15-16 h time on stream as shown in Table 5.1. Time-on-stream (TOS) performance of TiO_2 supported Fe-Cu bimetallic catalyst for CO_2 conversion and product selectivity are shown in Fig. 5.1 as examples. Fe-Cu(0.1)/TiO_2 and Fe-Cu(0.1)-K(0.1)/TiO_2 showed relatively stable CO_2 conversion and selectivities after 6-8 h on stream. CO_2 conversion of the catalysts slightly decreased with TOS, however, the decreasing rates were less than 0.5% per hour at 15-18 h on stream. From the initial relatively stable in CO_2 conversion with time on stream, it appears that the *in situ* activation is not really needed for the TiO_2 supported Fe-Cu bimetallic catalysts. Furthermore, the CH_4 selectivity of K-promoted catalyst kept constant at low level and did not change with time on stream.

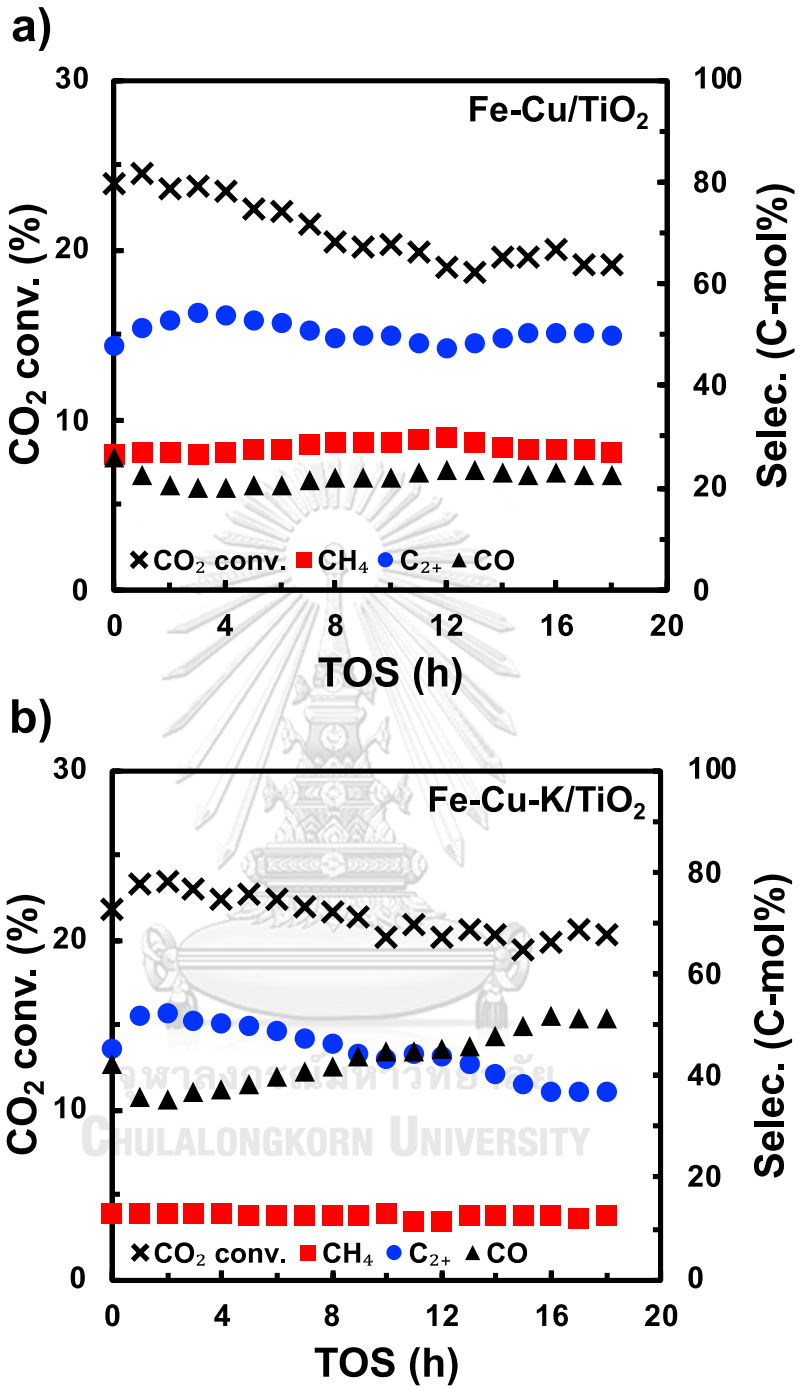

Figure 5.1 Catalytic stability of (a) Fe-Cu(0.1)/TiO_2 and (b) Fe-Cu(0.1)-K(0.1)/TiO_2 at time on stream (TOS). Reaction conditions: 573 K, 1.1 MPa, GHSV = 3600 mL (STP) g^{-1} h^{-1}.

Figure 5.2 illustrates the catalytic performance of K-promoted Fe-Cu bimetallic catalysts in the presence and absence of La promoter. Apparently, the addition of K promoter inhibited the CH_4 formation while promoted the CO STY suggesting that K promoter can suppress the methanation. The K addition showed a volcano-shaped trend on the C_5-C_7 formation with the increasing K/Fe atomic ratio, and the maximum C_5-C_7 STY value was obtained at K/Fe of 0.1 at at^{-1}. The K addition also yielded the increased light olefin content (C_2-C_4) and improved the chain growth probability of hydrocarbons as evidenced from the increased olefin to paraffin ratio (O/P) and **α** value (Table 5.1). However, a further increase in K/Fe up to 0.3 on both catalysts, namely with and without La, reduced the activity towards the hydrocarbon formation, and gave more CO. Such performance suggests that K addition suppressed the hydrogen adsorption and hydrogenation activity of the catalyst; the catalyst has low surface area compared with the bare TiO_2 support (SA = 44 $m^2 g^{-1}$) suggesting that K-oxide could cover the active site of the catalysts. The chemisorption properties of K-promoted Fe catalysts towards CO_2 and H_2 reported in the literatures indicate that the K addition could tune the surface H/C ratio by decreasing H_2 chemisorption capacity of Fe-based catalyst while enhancing CO_2 adsorption [119, 123, 147]. To verify the validity of this interpretation for Fe-Cu-K/TiO_2 catalyst, the CO_2 and H_2 chemisorption analysis was conducted which is discussed in Section 5.5 and 5.6.

Table 5.1 The activity of Fe-Cu(0.1)-K(Y)-La(Z)/TiO_2 catalyst [a]

Catalyst [b]	SA[c] (m^2 g^{-1})	PV[d] (cm^3 g^{-1})	D_p[e] (nm)	CO_2 conv. (%)	Prod. selec. (C-mol%)				STY (μmol g^{-1} s^{-1})				O/P[h]	α[i]
					CH_4	C_2-C_4	C_{5+}[f]	CO	CH_4	C_2-C_4	C_5-C_7[g]	CO		
TiO_2	43.8	0.42	34.9	-	-	-	-	-	-	-	-	-	-	-
Fe-Cu	36.7	0.29	32.2	19.5	27	29	21	23	0.60	0.23	0.023	0.46	0.10	0.41
Fe-Cu-K	41.4	0.29	31.8	19.9	12	21	16	51	0.27	0.17	0.028	0.98	0.38	0.52
Fe-Cu-La	41.3	0.30	27.0	22.5	25	31	19	25	0.61	0.28	0.033	0.61	0.05	0.44
Fe-Cu-K-La	37.6	0.27	31.7	23.2	13	25	29	33	0.31	0.21	0.045	0.76	0.52	0.56
Fe-Cu/K-La[j]	34.7	0.31	29.6	23.4	13	26	26	35	0.34	0.23	0.043	0.80	0.56	0.53
Fe-Cu/La/K[j]	41.3	0.33	34.6	24.2	15	28	25	32	0.40	0.25	0.043	0.75	0.37	0.51
Fe-Cu/K/La[j]	37.6	0.28	29.3	24.4	14	25	26	35	0.36	0.24	0.040	0.86	0.50	0.51

[a] Reaction conditions: 573 K, 1.1 MPa, GHSV=3600 mL (STP) g^{-1} h^{-1}.

[b] Total metal loading (Cu+Fe) = 15 wt% (support weight basis); Cu/(Cu+Fe) = K/Fe = La/Fe = 0.1 at at^{-1}.

[c] BET surface area [d] BJH desorption cumulative pore volume [e] BJH desorption average pore diameter

[f] Including small amounts of alcohols. [g] Only vapor phase. [h] Olefin to paraffin (O/P) ratio of C_2-C_4 hydrocarbons.

[i] Chain growth probability (α) of C_2–C_7 hydrocarbons determined by Anderson-Schulz-Flory (ASF) distribution equation (Appendix E).

[j] Prepared by sequential wet impregnation.

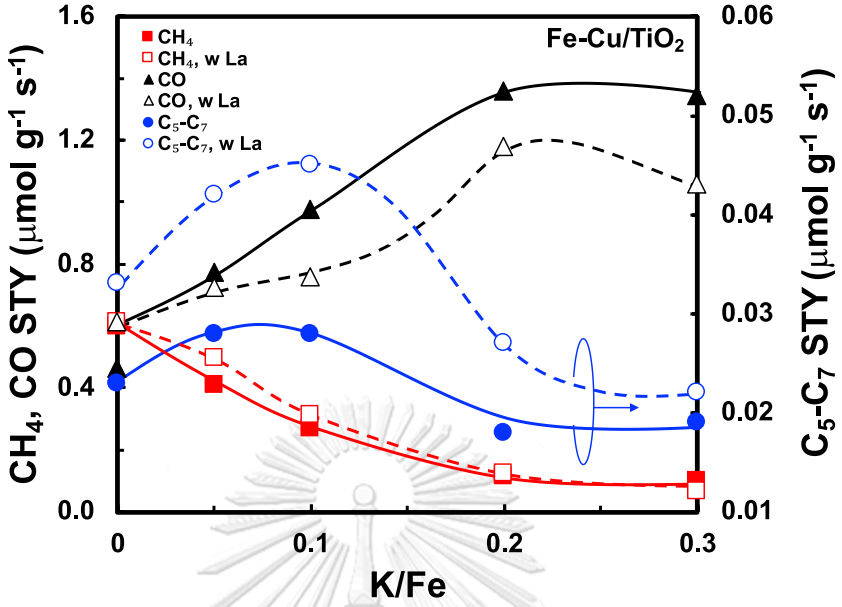

Figure 5.2 Effect of K/Fe atomic ratio on STYs of C_5-C_7, CH_4 and CO product over Fe-Cu(0.1)-K(Y)/TiO_2 and Fe-Cu(0.1)-K(Y)-La(0.1)/TiO_2 catalysts. Reaction conditions: 573 K, 1.1 MPa, GHSV = 3600 mL (STP) g^{-1} h^{-1}.

The effect of La addition on the catalytic performance of TiO_2-supported Fe bimetallic catalysts was also investigated. For comparison, the La/Fe atomic ratio of all Fe-Cu(0.1)-K(0.1)/TiO_2 catalysts was fixed at 0.1 at at^{-1}, as well as the K/Fe atomic ratio. Among the promoted bimetallic catalysts, the La-loaded Fe-Cu-K catalyst showed the maximum values of both C_{5+} selectivity and STY of C_5-C_7 hydrocarbons (Table 5.1). In comparison to both K-promoted and unpromoted Fe-Cu bimetallic catalysts, the La addition increased the C_5-C_7 STY to 0.045 and 0.033 μmol $g^{-1}s^{-1}$, respectively, which were about 1.5-fold of those corresponding catalysts without La addition (e.g., 0.028 and 0.023 μmol $g^{-1}s^{-1}$, respectively). Based on the positive effect of La on the higher hydrocarbon synthesis, a series of La-loaded Fe-Cu-K catalysts were tested, and corresponding activity performance is depicted in Fig. 5.2 (dotted line). The

presence of La clearly led to a shift from CO formation toward higher hydrocarbons (C_5-C_7). Such La loading-dependent behavior suggests that CO is possibly contributed to the synthesis of higher hydrocarbons. La addition showed no influence on the CH_4 synthesis since the La-loaded catalyst yielded almost identical STY and selectivity of CH_4 as the Fe-Cu-K/TiO_2 catalyst. This La-induced catalyst improvement on C_{5+} productivity from CO_2 hydrogenation was also found on Fe-K/La-Al_2O_3 catalyst, wherein La could enhance the *in situ* iron-carbide species during the CO_2 hydrogenation reaction, which is believed as the active sites for the formation of higher hydrocarbons in FTS and CO_2 hydrogenation [126].

From CO_2 hydrogenation using various Fe-Cu-K-La/TiO_2 catalysts (Fig. 5.2), the Fe-Cu(0.1)-K(0.1)-La(0.1) gave the highest STY and selectivity to C_5-C_7 hydrocarbons with the low amount of CH_4, a low value-added product. Thus, such efficient Fe-Cu-K-La/TiO_2 could be a promising catalyst for CO_2 hydrogenation to liquid-fuels. For comparison, a series of catalysts with similar composition was also papered by varied sequential wet impregnation including Fe-Cu/K/La, Fe-Cu/La/K, and Fe-Cu/K-La catalysts, activity performance of which is tabulated in Table 5.1. Apparently, these catalysts did not display any significant change of activity regarding to the different preparation sequence.

5.3 Plausible reaction pathways of CO_2 hydrogenation to hydrocarbons

The plausible reaction pathway of CO_2 hydrogenation over promoted and unpromoted Fe-Cu catalysts was also studied by varying the catalyst amount (0.002-0.600 g) at the same reaction conditions and the total gas flow rate was 12 mL (STP) min^{-1}. The obtained selectivity-conversion data for Fe-Cu(0.1)/TiO_2 and Fe-Cu(0.1)-K(0.1)-La(0.1)/TiO_2 are shown in Fig. 5.3a and 5.3b, respectively. At low CO_2 conversion for both catalysts, CO was more selective than hydrocarbons (CH_4 and C_{2+}) suggesting

that CO_2 was directly converted to CO *via* RWGS reaction. The extrapolated trend of C_{2+} selectivity approached zero at 0 % of CO_2 conversion on unpromoted catalyst, and the C_{2+} selectivity increased with decreasing CO formation. Such trend suggests that C_{2+} products are likely produced from CO through CO-FTS pathway. However, the RWGS reaction is not the only primary reaction of CO_2 conversion. Clearly, the extrapolated trend of CH_4 selectivity of unpromoted Fe-Cu catalyst did not reach zero at low CO_2 conversion (Fig. 5.3a) indicating the existence of the direct CO_2 hydrogenation to methane,

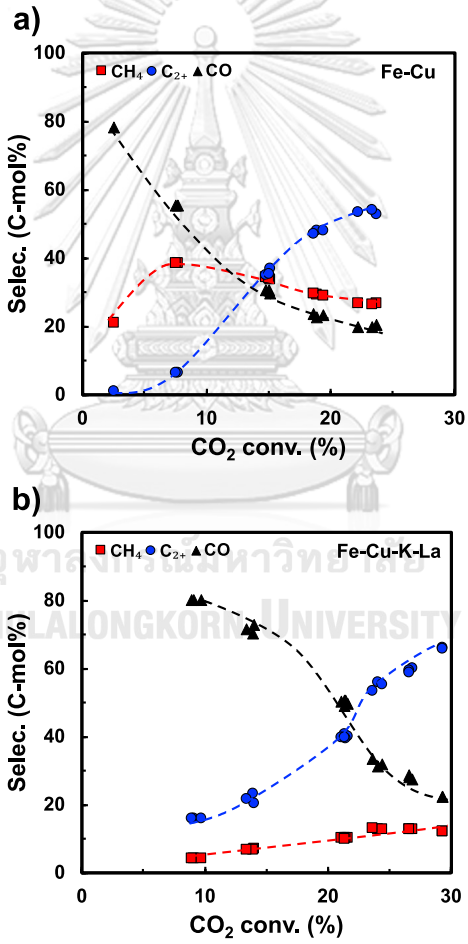

Figure 5.3 Selectivities to CH_4, CO and C_{2+} hydrocarbons versus CO_2 conversion over (a) Fe-Cu(0.1)/TiO_2 and (b) Fe-Cu(0.1)-K(0.1)-La(0.1)/TiO_2 catalysts. Reaction conditions: 573 K, 1.1 MPa, W/F=0.07-6.25 g h mol^{-1}.

namely CO_2 methanation. On the other hand, the CO_2 methanation significantly shifted to CO methanation with the presence of K and La promoters, which was evidenced by the increase in CH_4 selectivity with decreasing CO selectivity in the conversion range examined (Fig. 5.3b). Therefore, the plausible reaction pathways of CO_2 hydrogenation to hydrocarbon products are proposed in Fig. 5.4, wherein we suggest that CO and CH_4 are the primary products from direct CO_2 conversion, while C_{2+} hydrocarbon products are possibly produced through CO-FTS. The presence of K and La promoters on TiO_2 supported Fe-Cu bimetallic catalysts could shift CO_2 methanation toward CO methanation. However, the evidence from our recent DFT study [121] indicates that doping Cu to Fe can alter the kinetically favorable path of CO_2 dissociation to CO* toward CO_2 hydrogenation to HCOO* intermediate. It should be noted that the direct CO_2 hydrogenation to C_{2+} hydrocarbons could not be excluded.

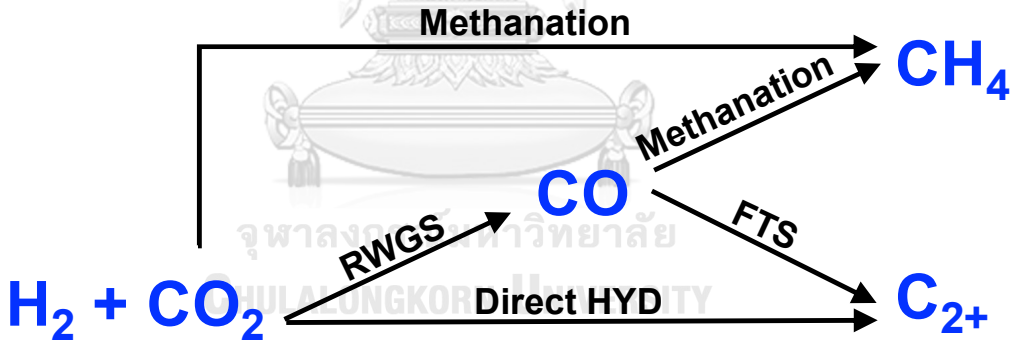

Figure 5.4 Proposed reaction pathways of CO_2 hydrogenation to hydrocarbon products.

5.4 Physical properties of prepared catalysts

The physical properties of calcined Fe-Cu(0.1)-K(*Y*)-La(*Z*)/TiO_2 catalysts are tabulated in Table 1. The BET surface area and pore volume of the calcined catalysts decreased with the loading of K and La promoter, while the average pore diameter was slightly reduced. The reduction in BET surface area and pore volume suggest that the small metal oxide particles are dispersed inside the pores of the TiO_2 support. Although, the K- and La-promoted Fe-Cu catalysts prepared by sequential impregnation method showed the difference in surface area and pore volume (< ±10%), these catalysts did not display any significant change in activity performance. Therefore, considering the relatively low BET surface area of the prepared catalysts (36.7-41.3 m^2 g^{-1}), the catalytic activity is not dependent on these physical properties.

The surface morphology of prepared catalyst was studied by using TEM-EDS and the micrograph showed the metal dispersion of Fe/TiO_2, Fe-Cu/TiO_2 and Fe-Cu-K/TiO_2 catalysts (Fig. 5.5). The agglomeration of Fe cluster on TiO_2 support was obviously found in unpromoted Fe-based catalysts (Fe/TiO_2 and Fe-Cu/TiO_2) (Figs. 5.5d and 5.5e). For Fe-Cu-K/TiO_2 catalyst, the good dispersion Fe cluster was observed (with no agglomeration) (Fig. 5.5f). Therefore, adding K-promoter could enhance the Fe dispersion of the TiO_2 supported Fe-based catalyst.

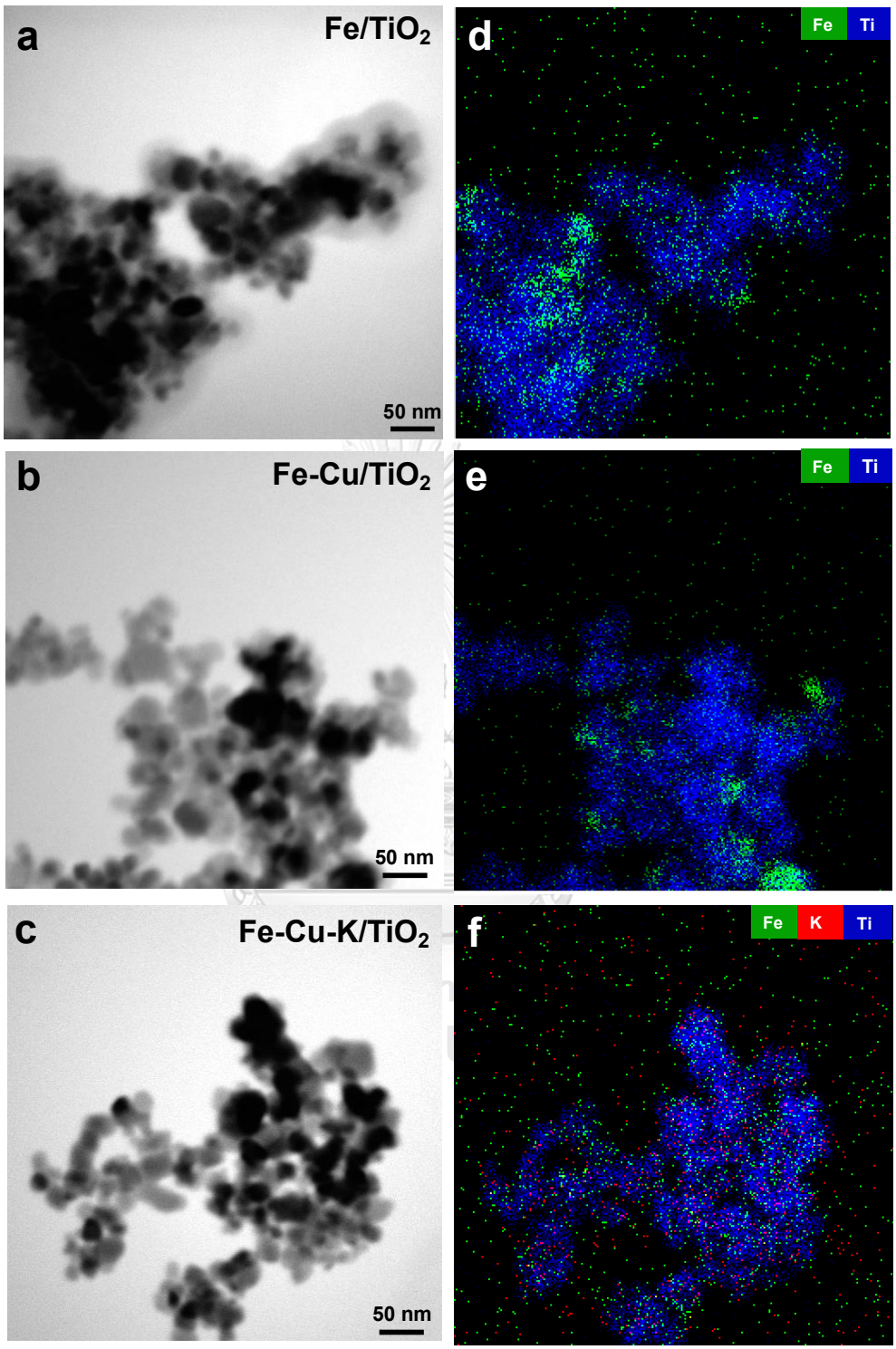

Figure 5.5 TEM images of calcined (a) Fe/TiO_2, (b) $Fe\text{-}Cu(0.1)/TiO_2$ and (c) $Fe\text{-}Cu(0.1)\text{-}K(0.1)/TiO_2$ catalysts and its corresponding TEM-EDS images (d-f), respectively.

5.5 CO_2 adsorption property

5.5.1 CO_2-TPD profiles

The CO_2 adsorption properties of reduced Fe-Cu(0.1)-K(*Y*)-La(*Z*)/TiO_2 catalysts were measured, and the resultant TPD profiles are presented in Fig. 5.6 For the bare TiO_2 support as a reference, only a small amount of CO_2 desorption was observed around 350-450 K, which CO_2 mainly originated from the monodentate carbonate and bicarbonate species formed on the TiO_2 surface observed from DRIFTS result [157, 158]. For reduced Fe-Cu catalyst, CO_2 desorption was clearly observed at 369 and 682 K. The signal of CO_2 desorption at low temperatures (350-450 K) was remarkably enhanced by the presence of a small amount of K (*Y*=0.1), while the desorption signals at higher temperatures (575-800 K) were clearly observed with the presence of La (*Z*=0.1).

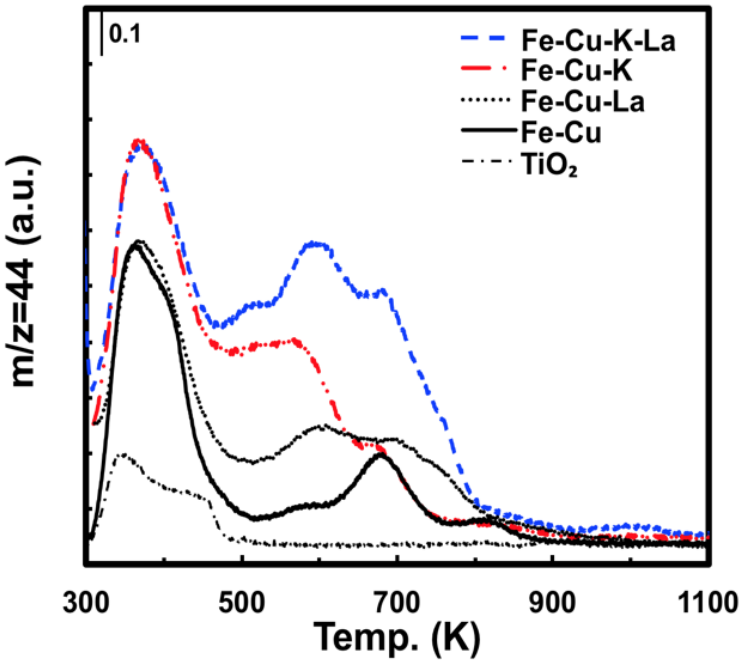

Figure 5.6 Effect of K and La promoters on the CO_2-TPD profiles of reduced Fe-Cu(0.1)-K(Y)-La(Z)/TiO_2 catalysts.

5.5.2 Deconvolution analysis of the CO_2-TPD profiles

To investigate quantitatively the effect of K and La promoter on the CO_2 adsorption properties quantitatively, the superimposed peaks in the CO_2-TPD profiles of Fe-Cu(0.1)-K(*Y*)-La(*Z*)/TiO_2 catalysts were deconvoluted using Gaussian functions, as depicted in Fig. 5.7. The deconvolution analysis exhibited 4 main Gaussian peaks corresponding to 4 types of desorbed CO_2 species on the surface, wherein Type I+II (desorbed below 550 K) and III+IV (desorbed around 550–700 K) were denoted as weakly- and moderately-adsorbed CO_2 species, respectively. The quantities of different types of adsorbed CO_2 estimated by integrating the Gaussian peaks are presented in Table 5.2.

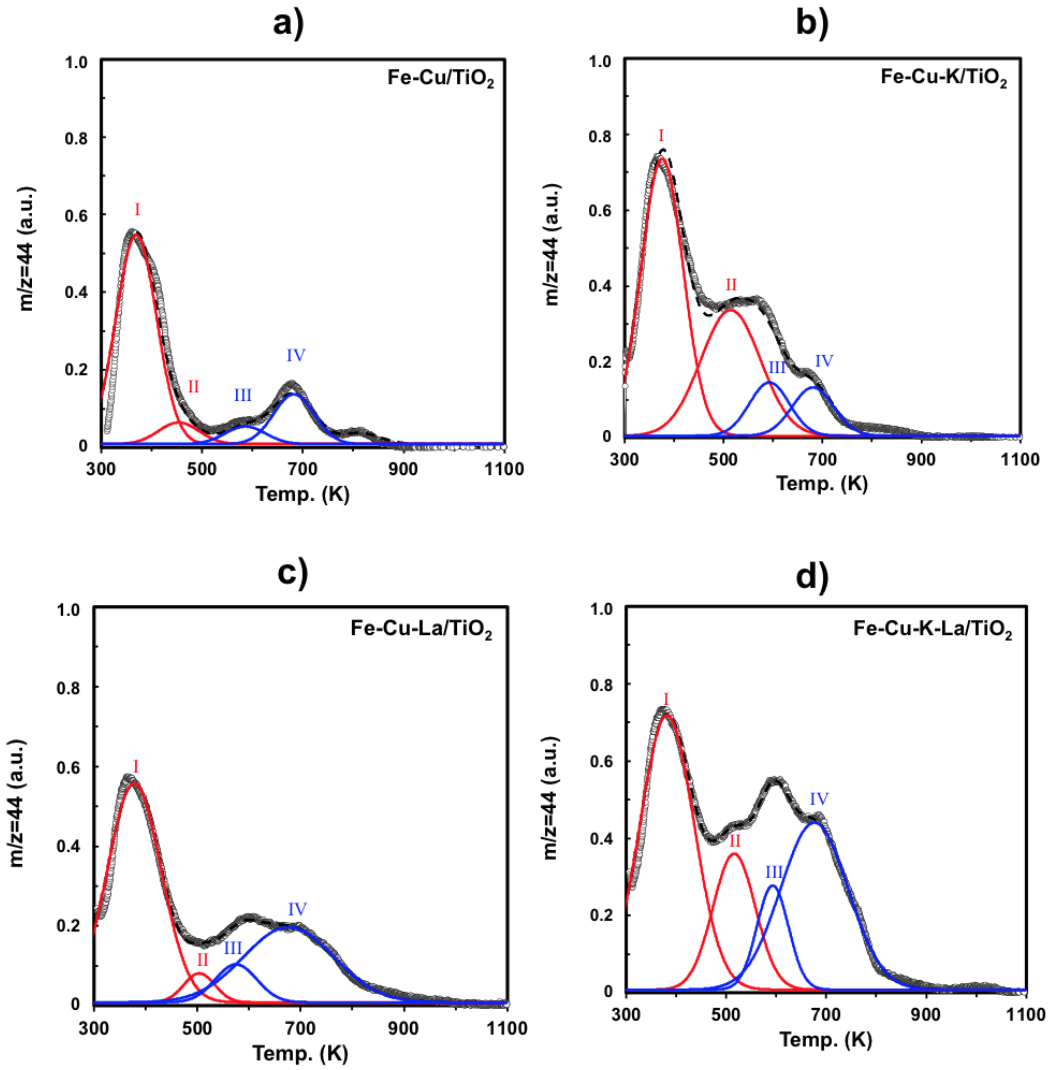

Figure 5.7 Deconvolution of CO_2-TPD profiles of the reduced (a) Fe-Cu(0.1)/TiO_2, (b) Fe-Cu(0.1)-K(0.1)/TiO_2, (c) Fe-Cu(0.1)-La(0.1)/TiO_2 and (d) Fe-Cu(0.1)-K(0.1)-La(0.1)/TiO_2 catalyst, (oooo) measured TPD profile, (——) deconvoluted peaks and (-------) summation of the deconvoluted peaks (I-IV).

Table 5.2 Amount of adsorbed CO_2 species over Fe-Cu(0.1)-K(Y)-La(Z)/TiO_2 catalysts.

Catalyst[a]	CO_2 Adsorption							
	Type I		Type II		Type III		Type IV	
	Temp. (K)	Amount (μmol g^{-1})	Temp. (K)	Amount (μmol g^{-1})	Temp. (K)	Amount (μmol g^{-1})	Temp. (K)	Amount (μmol g^{-1})
Fe-Cu	369	45.9	453	4.8	586	3.9	682	10.9
Fe-Cu-K(0.1)	375	65.8	514	42.3	593	12.0	681	11.2
Fe-Cu-La(0.1)	378	60.6	504	4.6	575	8.1	677	34.7
Fe-Cu-K(0.1)-La(0.1)	381	80.9	516	31.6	593	18.0	676	61.6

[a] Total metal loading (Cu+Fe) = 15 wt% (support weight basis); Cu/(Cu+Fe) = K/Fe = La/Fe = 0.1 at at^{-1}.

The K addition enhanced the amount of the weakly-adsorbed CO_2 species (Type I+II) significantly from 50.7 to 108.1 μmol g^{-1}, which was almost doubled. The K addition also increased the CO_2 adsorption at 593 K (Type III) due to the formation of the bidentate carbonate species on potassium ferrite ($K_2Fe_2O_4$) [159-161]. On the other hand, the presence of La obviously promoted the moderately-adsorbed CO_2 species especially the Type IV (676-682 K). The amount of moderately-adsorbed CO_2 of La-promoted catalyst (Fe-Cu-La = 42.8 and Fe-Cu-K-La = 79.6 μmol g^{-1}) was significantly higher than that of the catalyst without La (Fe-Cu = 14.8 and Fe-Cu-K = 23.2 μmol g^{-1}). Regarding La addition, the amount of weakly-adsorbed CO_2 species of the Fe-Cu-La (65.2 μmol g^{-1}) was slightly higher than that of the Fe-Cu catalyst (50.7 μmol g^{-1}).

5.5.3 *in situ* DRIFTS analysis of reduced catalyst

The adsorption states of CO_2 on the reduced catalyst were also investigated by *in situ* DRIFTS analysis and the interferograms as a function of adsorption time are shown in Fig. 5.8. For the bare TiO_2 support (Fig. 5.8a), four IR bands appeared at 1570, 1430, 1398, and 1345 cm^{-1}, wherein the bands at 1570 and 1345 cm^{-1} corresponded to monodentate carbonate, while the 1430 and 1398 cm^{-1} to bicarbonate species [157, 158]. Similar IR bands of bicarbonate species were also observed in the reduced Fe-Cu catalyst (Fig. 5.8b). Additional IR bands at 1672, 1630, 1243, and 1221 cm^{-1} were only observed in the spectra of K-promoted catalysts such as Fe-Cu-K and Fe-Cu-K-La (Fig. 5.8c and 5.8d, respectively). The bands at 1672 and 1243 cm^{-1} were attributed to bidentate carbonate species which were adsorbed on $K_2Fe_2O_4$ surface, while the bands at 1630 and 1221 cm^{-1} confirmed the presence of additional bicarbonate species [159-161]. In addition, the catalyst with the presence of La showed the additional IR bands at 1500, 1390, and 1362 cm^{-1} indicating the

existence of monodentate carbonate on the La_2O_3 surface would attribute to the formation of the moderately adsorbed CO_2 species since the monodentate carbonate is stable and can be decomposed at high temperature (above 673 K) [158, 162].

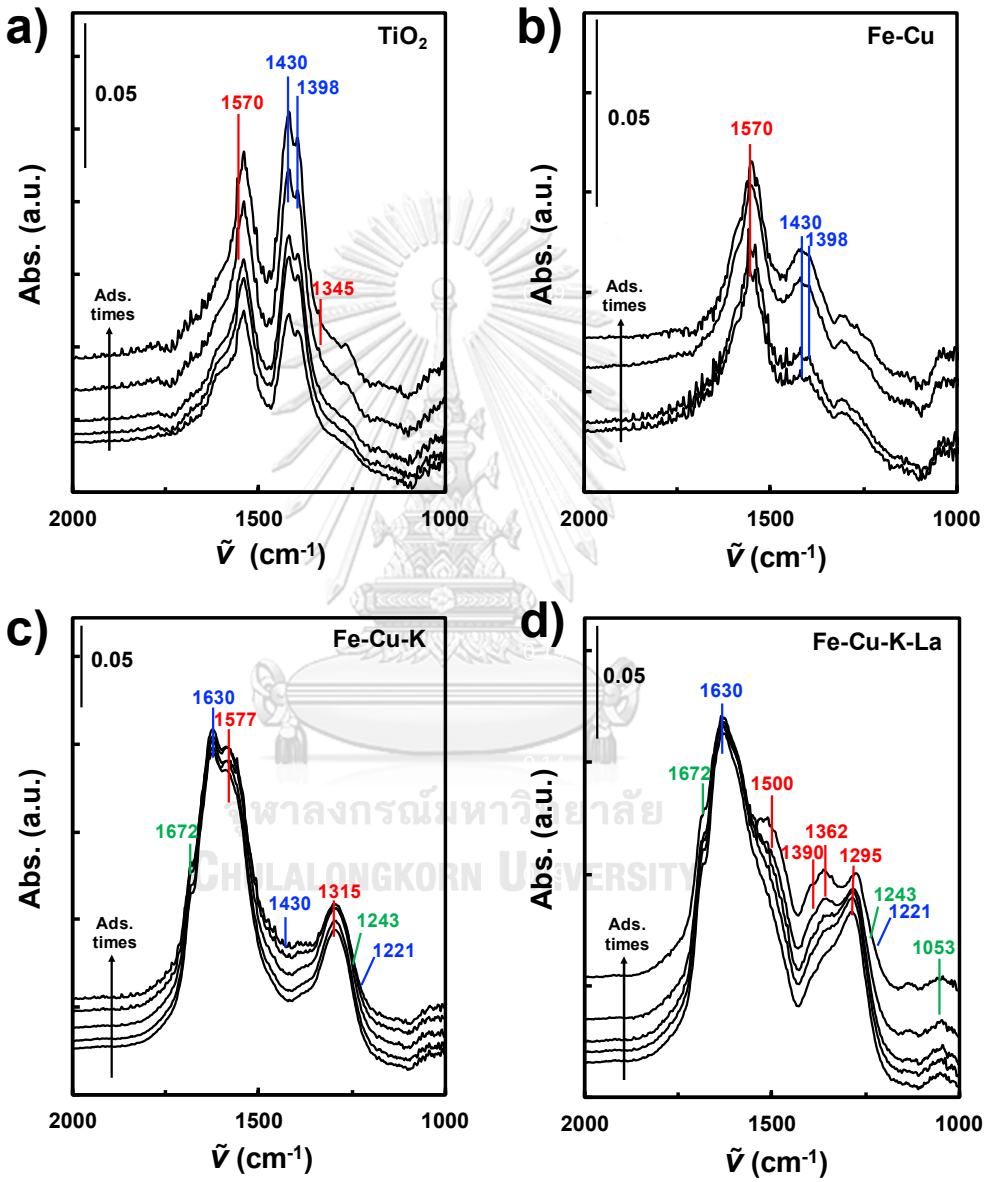

Figure 5.8 Change in the DRIFT spectra of CO_2 adsorbed on the (a) TiO_2 support, (b) reduced Fe-Cu(0.1)/TiO_2, (c) reduced Fe-Cu(0.1)-K(0.1)/TiO_2 and (d) Fe-Cu(0.1)-K(0.1)-La(0.1)/TiO_2 catalysts in the course of an adsorption time of (bottom to top) 3, 10, 20, 60 and 120 min.

5.6 H_2 adsorption property

The H_2 adsorption properties of reduced Fe-Cu(0.1)-K(*Y*)-La(*Z*)/TiO_2 catalysts were also studied by H_2-TPD, and the resultant profiles are depicted in Fig. 5.9. The bare TiO_2 support as reference did not show any adsorption towards H_2. The H_2-TPD profiles of unpromoted and promoted Fe-Cu catalysts mainly exhibited one peak around 400-500 K, which indicated that the existence of atomic adsorbed hydrogen species on the metal surface [163, 164] and quantities of adsorbed H_2 are presented in Table 5.3.

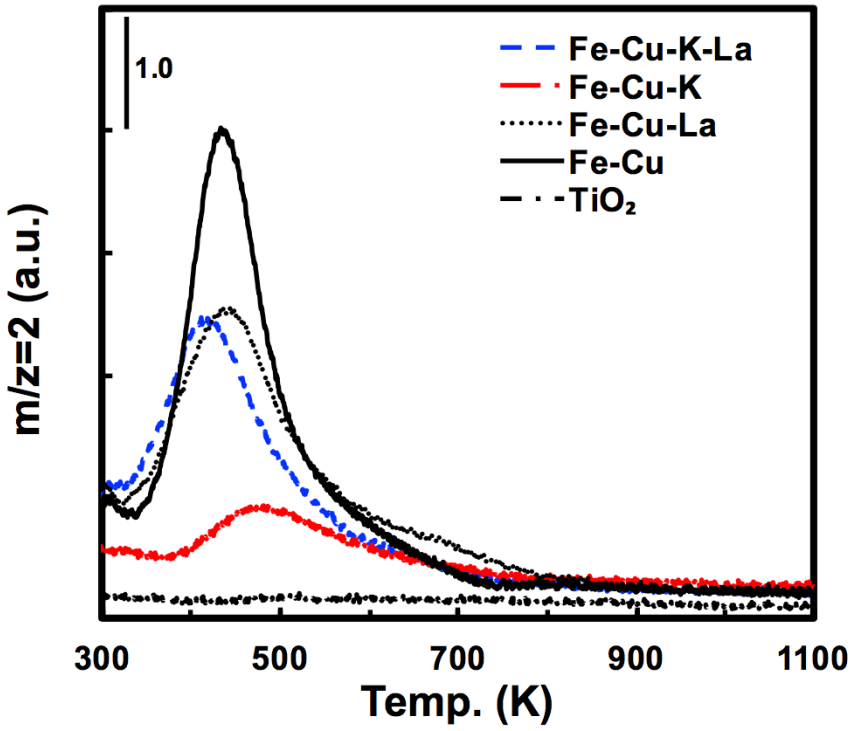

Figure 5.9 Effect of K and La promoters on the H_2-TPD profiles of reduced Fe-Cu(0.1)-K(Y)-La(Z)/TiO_2 catalysts.

Table 5.3 Amount of adsorbed H_2 species over Fe-Cu(0.1)-K(Y)-La(Z)/TiO_2 catalysts.

Catalyst[a]	**H_2 Adsorption**	
	Temp. (K)	Amount (μmol g^{-1})
Fe-Cu	432	559.4
Fe-Cu-K(0.1)	474	80.7
Fe-Cu-La(0.1)	436	525.2
Fe-Cu-K(0.1)-La(0.1)	415	438.9

[a] Total metal loading (Cu+Fe) = 15 wt% (support weight basis); Cu/(Cu+Fe) = K/Fe = La/Fe = 0.1 at at^{-1}.

For the presence of K promoter, the amount of weakly-adsorbed H_2 species was dramatically decreased from 559 μmol g^{-1} for Fe-Cu catalyst to only 81 μmol g^{-1} for Fe-Cu-K catalyst with 86% reduction. The Fe-Cu-K-La catalyst (439 μmol g^{-1}) showed a similar reduction in the amount of weakly-adsorbed H_2 compared with the unpromoted catalyst with only 21% reduction. Such negative impact suggests that the presence of K promoter can reduce the weak H_2 adsorption on the catalyst surface, and this similar behavior was also reported for the K/Fe/Al_2O_3 and Fe-Co/K/Al_2O_3 catalysts [123, 147]. On the other hand, the addition of La showed only a slight suppression effect on the amount of H_2 adsorption. The K addition has a higher impact on the H_2 adsorption property than the La addition, which might further influence the methanation and hydrogenation reaction. The total amount of adsorbed CO_2 and adsorbed H_2 species on Fe-Cu(0.1)-K(*Y*)-La(Z)/TiO_2 catalysts are shown in Fig. 5.10. It is worth noting that the correlation of adsorption properties with the catalyst activity remains to be discussed.

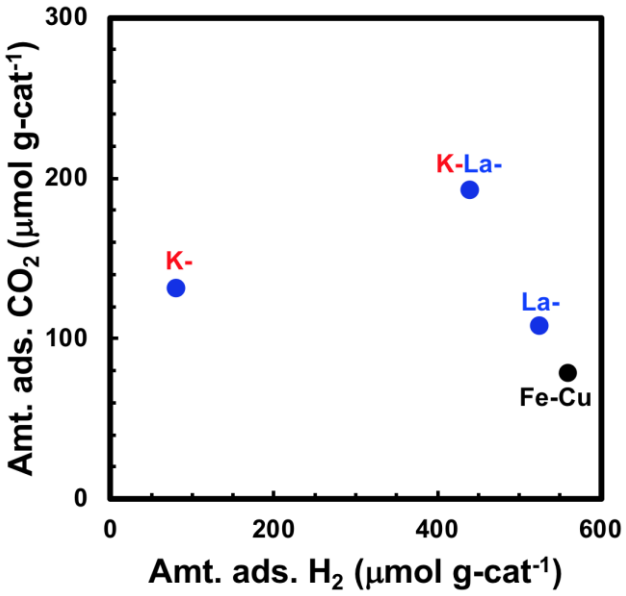

Figure 5.10 Effect of K and La promoters on the total amount of adsorbed CO_2 and adsorbed H_2 species of reduced Fe-Cu(0.1)-K(Y)-La(Z)/TiO_2 catalysts.

5.7 Surface adsorbed species on the spent catalyst

The DRIFTS and TPD analysis of the spent catalyst was used to investigate the surface adsorbed species formed during CO_2 hydrogenation to hydrocarbons. The DRIFTS spectra of the spent Fe-Cu/TiO_2, Fe-Cu-K/TiO_2 and Fe-Cu-K-La/TiO_2 catalysts after flushing the sample cell with N_2 at ambient temperature and pressure for 1 h are shown in Fig. 5.11a. Four major IR bands were observed at 1580, 1443, 1410 and 1367 cm^{-1}, wherein the bands at 1580 and 1367 cm^{-1} corresponded to the $\nu(CO)_{as}$ and $\nu(CO)_s$ of adsorbed formate species [158, 165]. The IR bands at 1443 and 1410 cm^{-1} were ascribed to the adsorbed carbonate species [157, 158, 166]. The spent catalysts were then reduced *in situ* in a H_2 flow at 523 K for 2 h followed by flushing with N_2. According to DRIFT spectra after H_2 reduction (Fig. 5.11b), it found to be that the intensities of the IR bands of adsorbed carbonate species on all spent catalysts were almost disappeared. However, in the case of promoted catalysts, namely Fe-Cu-K/TiO_2 and

Fe-Cu-K-La/TiO_2 catalysts, the IR bands of adsorbed formate species still being observed. DRIDTS analysis of the spent catalysts suggested that the adsorbed formate and carbonate species were formed on the Fe-Cu/TiO_2 catalyst during CO_2 hydrogenation to hydrocarbons and the formatted species had a higher stability on the K and La-promoted Fe-Cu bimetallic catalyst than unpromoted catalyst.

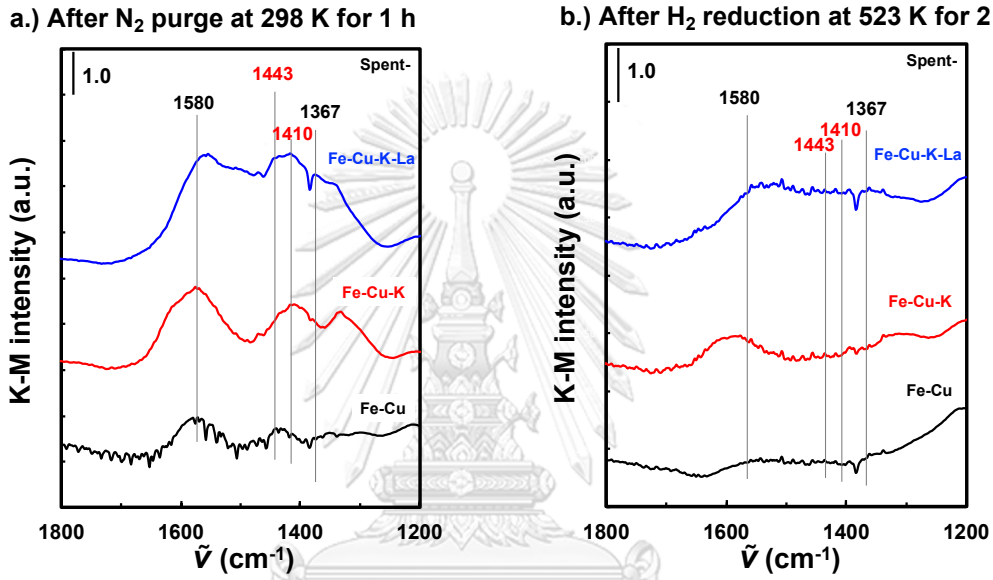

Figure 5.11 DRIFT spectra of the surface adsorbed species on spent Fe-Cu(0.1)-K(Y)-La(Z)/TiO_2 catalysts after (a) N_2 purge at 298 K for 1 h and then (b) followed by H_2 reduction at 523 K for 2 h.

The TPD analysis of spent catalyst was also carried out to investigate the presence of adsorbed surface species after CO_2 hydrogenation of Fe-Cu/TiO_2, Fe-Cu-K/TiO_2 and Fe-Cu-K-La/TiO_2 catalyst. The desorbed H_2, H_2O, CO and CO_2 were detected by the mass spectrometer during the TPD analysis as shown in Figure. 5.12. The H_2O signal was observed at low temperature (384 K) for all spent-catalysts due to the originated moisture. For all catalysts, the signals of CO_2 and H_2O appeared at the same temperature (640 K), corresponding to the decomposition of carbonate species.

Surprisingly, for spent-promoted catalysts (Fe-Cu-K/TiO_2 and Fe-Cu-K-La/TiO_2), the signal of H_2, CO, CO_2 and H_2O were only observed at the relative higher temperature (680 K) (see Fig. 5.12b and c), which is also the same temperature of decomposition of formate species and the adsorbed CO_2 species (Type IV) reported earlier [32, 33, 167]. It suggested that K and La promoter that enhance the adsorbed formate species on the catalyst's surface was found to be one of the moderately-adsorbed CO_2 species. The peaks observed at higher temperature than 900 K could be attributed to the decomposition of hydrocarbons species.

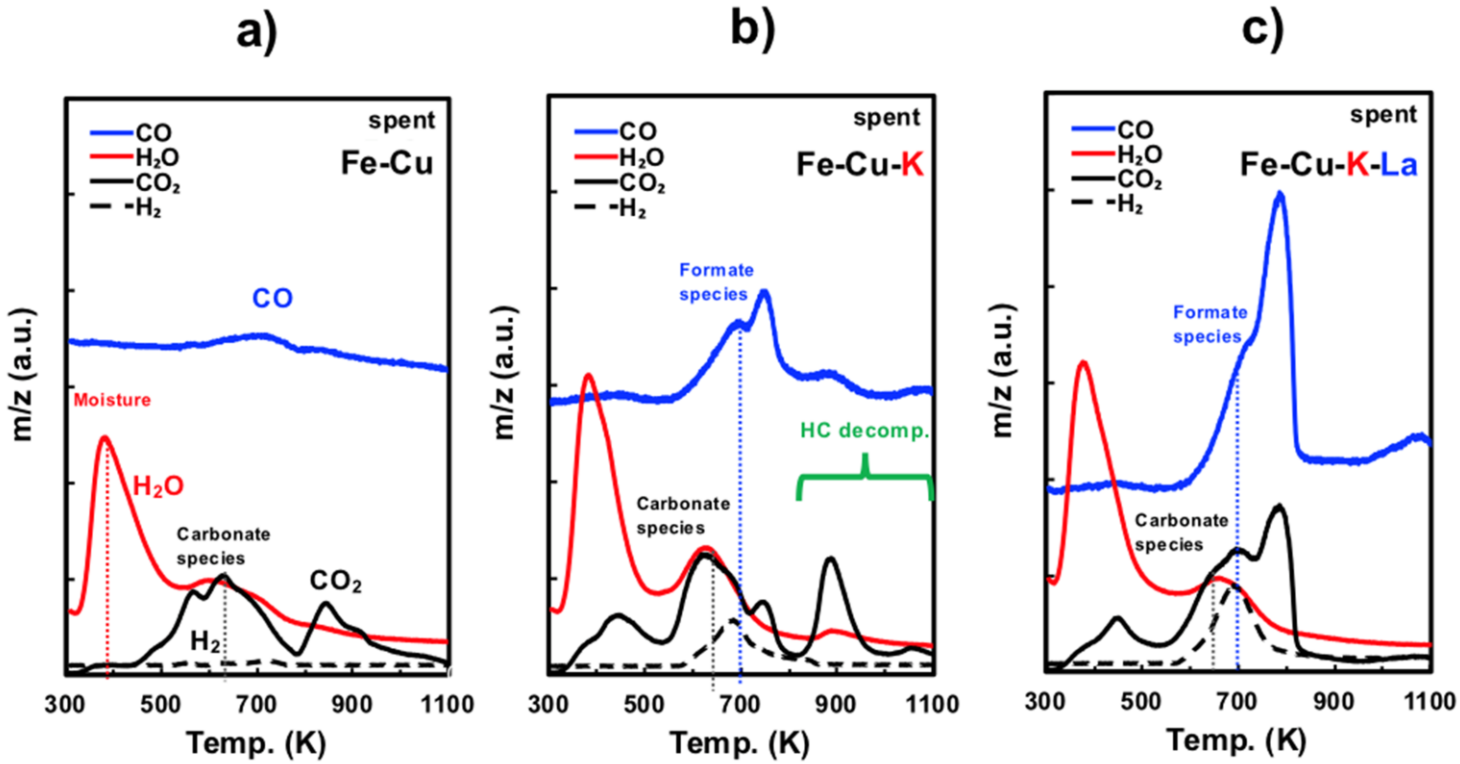

Figure 5.12 TPD signal of des. species over spent Fe-Cu(0.1)-K(Y)-La(Z)/TiO_2 catalyst surfaces.

5.8 Correlation of adsorption properties with the catalytic property

As discussed in Section 5.2, the Fe-Cu catalysts with K and La addition yielded a significant increase in the selectivity of higher hydrocarbons (C_{5+}). Furthermore, the Fe-Cu catalyst with K addition exhibited a dramatically decrease of CH_4 selectivity, while La addition enabled a notable enhancement of C_{5+} hydrocarbons selectivity. These results could be explained by the change of CO_2 and H_2 adsorption properties as discussed in Section 3.5 and 3.6, respectively.

Figure 5.13 illustrates the relation between the C_5-C_7 and CO STYs and the amount of various adsorbed CO_2 species identified by the CO_2-TPD analysis, along with the adsorption results on promoted and unpromoted catalysts. Evidently, for the catalyst with K promoter, the amount of weakly-adsorbed CO_2 (Type I+II) was apparently related to the CO formation rate. As reported, the existence of K could enhance the RWGS reaction by providing additional active sites for the formation of formate species on the catalyst surface, which was proposed as an important intermediate for RWGS reaction [33, 123]. On the other hand, the moderately-adsorbed CO_2 (Type III+IV), closely correlated to the La incorporation, played a crucial role on the C_5-C_7 STY. Thus, the single La-promoted and K-La promoted catalysts resulted the increase in the amount of moderately-adsorbed CO_2 species (Type III+IV), which could be a key intermediate for further hydrogenation to higher hydrocarbons (C_{5+}). From H_2-TPD results, the weakly-bonded H_2 species was dramatically decreased by the presence of K, and resulted in the suppression of CH_4 STY as shown in Fig. 5.14. This dependent behavior suggests that the amount of weakly-adsorbed H_2 plays an important role in the CH_4 formation.

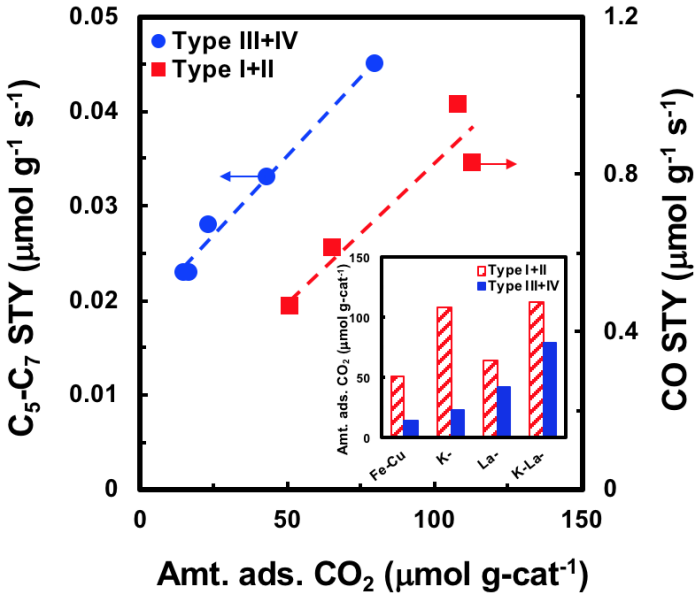

Figure 5.13 Effect of amount of desorbed CO_2 species on STY of C_5-C_7, CH_4 and CO products over Fe-Cu(0.1)-K(Y)-La(Z)/TiO_2 catalysts. Reaction conditions: 573 K, 1.1 MPa, GHSV = 3600 mL (STP) g^{-1} h^{-1}.

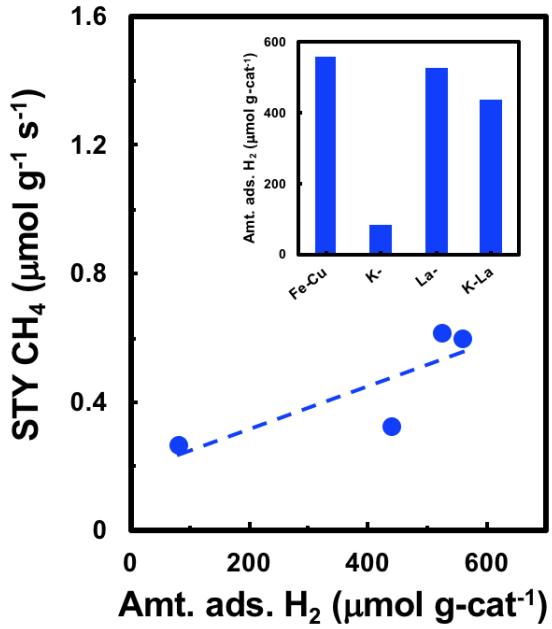

Figure 5.14 Effect of amount of weakly desorbed H_2 species on STY of C_5-C_7, CH_4 and CO products over Fe-Cu(0.1)-K(Y)-La(Z)/TiO_2 catalysts. Reaction conditions: 573 K, 1.1 MPa, GHSV = 3600 mL (STP) g^{-1} h^{-1}.

The changes of CO_2 and H_2 adsorbed properties on the catalyst surface were further analyzed in the form of surface H/C atomic ratios, the relation of which with the product selectivity is shown in Fig. 5.15.

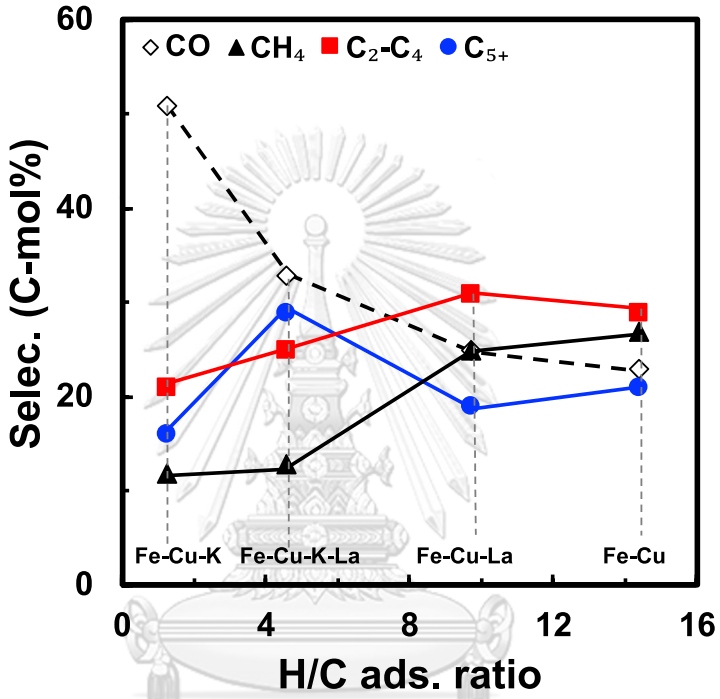

Figure 5.15 Effect of H/C adsorbed species (atomic ratio) on selectivity of CH_4, C_2-C_4, C_{5+} and CO products over Fe-Cu(0.1)-K(Y)-La(Z)/TiO_2 catalysts. Reaction conditions: 573 K, 1.1 MPa, GHSV = 3600 mL (STP) g^{-1} h^{-1}.

The CH_4 selectivity increased with the increasing H/C ratio, wherein a high relative H coverage on the surface could provide more chances of methanation reaction than C-C bond formation. Volcano-like trends of the selectivity of light hydrocarbons (C_2-C_4) and higher hydrocarbons (C_{5+}) with the surface H/C ratio were evidenced. However, their maximum selectivities appeared at different ranges of H/C ratio, the C_{5+} selectivity was at relatively lower region and the C_2-C_4 selectivity was at

higher. Possibly, the C-C bond formation would be favorable at a lower range of the H/C ratio (high C coverage), while a higher H coverage on the surface resulted in the direct hydrogenation reaction. However, a much higher CO selectivity than other hydrocarbon products was obtained at the lowest H/C ratio. This observation suggests that more unconverted CO was released probably due to the higher energy barrier for the subsequent hydrogenation [156, 168]. The addition of K and La promoter had a significant impact on the H/C atomic ratio of adsorbed H_2 and CO_2 species on the catalyst surface during CO_2 hydrogenation. As a result, the tailored H/C atomic ratio of adsorbed species on the catalyst surface influenced the catalyst performance and the product selectivity of CO_2 hydrogenation.

5.9 Influence of temperature on the CO_2 hydrogenation

The Fe-Cu-K-La/TiO_2 catalyst were also tested at various reaction temperatures (range of 523-623 K) as shown in Fig. 5.16 and Table 5.4. The CO_2 conversion and CO selectivity increased with increasing reaction temperature, while the opposite trend was observed for C_{2+} selectivity. These results are consistent with the thermodynamic equilibrium reported earlier in section 3.2. This is due to the fact that the RWGS is more favorable at high temperature than CO_2 hydrogenation to hydrocarbons. From thermodynamic point of view, the CO_2 conversion by RWGS reaction is limited at low temperature due to its endothermic reaction. However, the exothermic FTS reaction is also thermodynamically limited in this temperature range examined.

Table 5.4 Effect of temperature on CO_2 hydrogenation over Fe-Cu(0.1)-K(0.1)-La(0.1)/TiO_2 catalyst.

Temp.	CO_2 conv.	Selectivity (C-mol %)		
(K)	(%)	CH_4	CO	C_{2+}
523	17.0	12	28	60
548	21.4	14	31	55
573	22.8	13	33	54
598	25.3	13	49	38
623	26.3	14	69	17

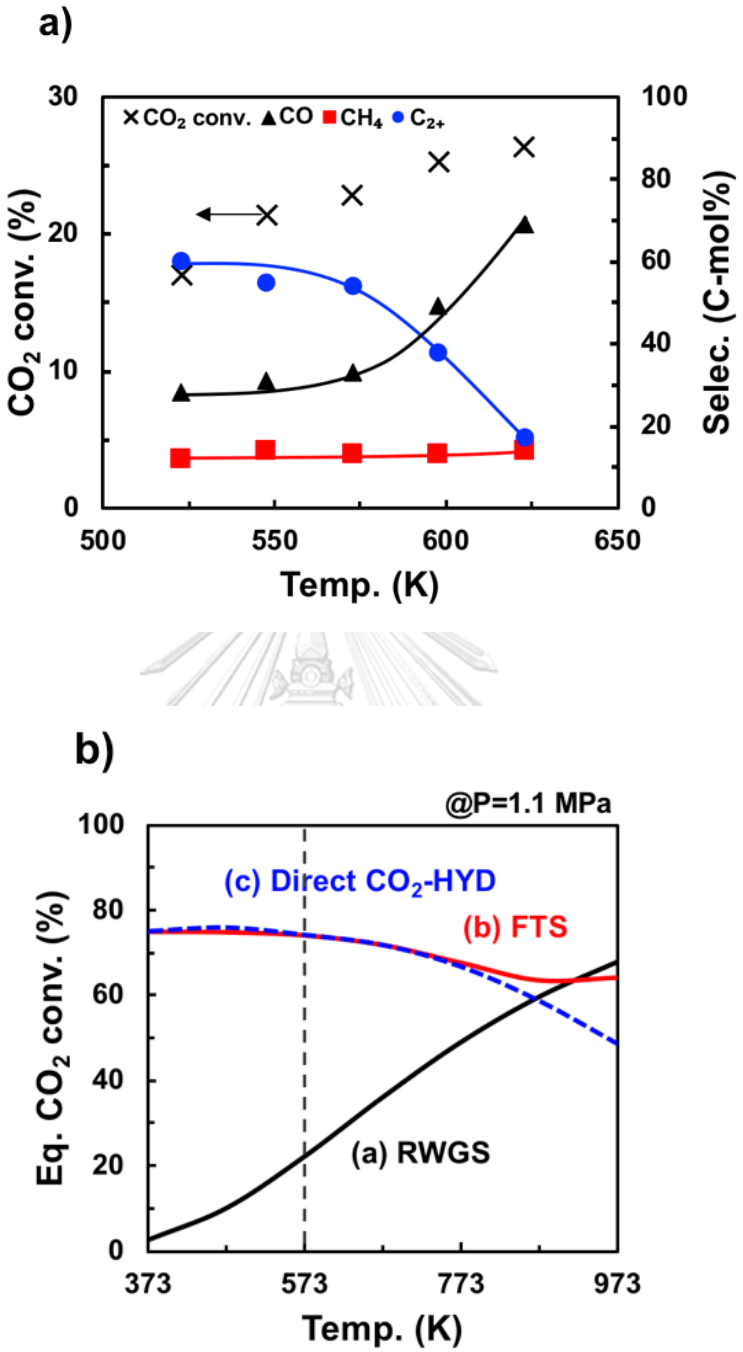

Figure 5.16 Influence of temperature on (a) CO_2 conv. and product selectivity for CO_2 hydrogenation over Fe-Cu(0.1)-K(0.1)-La(0.1)/TiO_2 (experimental) and (b) equilibrium CO_2 conversion (calculation).

CHAPTER VI

CONCLUSIONS AND RECOMMENDATIONS

6.1 Conclusions

(i) Comparative study of Fe-based catalysts for CO_2 hydrogenation to hydrocarbons

The CO_2 hydrogenation over TiO_2-supported monometallic (Fe, Co and Cu) catalysts was performed in a fixed-bed flow reactor. Among the monometallic supported on TiO_2 catalysts prepared, only Fe/TiO_2 catalyst exhibited the selectivity to higher hydrocarbons (C_{2+}). Although Co/TiO_2 catalyst gave much higher CO_2 conversion (55%) than Fe catalyst (16%), CH_4 was the dominant product. In contrast, Cu/TiO_2 catalyst produced CO as a main product, indicating its superior activity for the RWGS. The supported Fe monometallic catalyst were also prepared with different support material (e.g. γ-Al_2O_3) and the results suggested that the activity of Fe monometallic catalysts depended on the metal-support interaction and surface chemical properties, rather than the textural properties of support materials. Moreover, K as an effective promoter was added on Fe monometallic catalyst, that could suppress the CH_4 formation and improve selectivity to higher hydrocarbons as well as the olefins to paraffin ratio.

(ii) Fe-based bimetallic catalysts supported on TiO_2 for selective CO_2 hydrogenation to hydrocarbons

The titania-supported Fe-based bimetallic catalysts were examined for CO_2 hydrogenation in a fixed-bed flow reactor. The combination of Fe and a small amount

of second metal (Co and Cu) in TiO_2 supported catalysts can enhance the CO_2 conversion and the formation of hydrocarbons. The results show that the space-time yield (STY) of C_2-C_7 hydrocarbons approached the maximum at the M/(M+Fe) = 0.1 atom atom^{-1} for both M = Co and Cu. It is worth noting that the maximum C_2-C_7 STY hydrocarbons is significantly higher than those monometallic Fe/TiO_2, Co/TiO_2 and Cu/TiO_2 catalysts. A further Co addition promoted CH_4 formation to a dominant product due to the stronger hydrogenation ability of Co. On the other hand, adding more Cu into Fe evidently enhanced the RWGS reaction which exhibited a favorable production towards CO. However, these bimetallic Fe-Co/TiO_2 and Fe-Cu/TiO_2 still favored the CH_4 formation.

The incorporation of K and La as promoters could evidently improve the yield and selectivity to higher hydrocarbons. Adding K could suppress the CH_4 formation and also give high olefin content (C_2-C_4). However, an excessive K addition led to more CO STY. On the other hand, La could significantly shift CO toward the production of C_{5+} hydrocarbons, likely through CO-FTS reaction pathway, while it hardly showed any influence of La addition on the CH_4 synthesis since the La-loaded catalyst exhibited almost identical STY and selectivity of CH_4 as the non-La addition catalyst. Among all catalyst combinations, Fe-Cu(0.1)-K(0.1)-La(0.1)/TiO_2 catalyst gave the highest STY of C_{5-7} hydrocarbons, which is promising for the liquid-fuel production from CO_2 hydrogenation.

(iii) Higher hydrocarbons synthesis from CO_2 hydrogenation over K- and La- promoted Fe-Cu/TiO_2 catalysts

In the present work, the K- and La-promoted Fe-Cu/TiO_2 catalysts were found to be promising for CO_2 hydrogenation to C_{5+} higher hydrocarbons. The incorporation of K and La as promoters can improve both catalyst activity for CO_2 hydrogenation and

selectivity to higher hydrocarbons. The promoted catalyst (Fe-Cu-K-La/TiO_2) gave higher C_{5+} hydrocarbons selectivity (29 C-mol%) than the unpromoted catalyst (21 C-mol%). Through characterization of both promoted and unpromoted catalysts by CO_2-TPD, H_2-TPD and DRIFTS, the K addition can significantly reduce the amount of chemisorbed H_2 species and increase chemisorbed CO_2 species on catalyst surface, while La addition showed very limited influence on the amount of H_2 adsorption but increased in the amount of moderately-adsorbed CO_2 species (Type III+IV). Adding K appears to correlate to the suppression of CH_4 formation. The presence of La in Fe-Cu-K/TiO_2 catalyst enhanced the production of C_5-C_7 hydrocarbons, which may be in part due to the CO hydrogenation pathway relating to the increase of the moderately adsorbed CO_2 species (mainly monodentate carbonate species). Generally, the introduction of La and K promoters is capable of turning the surface chemisorbed H/C ratios, the variation of which appears to correlate to the product distribution evidently.

6.2 Recommendations

In this work, the Fe-Cu-K-La/TiO_2 exhibited the promising CO_2 hydrogenation activity and product selectivity to higher hydrocarbons. A further study of catalytic CO_2 hydrogenation to higher hydrocarbons, especially C_{5+} over heterogeneous catalysts should be concerned with following aspects:

1. This work revealed that Fe-based bimetallic promotion effect was related to the adsorption sites of H_2 and CO_2 species since the dispersion of active metal particle could play a crucial role on adsorption sites. Many literatures reported that the novel catalyst preparation including solution plasma and laser ablation technique could control the metal particle size, the metal dispersion, the deflect and the structure of the catalyst material. Therefore, the novel catalyst

preparation would be of interest in developing the Fe-based catalyst for CO_2 hydrogenation.

2. The catalytic CO_2 hydrogenation to higher hydrocarbons could occurred through RWGS and FTS reaction since water was formed from both reactions. Therefore, removing the produced water during the process could enhance the equilibrium conversion of CO_2 hydrogenation. The modification of catalyst hydrophobicity and water removing process (e.g. membrane separation) should be further studied.
3. In this work has been investigated the catalytic CO_2 hydrogenation using thermal process was investigated. It is worth noting that the electrochemical and photochemical catalytic process of CO_2 hydrogenation has been applied to improve in efficiency and become a more friendly environmental issue. Thus, the use of electrochemical and photochemical catalytic process in CO_2 hydrogenation should be carried out.

REFERENCES

REFERENCES

[1] S.C. Program, Carbon Dioxide Measurements, in, 2017, pp. Measurements by the Scripps CO_2 program are supported by the U.S. Department of Energy (DOE) and by Earth Networks, a technology company that is collaborating with Scripps to expand the global GHG monitoring network.

[2] U.S.E.I. Administration, Primary energy overview, in, U.S. Energy Information Administration, 2018.

[3] C. Federsel, R. Jackstell, M. Beller, State-of-the-Art Catalysts for Hydrogenation of Carbon Dioxide, Angewandte Chemie International Edition, 49 (2010) 6254-6257.

[4] M. Aresta, A. Dibenedetto, Utilisation of CO_2 as a chemical feedstock: opportunities and challenges, Dalton Transactions, (2007) 2975-2992.

[5] S.E. Schwartz, Uncertainty in climate sensitivity: Causes, consequences, challenges, Energy & Environmental Science, 1 (2008) 430.

[6] X.-l. Liu, China CO_2 Control Strategy under the Low-carbon Economy, Procedia Engineering, 37 (2012) 281-286.

[7] B. Hu, C. Guild, S.L. Suib, Thermal, electrochemical, and photochemical conversion of CO_2 to fuels and value-added products, Journal of CO_2 Utilization, 1 (2013) 18-27.

[8] U. Burghaus, Surface science perspective of carbon dioxide chemistry—Adsorption kinetics and dynamics of CO_2 on selected model surfaces, Catalysis Today, 148 (2009) 212-220.

[9] J. Ma, N. Sun, X. Zhang, N. Zhao, F. Xiao, W. Wei, Y. Sun, A short review of catalysis for CO_2 conversion, Catalysis Today, 148 (2009) 221-231.

[10] C. Song, Global challenges and strategies for control, conversion and utilization of CO_2 for sustainable development involving energy, catalysis, adsorption and chemical processing, Catalysis Today, 115 (2006) 2-32.

[11] S. Saeidi, N.A.S. Amin, M.R. Rahimpour, Hydrogenation of CO_2 to value-added products—A review and potential future developments, Journal of CO_2 Utilization, 5 (2014) 66-81.

[12] DOE/EPA, Fuel Economy. Internet Resource Developed by U.S. Department of Energy and U.S. Environmental Protection Agency, in, 2018.

[13] W. Wang, S. Wang, X. Ma, J. Gong, Recent advances in catalytic hydrogenation of carbon dioxide, Chemical Society Reviews, 40 (2011) 3703-3727.

[14] A. Baiker, Utilization of carbon dioxide in heterogeneous catalytic synthesis, Applied Organometallic Chemistry, 14 (2000) 751-762.

[15] W.C. Chueh, C. Falter, M. Abbott, D. Scipio, P. Furler, S.M. Haile, A. Steinfeld, High-Flux Solar-Driven Thermochemical Dissociation of CO_2 and H_2O Using Nonstoichiometric Ceria, Science, 330 (2010) 1797.

[16] G.A. Olah, A. Goeppert, G.K. Prakash, Chemical recycling of carbon dioxide to methanol and dimethyl ether: from greenhouse gas to renewable, environmentally carbon neutral fuels and synthetic hydrocarbons, Journal of Organometallic Chemistry, 74 (2009) 487-498.

[17] R. Satthawong, N. Koizumi, C. Song, P. Prasassarakich, Bimetallic Fe–Co catalysts for CO_2 hydrogenation to higher hydrocarbons, Journal of CO_2 Utilization, 3-4 (2013) 102-106.

[18] G. Centi, S. Perathoner, Heterogeneous Catalytic Reactions with CO_2: Status and Perspectives, in: S.-E. Park, J.-S. Chang, K.-W. Lee (Eds.) Studies in Surface Science and Catalysis, Elsevier, 2004, pp. 1-8.

[19] I. Omae, Aspects of carbon dioxide utilization, Catalysis Today, 115 (2006) 33-52.

[20] S. Moret, P.J. Dyson, G. Laurenczy, Direct synthesis of formic acid from carbon dioxide by hydrogenation in acidic media, Nature Communications, 5 (2014) 4017.

[21] M. Mikkelsen, M. Jorgensen, F.C. Krebs, The teraton challenge. A review of fixation and transformation of carbon dioxide, Energy & Environmental Science, 3 (2010) 43-81.

[22] G. Centi, S. Perathoner, Opportunities and prospects in the chemical recycling of carbon dioxide to fuels, Catalysis Today, 148 (2009) 191-205.

[23] W.-L. Dai, S.-L. Luo, S.-F. Yin, C.-T. Au, The direct transformation of carbon dioxide to organic carbonates over heterogeneous catalysts, Applied Catalysis A: General, 366 (2009) 2-12.

[24] T. Riedel, G. Schaub, K.W. Jun, K.W. Lee, Kinetics of CO_2 hydrogenation on a K-promoted Fe catalyst, Industrial & Engineering Chemistry Research, 40 (2001) 1355-1363.

[25] R.W. Dorner, D.R. Hardy, F.W. Williams, H.D. Willauer, K and Mn doped iron-based CO_2 hydrogenation catalysts: Detection of KAlH4 as part of the catalyst's active phase, Applied Catalysis A: General, 373 (2010) 112-121.

[26] S.-C. Lee, J.-H. Jang, B.-Y. Lee, J.-S. Kim, M. Kang, S.-B. Lee, M.-J. Choi, S.-J. Choung, Promotion of hydrocarbon selectivity in CO_2 hydrogenation by Ru component, Journal of Molecular Catalysis A: Chemical, 210 (2004) 131-141.

[27] A. Faur Ghenciu, Review of fuel processing catalysts for hydrogen production in PEM fuel cell systems, Current Opinion in Solid State and Materials Science, 6 (2002) 389-399.

[28] K. Zhao, Q. Bkour, X. Hou, S.W. Kang, J.C. Park, M.G. Norton, J.-I. Yang, S. Ha, Reverse water gas shift reaction over $CuFe/Al_2O_3$ catalyst in solid oxide electrolysis cell, Chemical Engineering Journal, 336 (2018) 20-27.

[29] G. Zhou, B. Dai, H. Xie, G. Zhang, K. Xiong, X. Zheng, CeCu composite catalyst for CO synthesis by reverse water–gas shift reaction: Effect of Ce/Cu mole ratio, Journal of CO_2 Utilization, 21 (2017) 292-301.

[30] E.L. Fornero, D.L. Chiavassa, A.L. Bonivardi, M.A. Baltanás, Transient analysis of the reverse water gas shift reaction on Cu/ZrO_2 and $Ga_2O_3/Cu/ZrO_2$ catalysts, Journal of CO_2 Utilization, 22 (2017) 289-298.

[31] C.-S. Chen, W.-H. Cheng, S.-S. Lin, Enhanced activity and stability of a Cu/SiO_2 catalyst for the reverse water gas shift reaction by an iron promoter, Chemical Communications, (2001) 1770-1771.

[32] C. Chen, Study of iron-promoted Cu/SiO_2 catalyst on high temperature reverse water gas shift reaction, Applied Catalysis A: General, 257 (2004) 97-106.

[33] C.-S. Chen, W.-H. Cheng, S.-S. Lin, Study of reverse water gas shift reaction by TPD, TPR and CO_2 hydrogenation over potassium-promoted Cu/SiO_2 catalyst, Applied Catalysis A: General, 238 (2003) 55-67.

[34] L. Wang, H. Liu, Y. Liu, Y. Chen, S. Yang, Influence of preparation method on performance of $Ni-CeO_2$ catalysts for reverse water-gas shift reaction, Journal of Rare Earths, 31 (2013) 559-564.

[35] F.-m. Sun, C.-f. Yan, Z.-d. Wang, C.-q. Guo, S.-l. Huang, Ni/Ce–Zr–O catalyst for high CO_2 conversion during reverse water gas shift reaction (RWGS), International Journal of Hydrogen Energy, 40 (2015) 15985-15993.

[36] L. Wang, H. Liu, Y. Liu, Y. Chen, S. Yang, Effect of precipitants on $Ni-CeO_2$ catalysts prepared by a co-precipitation method for the reverse water-gas shift reaction, Journal of Rare Earths, 31 (2013) 969-974.

[37] A. Goguet, F. Meunier, J. Breen, R. Burch, M. Petch, A. Faurghenciu, Study of the origin of the deactivation of a Pt/CeO catalyst during reverse water gas shift (RWGS) reaction, Journal of Catalysis, 226 (2004) 382-392.

[38] A. Goguet, S. Shekhtman, R. Burch, C. Hardacre, F. Meunier, G. Yablonsky, Pulse-response TAP studies of the reverse water–gas shift reaction over a Pt/CeO_2 catalyst, Journal of Catalysis, 237 (2006) 102-110.

[39] S.-I. Fujita, M. Usui, N. Takezawa, Mechanism of the reverse water gas shift reaction over Cu/ZnO catalyst, Journal of Catalysis, 134 (1992) 220-225.

[40] Q. Zhang, L. Guo, Z. Hao, Exploration of high-performance W_6S_8 -supported single-atom Rh 1 catalysts for reverse water–gas shift reaction and methanol formation via DFT computational study, Polyhedron, 146 (2018) 108-120.

[41] B. Liang, H. Duan, X. Su, X. Chen, Y. Huang, X. Chen, J.J. Delgado, T. Zhang, Promoting role of potassium in the reverse water gas shift reaction on Pt/mullite catalyst, Catalysis Today, 281 (2017) 319-326.

[42] C.-S. Chen, W.-H. Cheng, S.-S. Lin, Mechanism of CO formation in reverse water–gas shift reaction over Cu/Al_2O_3 catalyst, Catalysis Letters, 68 (2000) 45-48.

[43] V. Arunajatesan, B. Subramaniam, K.W. Hutchenson, F.E. Herkes, In situ FTIR investigations of reverse water gas shift reaction activity at supercritical conditions, Chemical Engineering Science, 62 (2007) 5062-5069.

[44] T.A. Semelsberger, R.L. Borup, H.L. Greene, Dimethyl ether (DME) as an alternative fuel, Journal of Power Sources, 156 (2006) 497-511.

[45] M. Matzen, Y. Demirel, Methanol and dimethyl ether from renewable hydrogen and carbon dioxide: Alternative fuels production and life-cycle assessment, Journal of Cleaner Production, 139 (2016) 1068-1077.

[46] J. McCandless, DME as an Automotive Fuel: Technical, in: Economic and Social Perspectives Energy Frontiers Conference, 2001.

[47] R.S. T. Fleisch, Beyond of GTL-FT: large-scale gas conversion through oxygenates, in: 7th Natural Gas Conversion Symposium, Dalian, China, 2004.

[48] H.H.-L. G.R. Jones, D. Romani, R.A. Sills, DME for power generation fuel: supplying India's southern region in: PetroTech conference, New Delhi, India, 2001.

[49] J.M.W. A. Basu, DME as power generation fuel: performance in gas turbines, in: PetroTech conference, New Delhi, India, 2001.

[50] S.D. Badmaev, G.G. Volkova, V.D. Belyaev, V.A. Sobyanin, Steam reforming of dimethyl ether to hydrogen-rich gas, Reaction Kinetics and Catalysis Letters, 90 (2007) 205-211.

[51] V.V. Galvita, G.L. Semin, V.D. Belyaev, T.M. Yurieva, V.A. Sobyanin, Production of hydrogen from dimethyl ether, Applied Catalysis A: General, 216 (2001) 85-90.

[52] K. Takeishi, H. Suzuki, Steam reforming of dimethyl ether, Applied Catalysis A: General, 260 (2004) 111-117.

[53] F. Frusteri, M. Migliori, C. Cannilla, L. Frusteri, E. Catizzone, A. Aloise, G. Giordano, G. Bonura, Direct CO_2-to-DME hydrogenation reaction: New evidences of a superior behaviour of FER-based hybrid systems to obtain high DME yield, Journal of CO_2 Utilization, 18 (2017) 353-361.

[54] G. Bonura, M. Migliori, L. Frusteri, C. Cannilla, E. Catizzone, G. Giordano, F. Frusteri, Acidity control of zeolite functionality on activity and stability of hybrid catalysts during DME production via CO_2 hydrogenation, Journal of CO_2 Utilization, 24 (2018) 398-406.

[55] G. Jia, Y. Tan, Y. Han, A Comparative Study on the Thermodynamics of Dimethyl Ether Synthesis from CO Hydrogenation and CO_2 Hydrogenation, Industrial & Engineering Chemistry Research, 45 (2006) 1152-1159.

[56] A. Goeppert, M. Czaun, J.-P. Jones, G.K. Surya Prakash, G.A. Olah, Recycling of carbon dioxide to methanol and derived products – closing the loop, Chemical Society Reviews, 43 (2014) 7995-8048.

[57] G. Bonura, C. Cannilla, L. Frusteri, A. Mezzapica, F. Frusteri, DME production by CO_2 hydrogenation: Key factors affecting the behaviour of CuZnZr/ferrierite catalysts, Catalysis Today, 281 (2017) 337-344.

[58] G. Bonura, M. Cordaro, L. Spadaro, C. Cannilla, F. Arena, F. Frusteri, Hybrid Cu–ZnO–ZrO_2/H-ZSM5 system for the direct synthesis of DME by CO_2 hydrogenation, Applied Catalysis B: Environmental, 140-141 (2013) 16-24.

[59] F. Frusteri, M. Cordaro, C. Cannilla, G. Bonura, Multifunctionality of Cu–ZnO–ZrO_2/H-ZSM5 catalysts for the one-step CO_2-to-DME hydrogenation reaction, Applied Catalysis B: Environmental, 162 (2015) 57-65.

[60] Y. Zhang, D. Li, Y. Zhang, Y. Cao, S. Zhang, K. Wang, F. Ding, J. Wu, V-modified CuO–ZnO–ZrO_2/HZSM-5 catalyst for efficient direct synthesis of DME from CO_2 hydrogenation, Catalysis Communications, 55 (2014) 49-52.

[61] Y. Suwannapichat, T. Numpilai, N. Chanlek, K. Faungnawakij, M. Chareonpanich, J. Limtrakul, T. Witoon, Direct synthesis of dimethyl ether from CO_2 hydrogenation over novel hybrid catalysts containing a Cu ZnO ZrO_2 catalyst admixed with WO_x/Al_2O_3 catalysts: Effects of pore size of Al_2O_3 support and W loading content, Energy Conversion and Management, 159 (2018) 20-29.

[62] Z.-z. Qin, X.-h. Zhou, T.-m. Su, Y.-x. Jiang, H.-b. Ji, Hydrogenation of CO_2 to dimethyl ether on La-, Ce-modified Cu-Fe/HZSM-5 catalysts, Catalysis Communications, 75 (2016) 78-82.

[63] T.A. Semelsberger, K.C. Ott, R.L. Borup, H.L. Greene, Generating hydrogen-rich fuel-cell feeds from dimethyl ether (DME) using Cu/Zn supported on various solid-acid substrates, Applied Catalysis A: General, 309 (2006) 210-223.

[64] F. Yaripour, F. Baghaei, I. Schmidt, J. Perregaard, Synthesis of dimethyl ether from methanol over aluminium phosphate and silica–titania catalysts, Catalysis Communications, 6 (2005) 542-549.

[65] A.T. Aguayo, J. Ereña, D. Mier, J.M. Arandes, M. Olazar, J. Bilbao, Kinetic Modeling of Dimethyl Ether Synthesis in a Single Step on a CuO–ZnO–Al_2O_3/**γ**-Al_2O_3 Catalyst, Industrial & Engineering Chemistry Research, 46 (2007) 5522-5530.

[66] T. Wang, J. Wang, Y. Jin, Slurry Reactors for Gas-to-Liquid Processes: A Review, Industrial & Engineering Chemistry Research, 46 (2007) 5824-5847.

[67] T. Lu, Y. Hou, W. Wu, M. Niu, Y. Wang, Formic acid and acetic acid production from corn cob by catalytic oxidation using O_2, Fuel Processing Technology, 171 (2018) 133-139.

[68] C. Rice, S. Ha, R.I. Masel, P. Waszczuk, A. Wieckowski, T. Barnard, Direct formic acid fuel cells, Journal of Power Sources, 111 (2002) 83-89.

[69] N.V. Rees, R.G. Compton, Sustainable energy: a review of formic acid electrochemical fuel cells, Journal of Solid State Electrochemistry, 15 (2011) 2095-2100.

[70] T. Zell, B. Butschke, Y. Ben-David, D. Milstein, Efficient hydrogen liberation from formic acid catalyzed by a well-defined iron pincer complex under mild conditions, Chemistry, 19 (2013) 8068-8072.

[71] Z.L. Wang, J.M. Yan, Y. Ping, H.L. Wang, W.T. Zheng, Q. Jiang, An efficient CoAuPd/C catalyst for hydrogen generation from formic acid at room temperature, Angewandte Chemie International Edition in English, 52 (2013) 4406-4409.

[72] T.C. Johnson, D.J. Morris, M. Wills, Hydrogen generation from formic acid and alcohols using homogeneous catalysts, Chemical Society Reviews, 39 (2010) 81-88.

[73] Z. Zhang, S. Hu, J. Song, W. Li, G. Yang, B. Han, Hydrogenation of CO_2 to Formic Acid Promoted by a Diamine-Functionalized Ionic Liquid, ChemSusChem, 2 (2009) 234-238.

[74] P.G. Jessop, F. Joó, C.-C. Tai, Recent advances in the homogeneous hydrogenation of carbon dioxide, Coordination Chemistry Reviews, 248 (2004) 2425-2442.

[75] S. Ogo, R. Kabe, H. Hayashi, R. Harada, S. Fukuzumi, Mechanistic investigation of CO2 hydrogenation by Ru(II) and Ir(III) aqua complexes under acidic conditions: two catalytic systems differing in the nature of the rate determining step, Dalton Transactions, (2006) 4657-4663.

[76] P.G. Jessop, Y. Hsiao, T. Ikariya, R. Noyori, Homogeneous Catalysis in Supercritical Fluids: Hydrogenation of Supercritical Carbon Dioxide to Formic Acid, Alkyl Formates, and Formamides, Journal of the American Chemical Society, 118 (1996) 344-355.

[77] P.G. Jessop, T. Ikariya, R. Noyori, Homogeneous catalytic hydrogenation of supercritical carbon dioxide, Nature, 368 (1994) 231.

[78] P. Daw, S. Chakraborty, G. Leitus, Y. Diskin-Posner, Y. Ben-David, D. Milstein, Selective N-Formylation of Amines with H_2 and CO_2 Catalyzed by Cobalt Pincer Complexes, ACS Catalysis, 7 (2017) 2500-2504.

[79] S. Jones, C.J. Warner, Trichlorosilane mediated asymmetric reductions of the C=N bond, Organic and Biomolecular Chemistry, 10 (2012) 2189-2200.

[80] P. Ganapati Reddy, G.D. Kishore Kumar, S. Baskaran, A convenient method for the N-formylation of secondary amines and anilines using ammonium formate, Tetrahedron Letters, 41 (2000) 9149-9151.

[81] P. Haynes, L.H. Slaugh, J.F. Kohnle, Formamides from carbon dioxide, amines and hydrogen in the presence of metal complexes, Tetrahedron Letters, 11 (1970) 365-368.

[82] P.G. Jessop, T. Ikariya, R. Noyori, Homogeneous Hydrogenation of Carbon Dioxide, Chemical Reviews, 95 (1995) 259-272.

[83] F. Liu, M.B. Abrams, R.T. Baker, W. Tumas, Phase-separable catalysis using room temperature ionic liquids and supercritical carbon dioxide, Chemical Communications, (2001) 433-434.

[84] P.G. Jessop, Y. Hsiao, T. Ikariya, R. Noyori, Catalytic Production of Dimethylformamide from Supercritical Carbon Dioxide, Journal of the American Chemical Society, 116 (1994) 8851-8852.

[85] A. Behr, P. Ebbinghaus, F. Naendrup, Process Concepts for the Transition Metal Catalyzed Syntheses of Formic Acid and Dimethylformamide Based on Carbon Dioxide, Chemical Engineering & Technology, 27 (2004) 495-501.

[86] R. Kuhlmann, S. Schmitz, K. Haßmann, A. Prüllage, A. Behr, Synthesis of N,N-dimethylformamide from carbon dioxide in aqueous biphasic solvent systems, Applied Catalysis A: General, 539 (2017) 90-96.

[87] L. Zhang, Z. Han, X. Zhao, Z. Wang, K. Ding, Highly Efficient Ruthenium-Catalyzed N-Formylation of Amines with H_2 and CO_2, Angewandte Chemie International Edition in English, 54 (2015) 6186-6189.

[88] A. Olah George, Towards Oil Independence Through Renewable Methanol Chemistry, Angewandte Chemie International Edition, 52 (2012) 104-107.

[89] T. Inui, T. Takeguchi, Effective conversion of carbon dioxide and hydrogen to hydrocarbons, Catalysis Today, 10 (1991) 95-106.

[90] X.M. Liu, G.Q. Lu, Z.F. Yan, J. Beltramini, Recent advances in catalysts for methanol synthesis via hydrogenation of CO and CO_2, Industrial & Engineering Chemistry Research, 42 (2003) 6518-6530.

[91] X. Jiang, N. Koizumi, X. Guo, C. Song, Bimetallic Pd–Cu catalysts for selective CO2 hydrogenation to methanol, Applied Catalysis B: Environmental, 170–171 (2015) 173-185.

[92] N. Koizumi, X. Jiang, J. Kugai, C. Song, Effects of mesoporous silica supports and alkaline promoters on activity of Pd catalysts in CO_2 hydrogenation for methanol synthesis, Catalysis Today, 194 (2012) 16-24.

[93] E.L. Kunkes, F. Studt, F. Abild-Pedersen, R. Schlögl, M. Behrens, Hydrogenation of CO_2 to methanol and CO on Cu/ZnO/Al_2O_3: Is there a common intermediate or not?, Journal of Catalysis, 328 (2015) 43-48.

[94] H. Ren, C.-H. Xu, H.-Y. Zhao, Y.-X. Wang, J. Liu, J.-Y. Liu, Methanol synthesis from CO_2 hydrogenation over Cu/γ-Al_2O_3 catalysts modified by ZnO, ZrO_2 and MgO, Journal of Industrial and Engineering Chemistry, 28 (2015) 261-267.

[95] L. Zhang, Y. Zhang, S. Chen, Effect of promoter SiO_2, TiO_2 or SiO_2-TiO_2 on the performance of CuO-ZnO-Al_2O_3 catalyst for methanol synthesis from CO_2 hydrogenation, Applied Catalysis A: General, 415–416 (2012) 118-123.

[96] I.A. Fisher, A.T. Bell, In-SituInfrared Study of Methanol Synthesis from H_2/CO_2 over Cu/SiO_2 and $Cu/ZrO_2/SiO_2$, Journal of Catalysis, 172 (1997) 222-237.

[97] R.A. Koeppel, A. Baiker, A. Wokaun, Copper/zirconia catalysts for the synthesis of methanol from carbon dioxide: Influence of preparation variables on structural and catalytic properties of catalysts, Applied Catalysis A: General, 84 (1992) 77-102.

[98] W.P.A. Jansen, J. Beckers, J.C. v. d. Heuvel, A.W. Denier v. d. Gon, A. Bliek, H.H. Brongersma, Dynamic Behavior of the Surface Structure of $Cu/ZnO/_{SiO2}$ Catalysts, Journal of Catalysis, 210 (2002) 229-236.

[99] J. Liu, J. Shi, D. He, Q. Zhang, X. Wu, Y. Liang, Q. Zhu, Surface active structure of ultra-fine Cu/ZrO_2 catalysts used for the CO_2+H_2 to methanol reaction, Applied Catalysis A: General, 218 (2001) 113-119.

[100] X.-M. Liu, G.Q. Lu, Z.-F. Yan, Nanocrystalline zirconia as catalyst support in methanol synthesis, Applied Catalysis A: General, 279 (2005) 241-245.

[101] M. Saito, T. Fujitani, M. Takeuchi, T. Watanabe, Development of copper/zinc oxide-based multicomponent catalysts for methanol synthesis from carbon dioxide and hydrogen, Applied Catalysis A: General, 138 (1996) 311-318.

[102] S.H. Liu, H.P. Wang, H.C. Wang, Y.W. Yang, In situ EXAFS studies of copper on ZrO_2 during catalytic hydrogenation of CO_2, Journal of Electron Spectroscopy and Related Phenomena, 144-147 (2005) 373-376.

[103] Q.-L. Tang, Q.-J. Hong, Z.-P. Liu, CO2 fixation into methanol at Cu/ZrO_2 interface from first principles kinetic Monte Carlo, Journal of Catalysis, 263 (2009) 114-122.

[104] T.C. Schilke, I.A. Fisher, A.T. Bell, In SituInfrared Study of Methanol Synthesis from CO_2/H_2 on Titania and Zirconia Promoted Cu/SiO_2, Journal of Catalysis, 184 (1999) 144-156.

[105] D.L. Chiavassa, S.E. Collins, A.L. Bonivardi, M.A. Baltanás, Methanol synthesis from CO_2/H_2 using Ga_2O_3–Pd/silica catalysts: Kinetic modeling, Chemical Engineering Journal, 150 (2009) 204-212.

[106] H.-W. Lim, M.-J. Park, S.-H. Kang, H.-J. Chae, J.W. Bae, K.-W. Jun, Modeling of the Kinetics for Methanol Synthesis using $Cu/ZnO/Al_2O_3/ZrO_2$ Catalyst: Influence of

Carbon Dioxide during Hydrogenation, Industrial & Engineering Chemistry Research, 48 (2009) 10448-10455.

[107] J. Słoczyński, R. Grabowski, A. Kozłowska, P. Olszewski, M. Lachowska, J. Skrzypek, J. Stoch, Effect of Mg and Mn oxide additions on structural and adsorptive properties of $Cu/ZnO/ZrO_2$ catalysts for the methanol synthesis from CO_2, Applied Catalysis A: General, 249 (2003) 129-138.

[108] Y. Nitta, O. Suwata, Y. Ikeda, Y. Okamoto, T. Imanaka, Copper-zirconia catalysts for methanol synthesis from carbon dioxide: Effect of ZnO addition to $Cu-ZrO_2$ catalysts, Catalysis Letters, 26 (1994) 345-354.

[109] C. Schild, A. Wokaun, A. Baiker, On the mechanism of CO and CO_2 hydrogenation reactions on zirconia-supported catalysts: a diffuse reflectance FTIR study: Part II. Surface species on copper/zirconia catalysts: implications for methanoi synthesis selectivity, Journal of Molecular Catalysis, 63 (1990) 243-254.

[110] J. Weigel, R.A. Koeppel, A. Baiker, A. Wokaun, Surface Species in CO and CO_2 Hydrogenation over Copper/Zirconia: On the Methanol Synthesis Mechanism, Langmuir, 12 (1996) 5319-5329.

[111] S. Collins, M. Baltanas, A. Bonivardi, An infrared study of the intermediates of methanol synthesis from carbon dioxide over Pd/-GaO, Journal of Catalysis, 226 (2004) 410-421.

[112] Y. Yang, J. Evans, J.A. Rodriguez, M.G. White, P. Liu, Fundamental studies of methanol synthesis from CO_2 hydrogenation on Cu(111), Cu clusters, and Cu/ZnO(0001), Physical Chemistry Chemical Physics, 12 (2010) 9909-9917.

[113] T. Inui, T. Yamamoto, M. Inoue, H. Hara, T. Takeguchi, J.-B. Kim, Highly effective synthesis of ethanol by CO_2-hydrogenation on well balanced multi-functional FT-type composite catalysts, Applied Catalysis A: General, 186 (1999) 395-406.

[114] T. Inui, T. Yamamoto, Effective synthesis of ethanol from CO_2 on polyfunctional composite catalysts, Catalysis Today, 45 (1998) 209-214.

[115] K.-i. Tominaga, Y. Sasaki, Ruthenium complex-catalyzed hydroformylation of alkenes with carbon dioxide, Catalysis Communications, 1 (2000) 1-3.

[116] K. Fujimoto, T. Shikada, Selective synthesis of C2-C5 hydrocarbons from carbon dioxide utilizing a hybrid catalyst composed of a methanol synthesis catalyst and zeolite, Applied Catalysis, 31 (1987) 13-23.

[117] S. Krishnamoorthy, A. Li, E. Iglesia, Pathways for CO_2 formation and conversion during Fischer–Tropsch synthesis on iron-based catalysts, Catalysis Letters, 80 (2002) 77-86.

[118] T. Li, H. Wang, Y. Yang, H. Xiang, Y. Li, Study on an iron–nickel bimetallic Fischer–Tropsch synthesis catalyst, Fuel Processing Technology, 118 (2014) 117-124.

[119] T. Riedel, M. Claeys, H. Schulz, G. Schaub, S.-S. Nam, K.-W. Jun, M.-J.C.G. Kishan, K.-W. Lee, Comparative study of Fischer–Tropsch synthesis with H_2-CO and H_2-CO_2 syngas using Fe- and Co-based catalysts, Applied Catalysis A: General, 186 (1999) 201-213.

[120] S.-C. Lee, J.-S. Kim, W.C. Shin, M.-J. Choi, S.-J. Choung, Catalyst deactivation during hydrogenation of carbon dioxide: Effect of catalyst position in the packed bed reactor, Journal of Molecular Catalysis A: Chemical, 301 (2009) 98-105.

[121] X. Nie, H. Wang, M.J. Janik, Y. Chen, X. Guo, C. Song, Mechanistic Insight into C–C Coupling over Fe–Cu Bimetallic Catalysts in CO_2 Hydrogenation, The Journal of Physical Chemistry C, 121 (2017) 13164-13174.

[122] R. Satthawong, N. Koizumi, C. Song, P. Prasassarakich, Comparative study on CO_2 hydrogenation to higher hydrocarbons over Fe-based bimetallic catalysts, Topics in Catalysis, 57 (2013) 588-594.

[123] R. Satthawong, N. Koizumi, C. Song, P. Prasassarakich, Light olefin synthesis from CO_2 hydrogenation over K-promoted Fe-Co bimetallic catalysts, Catalysis Today, 251 (2015) 34-40.

[124] J. Barrault, A. Guilleminot, J.C. Achard, V. Paul-Boncour, A. Percheron-Guegan, Hydrogenation of carbon monoxide on carbon-supported cobalt rare earth catalysts, Applied Catalysis, 21 (1986) 307-312.

[125] U. Rodemerck, M. Holeňa, E. Wagner, Q. Smejkal, A. Barkschat, M. Baerns, Catalyst Development for CO2Hydrogenation to Fuels, ChemCatChem, 5 (2013) 1948-1955.

[126] S.-S. Nam, G. Kishan, M.-W. Lee, M.-J. Choi, K.-W. Lee, Effect of lanthanum loading in Fe–K/La–Al_2O_3 catalysts for CO_2 hydrogenation to hydrocarbons, Applied Organometallic Chemistry, 14 (2000) 794-798.

[127] S. Hinchiranan, Y. Zhang, S. Nagamori, T. Vitidsant, N. Tsubaki, TiO_2 promoted Co/SiO2 catalysts for Fischer–Tropsch synthesis, Fuel Processing Technology, 89 (2008) 455-459.

[128] J. Xiao, D. Mao, X. Guo, J. Yu, Effect of TiO_2, ZrO_2, and TiO_2–ZrO_2 on the performance of CuO–ZnO catalyst for CO_2 hydrogenation to methanol, Applied Surface Science, 338 (2015) 146-153.

[129] G.V. Schulz, Über die Beziehung zwischen Reaktionsgeschwindigkeit und Zusammensetzung des Reaktionsproduktes bei Makropolymerisationsvorgängen, Zeitschrift Fur Physikalische Chemie-Abteilung B-Chemie Der Elementarprozesse Aufbau Der Materie, 30 (1935) 379-398.

[130] P.J. Flory, Molecular Size Distribution in Linear Condensation Polymers1, Journal of the American Chemical Society, 58 (1936) 1877-1885.

[131] R.B. Anderson, R.A. Friedel, H.H. Storch, Fischer-Tropsch Reaction Mechanism Involving Stepwise Growth of Carbon Chain, The Journal of Chemical Physics, 19 (1951) 313-319.

[132] H.D. Willauer, R. Ananth, M.T. Olsen, D.M. Drab, D.R. Hardy, F.W. Williams, Modeling and kinetic analysis of CO_2 hydrogenation using a Mn and K-promoted Fe catalyst in a fixed-bed reactor, Journal of CO_2 Utilization, 3-4 (2013) 56-64.

[133] K.J.A. Raj, B. Viswanathan, Effect of surface area, pore volume and particle size of P25 titania on the phase transformation of anatase to rutile, Indian Journal of Chemistry, 48A (2009) 1378-1382.

[134] T.L. Thompson, J.T. Yates, Surface Science Studies of the Photoactivation of TiO_2 New Photochemical Processes, Chemical Reviews, 106 (2006) 4428-4453.

[135] G. Colón, J.M. Sánchez-España, M.C. Hidalgo, J.A. Navío, Effect of TiO_2 acidic pretreatment on the photocatalytic properties for phenol degradation, Journal of Photochemistry and Photobiology A: Chemistry, 179 (2006) 20-27.

[136] J.C. Yu, J. Lin, R.W.M. Kwok, Ti_1-xZr_xO_2 Solid Solutions for the Photocatalytic Degradation of Acetone in Air, The Journal of Physical Chemistry B, 102 (1998) 5094-5098.

[137] G. Weatherbee, Hydrogenation of CO_2 on group VIII metals IV. Specific activities and selectivities of silica-supported Co, Fe, and Ru, Journal of Catalysis, 87 (1984) 352-362.

[138] F.-W. Chang, M.-S. Kuo, M.-T. Tsay, M.-C. Hsieh, Hydrogenation of CO_2 over nickel catalysts on rice husk ash-alumina prepared by incipient wetness impregnation, Applied Catalysis A: General, 247 (2003) 309-320.

[139] T.Z. Li, Y. Yang, C.H. Zhang, Z.C. Tao, H.J. Wan, X. An, H.W. Xiang, Y.W. Li, Effect of manganese incorporation manner on an iron-based catalyst for Fischer-Tropsch synthesis, Journal of Natural Gas Chemistry, 16 (2007) 244-251.

[140] R.W. Dorner, D.R. Hardy, F.W. Williams, H.D. Willauer, C2-C5+ olefin production from CO_2 hydrogenation using ceria modified Fe/Mn/K catalysts, Catalysis Communications, 15 (2011) 88-92.

[141] M. Fujiwara, T. Satake, K. Shiokawa, H. Sakurai, CO_2 hydrogenation for C2+ hydrocarbon synthesis over composite catalyst using surface modified HB zeolite, Applied Catalysis B: Environmental, 179 (2015) 37-43.

[142] S. Hu, M. Liu, F. Ding, C. Song, G. Zhang, X. Guo, Hydrothermally stable MOFs for CO_2 hydrogenation over iron-based catalyst to light olefins, Journal of CO_2 Utilization, 15 (2016) 89-95.

[143] W. Arabczyk, D. Moszyński, U. Narkiewicz, R. Pelka, M. Podsiadły, Poisoning of iron catalyst by sulfur, Catalysis Today, 124 (2007) 43-48.

[144] T. Salmi, R. Hakkarainen, Kinetic Study of the Low-Temperature Water-Gas Shift Reaction over a Cu—ZnO Catalyst, Applied Catalysis, 49 (1989) 285-306.

[145] J. Graciani, K. Mudiyanselage, F. Xu, A.E. Baber, J. Evans, S.D. Senanayake, D.J. Stacchiola, P. Liu, J. Hrbek, J.F. Sanz, J.A. Rodriguez, Highly active copper-ceria and copper-ceria-titania catalysts for methanol synthesis from CO_2, Science, 345 (2014) 546.

[146] J.A. Rodriguez, J. Evans, L. Feria, A.B. Vidal, P. Liu, K. Nakamura, F. Illas, CO_2 hydrogenation on Au/TiC, Cu/TiC, and Ni/TiC catalysts: Production of CO, methanol, and methane, Journal of Catalysis, 307 (2013) 162-169.

[147] M.L. Cubeiro, H. Morales, M.R. Goldwasser, M.J. Pérez-Zurita, F. González-Jiménez, Promoter Effect of Potassium on an Iron Catalyst in the Carbon Dioxide Hydrogenation Reaction, Reaction Kinetics and Catalysis Letters, 69 (2000) 259-264.

[148] P.H. Choi, K.-W. Jun, S.-J. Lee, M.-J. Choi, K.-W. Lee, Hydrogenation of carbon dioxide over alumina supported Fe-K catalysts, Catalysis Letters, 40 (1996) 115-118.

[149] R. Shannon, Revised effective ionic radii and systematic studies of interatomic distances in halides and chalcogenides, Acta Crystallographica Section A, 32 (1976) 751-767.

[150] R. Brown, M.E. Cooper, D.A. Whan, Temperature programmed reduction of alumina-supported iron, cobalt and nickel bimetallic catalysts, Applied Catalysis, 3 (1982) 177-186.

[151] D.J. Duvenhage, N.J. Coville, Fe:$CoTiO_2$ bimetallic catalysts for the Fischer-Tropsch reaction I. Characterization and reactor studies, Applied Catalysis A: General, 153 (1997) 43-67.

[152] G. Pecchi, P. Reyes, T. López, R. Gómez, A. Moreno, J.L.G. Fierro, Effect of precursors on surface and catalytic properties of Fe/TiO_2 catalysts, Journal of Chemical Technology & Biotechnology, 77 (2002) 944-949.

[153] S. Lögdberg, D. Tristantini, Ø. Borg, L. Ilver, B. Gevert, S. Järås, E.A. Blekkan, A. Holmen, Hydrocarbon production via Fischer–Tropsch synthesis from H_2-poor syngas over different Fe-Co/γ-Al_2O_3 bimetallic catalysts, Applied Catalysis B: Environmental, 89 (2009) 167-182.

[154] W. Wang, X. Jiang, X. Wang, C. Song, Fe–Cu Bimetallic Catalysts for Selective CO_2 Hydrogenation to Olefin-Rich C2+ Hydrocarbons, Industrial & Engineering Chemistry Research, 57 (2018) 4535-4542.

[155] W. Li, X. Nie, X. Jiang, A. Zhang, F. Ding, M. Liu, Z. Liu, X. Guo, C. Song, ZrO_2 support imparts superior activity and stability of Co catalysts for CO_2 methanation, Applied Catalysis B: Environmental, 220 (2018) 397-408.

[156] X. Nie, H. Wang, M.J. Janik, X. Guo, C. Song, Computational Investigation of Fe–Cu Bimetallic Catalysts for CO_2 Hydrogenation, The Journal of Physical Chemistry C, 120 (2016) 9364-9373.

[157] G. Martra, Lewis acid and base sites at the surface of microcrystalline TiO_2 anatase: relationships between surface morphology and chemical behaviour, Applied Catalysis A: General, 200 (2000) 275-285.

[158] G. Busca, V. Lorenzelli, Infrared spectroscopic identification of species arising from reactive adsorption of carbon oxides on metal oxide surfaces, Materials Chemistry, 7 (1982) 89-126.

[159] T. Montanari, L. Castoldi, L. Lietti, G. Busca, Basic catalysis and catalysis assisted by basicity: FT-IR and TPD characterization of potassium-doped alumina, Applied Catalysis A: General, 400 (2011) 61-69.

[160] M. Kantschewa, E.V. Albano, G. Etrtl, H. Kno¨zinger, Infrared and x-ray photoelectron spectroscopy study of K_2CO_3/γ-Al_2O_3, Applied Catalysis, 8 (1983) 71-84.

[161] T. Hirano, Roles of potassium in potassium-promoted iron oxide catalyst for dehydrogenation of ethylbenzene, Applied Catalysis, 26 (1986) 65-79.

[162] H. Tsuji, A. Okamura-Yoshida, T. Shishido, H. Hattori, Dynamic Behavior of Carbonate Species on Metal Oxide Surface: Oxygen Scrambling between Adsorbed Carbon Dioxide and Oxide Surface, Langmuir, 19 (2003) 8793-8800.

[163] J.M. Zowtiak, C.H. Bartholomew, The kinetics of H_2 adsorption on and desorption from cobalt and the effects of support thereon, Journal of Catalysis, 83 (1983) 107-120.

[164] F. Bozso, G. Ertl, M. Grunze, M. Weiss, Chemisorption of hydrogen on iron surfaces, Applications of Surface Science, 1 (1977) 103-119.

[165] P. Panagiotopoulou, Hydrogenation of CO_2 over supported noble metal catalysts, Applied Catalysis A: General, 542 (2017) 63-70.

[166] L. Mino, G. Spoto, A.M. Ferrari, CO_2 Capture by TiO_2 Anatase Surfaces: A Combined DFT and FTIR Study, The Journal of Physical Chemistry C, 118 (2014) 25016-25026.

[167] T. Meisel, Z. Halmos, K. Seybold, E. Pungor, The thermal decomposition of alkali metal formates, Journal of thermal analysis, 7 (1975) 73-80.

[168] Y. Santiago-Rodríguez, E. Barreto-Rodríguez, M.C. Curet-Arana, Quantum mechanical study of CO_2 and CO hydrogenation on Cu(111) surfaces doped with Ga, Mg, and Ti, Journal of Molecular Catalysis A: Chemical, 423 (2016) 319-332.

[169] R.W. Dorner, D.R. Hardy, F.W. Williams, H.D. Willauer, Heterogeneous catalytic CO_2 conversion to value-added hydrocarbons, Energy & Environmental Science, 3 (2010) 884.

[170] M.-J. Choi, J.-S. Kim, H.-K. Kim, S.-B. Lee, Y. Kang, K.-W. Lee, Hydrogenation of CO_2 over Fe-K based catalysts in a fixed bed reactors at elevated pressure, Korean Journal of Chemical Engineering, 18 (2001) 646-651.

[171] H.S. Fogler, Elements of chemical reaction engineering, Third edition. Upper Saddle River, N.J. : Prentice Hall PTR, [1999] ©1999, 1999.

APPENDICES

APPENDIX A

Gas Product Analysis

The gas product including Ar, CO, CH_4 and CO_2 were analyzed online using an Agilent 3000 micro GC with molecular sieve type column for Ar, CO, CH_4 and Plot-Q column for CO_2, respectively. The GC-TCD condition and temperature program used for the analyses are described in Table A-1.

Table A-1 Condition and temperature program for micro GC analysis.

Parameters	Molecular Sieve	Plot Q
Carrier gas	Helium	Helium
Internal standard	Argon	Argon
Injector temperature (°C)	100	100
Column temperature (°C)	60	70
Column pressure (psi)	20	20
Sample pump (s)	10	10
Injection time (ms)	100	100
Run time (s)	300	600

The gas-phase hydrocarbon products were analyzed online using SRI 8610C GC (Porapak Q column) equipped with FID. The GC-FID condition and temperature program used for the analyses are described in Table A-2.

Table A-2 Condition and temperature program for GC-FID analysis.

Parameters	Molecular Sieve
Carrier gas	Helium
Injector temperature (°C)	165
Detector temperature (°C)	250
Injection volume (ml)	3
Oven temperature program	
Initial temperature (°C)	40
Hold time (min)	0
Ramp rate (°C min^{-1})	5
Final temperature (°C)	100
Hold time (min)	0
Ramp rate (°C min^{-1})	2.5
Final temperature (°C)	200
Hold time (min)	0

APPENDIX B

Liquid Hydrocarbon Product Analysis

The liquid hydrocarbons collected from an ice cooled condenser connected to the reactor system were analyzed after the CO_2 hydrogenation reaction using the GC/MS (Agilent, 7890) with a capillary column RTX-PAH (60 m x 0.25 mm I.D. x 0.25 μm film thickness). The condition and temperature program for GC/MS are described in Table B-1.

Table B-1 Condition and temperature program for GC/MS analysis.

Parameters	Molecular Sieve
Carrier gas	Helium
Column inlet pressure (kPa)	23
Column flow (mL min^{-1})	0.7
Split mode injector	20:1
Total flow (mL min^{-1})	15.2
Carrier gas flow rate (mL min^{-1})	15.2
Injector temperature (°C)	290
Detector temperature (°C)	270
Injection volume (μl)	1
Oven temperature program	
Initial temperature (°C)	40
Hold time (min)	10
Ramp rate (°C min^{-1})	5
Final temperature (°C)	120
Hold time (min)	2
Ramp rate (°C min^{-1})	4
Final temperature (°C)	250
Hold time (min)	5

APPENDIX C

The equilibrium CO_2 conversion from ASPEN HYSYS 7.1

Table C-1 Equilibrium CO_2 conversion at constant molar ratio (H_2/CO_2 = 3) and various reaction temperatures.

	(a) RWGS	(b) FTS	(c) Direct CO_2-HYD
Temp. (K)	CO_2 conv. (%)	CO_2 conv. (%)	CO_2 conv. (%)
373	2.78	75.00	75.00
473	10.23	74.87	75.87
573	22.30	74.14	74.13
673	36.12	71.9	71.76
773	48.97	67.74	66.68
873	59.56	63.65	58.66
973	67.74	64.26	48.56

Table C-2 Equilibrium CO_2 conversion at constant molar ratio (H_2/CO_2 = 3) and various reaction pressures.

	(a) RWGS	(b) FTS	(c) Direct CO_2-HYD
Press. (MPa)	CO_2 conv. (%)	CO_2 conv. (%)	CO_2 conv. (%)
0.10	22.22	72.20	72.17
0.51	22.25	73.73	73.71
1.01	22.30	74.1	74.09
1.10	22.30	74.14	74.13
1.52	22.34	74.27	74.27
2.03	22.38	74.38	74.37
2.53	22.42	74.45	74.44
4.05	22.42	74.58	74.57

APPENDIX D

Calculation of CO_2 Conversion and Product Selectivity

The catalytic CO_2 hydrogenation activity was obtained from GC-TCD analyses (using Ar as an internal standard) and can be written in terms of mole percent conversion of CO_2. Calculation procedures are as follow:

$$CO_2 \text{ conversion } (\%) = \left[1 - \frac{\left(CO_2/Ar\right)_{out}}{\left(CO_2/Ar\right)_{in}}\right] \times 100 \qquad \text{(D-1)}$$

where $\left(CO_2/Ar\right)_{in}$ = ratio of CO_2 to Ar concentration at the reactor inlet

$\left(CO_2/Ar\right)_{out}$ = ratio of CO_2 to Ar concentration at the reactor outlet

Example: CO_2 conversion of Fe-Co(0.1)-K(0.1)-La(0.1)/TiO_2 catalyst

Form Table D-1: at 16 hour-on-stream; Ar area = 431342 and CO_2 area = 1042200

$(CO_2/Ar)_{out}$ = 1042200 / 431342 = 2.416

$(CO_2/Ar)_{in}$ can be estimated from the ratio of CO_2 area to Ar area measured at 1.1 MPa (ambient temperature) before CO_2 hydrogenation

$(CO_2/Ar)_{out}$ = 3.087

Hence, CO_2 conversion = [1 – (2.416 / 3.087)] x 100 = 21.7%

Table D-1 GC-TCD data of CO_2 hydrogenation over Fe-Cu(0.1)-K(0.1)-La(0.1) catalyst.

TOS (h)	Area			
	Ar	CH_4	CO	CO_2
0.0	398981	43830	251533	958745
1.0	429489	56955	203807	1004440
2.0	445046	64519	174765	1026030
3.0	447148	67378	164505	1031730
4.0	448374	68690	163690	1030920
5.0	444311	68410	164510	1032030
6.0	442667	68122	169911	1027940
7.0	441684	67795	174226	1034790
8.0	441708	67413	182050	1032350
9.0	437076	66261	187331	1030370
10.0	430783	64754	174948	1032700
11.0	430938	64528	185100	1032000
12.0	431116	63674	194487	1028950
13.0	431254	62425	173698	1032500
14.0	431566	64261	177908	1036980
15.0	434350	67360	177908	1044920
16.0	431342	61837	175760	1042200
17.0	426581	51028	187820	1038730

The product space-time yield (STY) was expressed in the moles of product per weight of the catalyst per reaction time (μmol g^{-1} s^{-1}) and can estimated as follows:

Example: CH_4 STY of Fe-Co(0.1)-K(0.1)-La(0.1)/TiO_2 catalyst

Feed gas flow rate (24 vol% CO_2/ 72 vol% H_2/ 4 vol% Ar) = 12 mL(STP) min^{-1}

Catalyst weight = 0.2005 g

Gas constant = 0.082 L at, K^{-1} mol^{-1}

First the CO_2 flow rate is calculated;

CO_2 flow rate = [(Feed gas flow rate (mL(STP) min^{-1}) x 0.001 / 0.082 / 273.15 x 60) / (Catalysts weight (g) / 1000)] x 0.24

= [(12 x 0.001 / 0.082 / 273.15 x 60) / (0.2005 / 1000)] x 0.24

= 38.48 mol kg-cat^{-1} h^{-1}

To calculate the STY, the calibration data of Ar, CH_4 and CO_2 for GC-TCD are required. By plotting out between gas concentration (y-axis) and area of the peak (x-axis) and the slope will be used for qualitative calculation. From the calibration curve of Ar, CH_4 and CO_2 (Fig. C-1), the slopes are listed below:

Slope of Ar curve = 1.2550E-05

Slope of CH_4 curve = 1.4011E-05

Slope of CO_2 curve = 2.3222E-05

Form Table D-1 at 16 hour-on-stream; Ar area = 431342 and CH_4 area = 61837

CH_4 STY = CO_2 flow rate x (CH_4 area x Slope pf CH_4 curve) / (Ar area x Slope of Ar curve) / [$(CO_2/Ar)_{in}$ x (Slope of CO_2 curve/Slope of Ar curve)]

= 38.48 x (61837 x 1.4011E-05) / (431342 x 1.4011E-05) / [3.087 x (2.3222E-05 / 1.2550E-05)]

= 0.966 mol kg-cat^{-1} h^{-1}

= 0.268 μmol g-cat^{-1} s^{-1} #

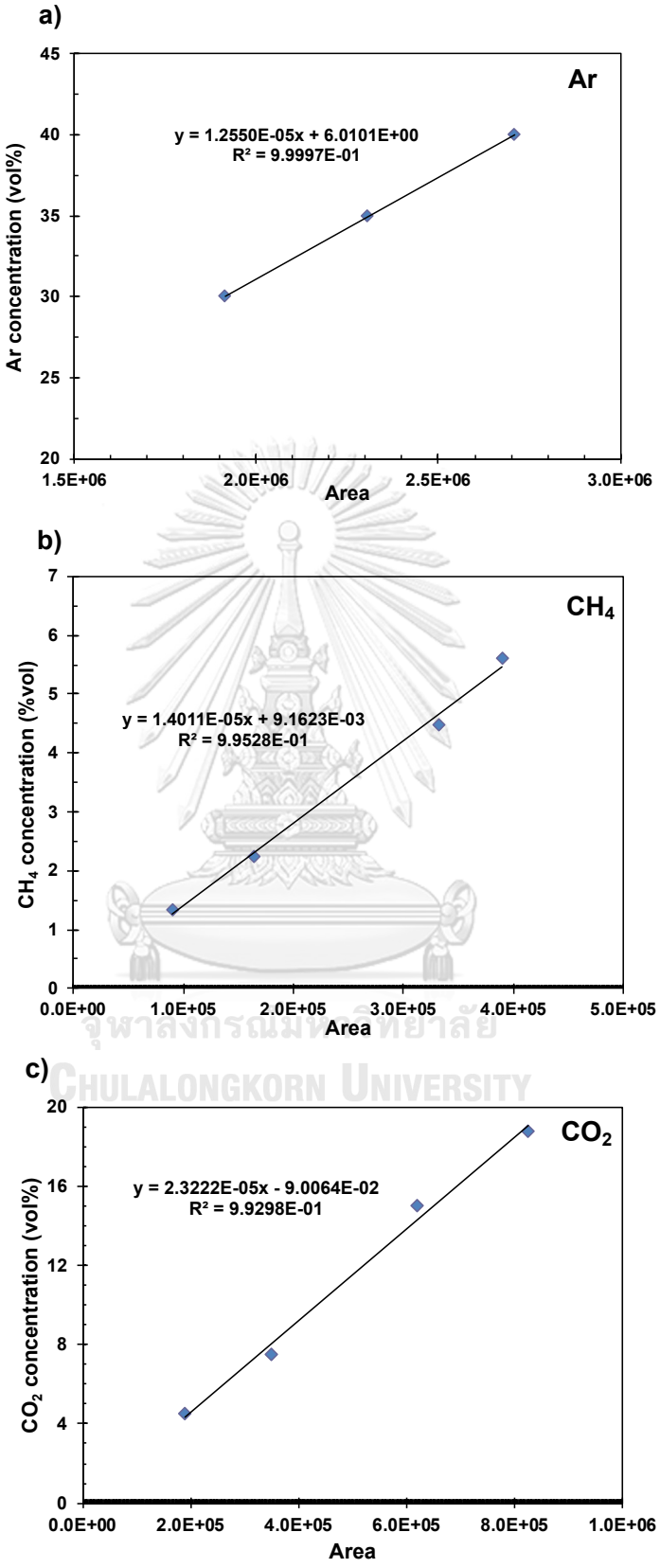

Figure D-1 The calibration curve. (a) Ar, (b) CH_4 and (c) CO_2.

The gaseous hydrocarbons were analyzed online by GC-FID. The selectivity of these gaseous hydrocarbons (C_1 – C_7) was expressed in carbon mole percent (%) and calculated as follows:.

$$S_i\ (\text{C-mol\%}) = \left(\frac{\text{mole}_i}{\text{mole}_{CO_2(\text{converted})}} \right) \times 100 \qquad \text{(D-2)}$$

where S_i = percent product selectivity of produced product i

mole_i = mole of produced product i

$\text{mole}_{CO_2(\text{converted})}$ = mole of converted CO_2

Example: Product selectivity of Fe-Co(0.1)-K(0.1)-La(0.1)/TiO_2 catalyst:

From Table D-1 the CO_2 conversion could be calculated:

The CO_2 conversion @16 h = 21.73%

The CO_2 conversion @17 h = 21.13%

Then, $\text{mole}_{CO_2(\text{converted})}$ = (CO_2 flow rate) x (%CO_2 conv. @16 h + %CO_2 conv. @17 h) /2 / 100

= (38.48) x (21.73 + 21.13) / 2 / 100

= 8.24 mol

From Table D-1 the CH_4 STY could be calculated:

The CH_4 STY @16 h = 1.0873 mol kg-cat^{-1} h^{-1}

The CH_4 STY @17 h = 0.9073 mol kg-cat^{-1} h^{-1}

Then, mole_{CH_4} = (CH_4 STY @16 h + CH_4 STY @17 h) / 2

= (1.0873 + 0.9073) / 2

= 0.9973 mol

Hence, from Eq. D-2 S_{CH_4} = (0.9973 / 8.24) x 100

= 12 C-mol% #

APPENDIX E

Calculation of Chain Growth Probability

Since CO_2 hydrogenation over Fe-based catalysts mostly proceeds *via* reverse water-gas shift reaction followed by Fischer-Tropsch synthesis, so the hydrocarbon product distribution generally follows an Anderson-Schulz-Flory distribution, where the hydrocarbon chain is formed step-wise by insertion of C_1 intermediates with constant growth proability (α) [129-131]. The Anderson-Schulz-Flory distribution can be written as the following equation,

$$W_N = N(1 - \alpha)^2 \alpha^{N-1} \quad \text{(E-1)}$$

$$\frac{W_N}{N} = \frac{(1 - \alpha)^2}{\alpha} \alpha^N \quad \text{(E-2)}$$

$$\ln\left(\frac{W_N}{N}\right) = \ln\left(\frac{(1 - \alpha)^2}{\alpha}\right) + N \ln \alpha^N \quad \text{(E-3)}$$

where W_N = carbon weight fraction of hydrocarbon containing N carbon

N = carbon number

α = chain growth probability

The chain growth probability (α) can be calculated from the slope of the plot between the carbon number (N) and natural logarithm of hydrocarbon weight fraction to carbon number ratio ($\ln(W_N/N)$) or natural logarithm of the carbon mole fraction of hydrocarbon containing N carbon ($\ln M_N$)

Example: Chain growth probability of gaseous product from CO_2 hydrogenation over Fe-Cu(0.1)-K(0.1)-La(0.1)/TiO_2 catalyst

First, the area of each hydrocarbon containing N carbon from GC-FID data as shown in Table E-1 is calculated.

Table E-1 GC-FID data of CO_2 hydrogenation over Fe-Cu(0.1)-K(0.1)-La(0.1) catalyst.

Component	Retention time (min)	Area
CH_4	0.933	767.2980
C_2H_4	2.683	49.3330
C_2H_6	3.416	401.0050
C_3H_6	8.233	334.1460
C_3H_8	8.683	274.3615
C_4H_8	14.700	129.2870
C_4H_{10}	15.416	333.0400
C_5H_{10}	22.550	69.0730
C_5H_{12}	23.333	256.7960
C_6H_{14}	31.566	196.8835
C_7H_{16}	39.500	129.1130

Area of C_4 hydrocarbon = 129.2870 + 333.0400 = 462.327 #

Carbon number (N)	Area
1	767.2980
2	450.3380
3	608.5075
4	462.3270
5	325.8690
6	196.8840
7	129.1130

The carbon weight fraction of hydrocarbon containing N carbon (W_N) is then calculated by divided the area of each hydrocarbon containing N carbon with the total area.

Total area = 2940.3360

W_4 = 462.3270 / 2940.3360 = 0.1572

Then, $\ln(W_N/N)$ is calculated and plotted with carbon number (N).

Carbon number (N)	W_N	W_N/N	$\ln(W_N/N)$
1	0.2610	0.2610	-1.3434
2	0.1532	0.0766	-2.5694
3	0.2070	0.0690	-2.6739
4	0.1572	0.0393	-3.2363
5	0.1108	0.0222	-3.8092
6	0.0670	0.0112	-4.4954
7	0.0439	0.0063	-5.0715
Total	1.0000		

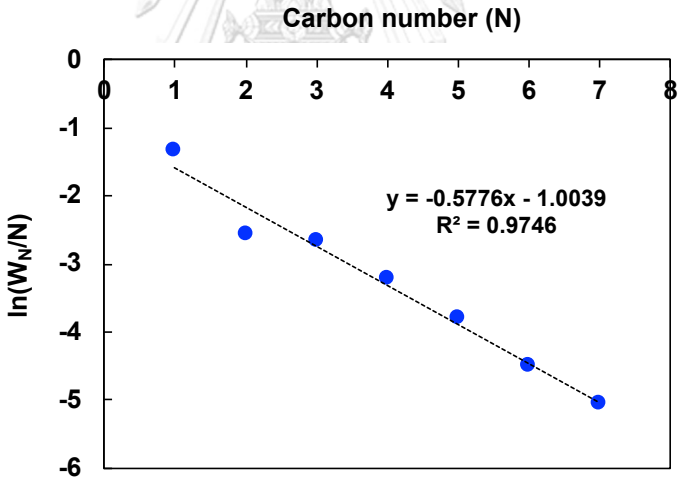

Figure E-1 ASF plot of the gaseous hydrocarbon products for the Fe-Cu(0.1)-K(0.1)-La(0.1)/TiO_2 catalysts.

According to Eq. E-3, the slope of Fig. E-1 is $\ln(\alpha)$. Then, the chain growth probability (α) can be calculated.

Slope = $\ln(\alpha)$ = -0.5776

α = 0.56 #

APPENDIX F

H_2-TPR of Fe-Cu bimetallic catalysts

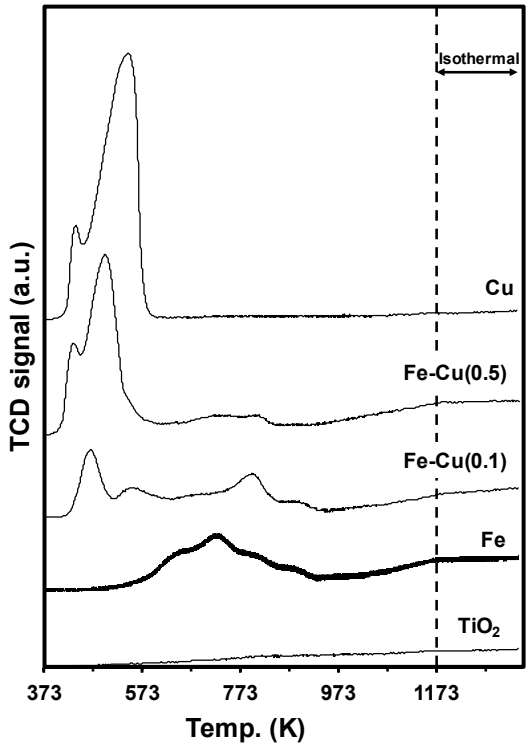

Figure F-1 Effect of combining Fe and Cu on the H_2-TPR profiles of the calcined Fe-Cu(X)/TiO_2 catalysts.

APPENDIX G

Chromatograms of gas product over Fe-Cu(0.1)-K(*X*)/TiO_2 catalysts

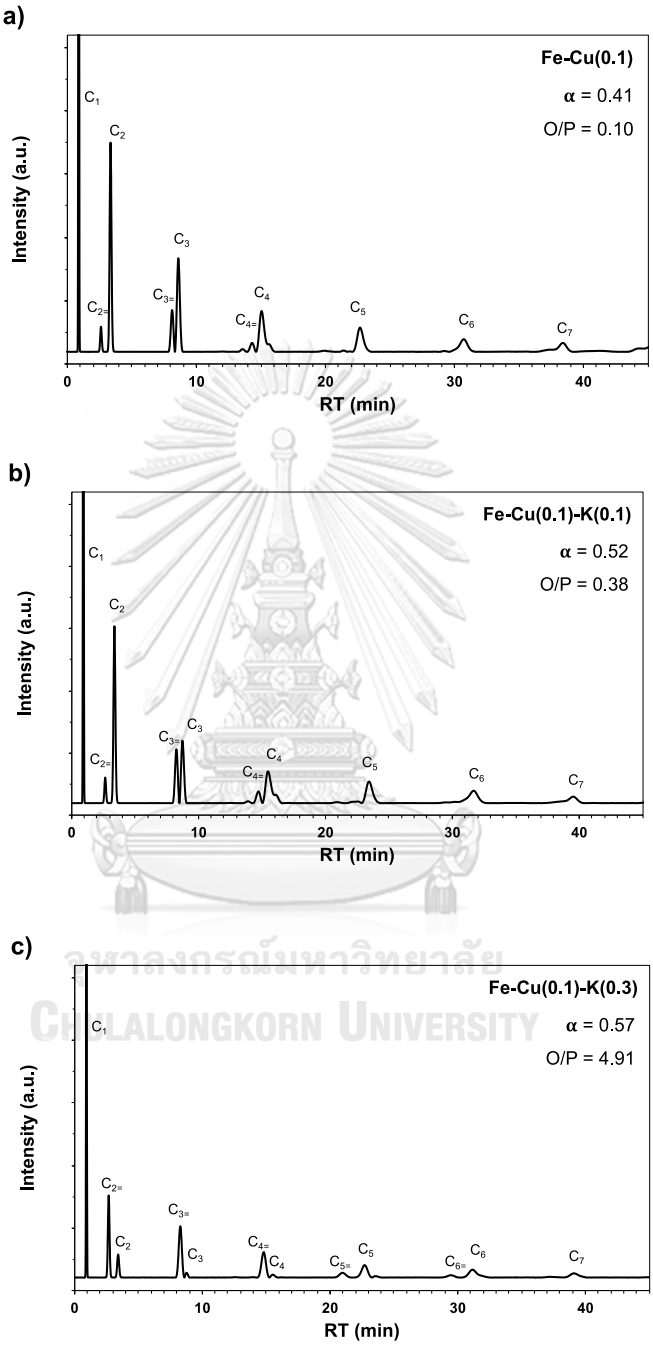

Figure G-1 GC-FID chromatograms of gas-phase hydrocarbons from CO_2 hydrogenation over Fe-Cu(0.1)-K(X)/TiO_2 with different K/Fe atomic ratio. (a) X = 0, (b) X = 0.1 and (c) X = 0.3.

APPENDIX H

KINETICS AND MODELLING OF Fe-BASED CATALYSTS FOR CO_2 HYDROGENATION TO HIGHER HYDROCARBONS

H-1 Introduction

The catalytic CO_2 hydrogenation to hydrocarbon is a potential way for CO_2 utilization. One limitation of using CO_2 as a feedstock for hydrocarbon production concerns the high energy barrier for polymerization and the need for a source of hydrogen. Recently, some reports suggested that the electrochemical and photochemical catalytic CO_2 conversion processes continue to improve in efficiencies, the thermal processes remain one of the few proven methods for producing high yields of higher hydrocarbons greater than methane [24, 132, 169, 170].

According to Chapter IV and V, for CO_2 hydrogenation using an optimized Fe-Cu-K-La catalyst impregnated on TiO_2 in a fixed-bed reactor with thermal process, CO_2 conversion levels could be achieved as high as 23%. The modelling and kinetic analysis could be applied to the further tailor catalyst properties and reactor design in effort to facilitate greater CO_2 conversion. The kinetic studies should be performed on the specific catalyst and operating conditions for process design and scale-up [24, 132].

In this study on the APPEN PLUS simulation of CO_2 hydrogenation, the obtained activity results of Fe-Cu(0.1)-K(0.1)-La(0.1)/TiO_2 catalyst were used to modify the kinetic parameters of Langmuir-Hinshelwood model and predict the optimal reactor size and conditions for hydrocarbon production.

H-2 Kinetic analysis over Fe-Cu-K-La/TiO_2 catalyst

The kinetic rate parameters of CO_2 hydrogenation over optimized Fe-Cu(0.1)-K(0.1)-La(0.1)/TiO_2 catalyst were determined by varying the gas hourly space velocity (GHSV) at constant reaction condition (573 K and 1.1 MPa). The reactor tube was loaded with the desired amounts of catalyst (0.002-0.600 g) diluted with amorphous SiO_2 (Davisil Grade 62, particle size = 75-250 × 10^{-6} m) to maintain an aspect ratio of approximately 6.0. The rates of CO_2 change with various inlet CO_2 concentration (at about 16-18 h on stream) were used to estimate the kinetic rate parameters as shown in Fig. F-1 and Table. F-1.

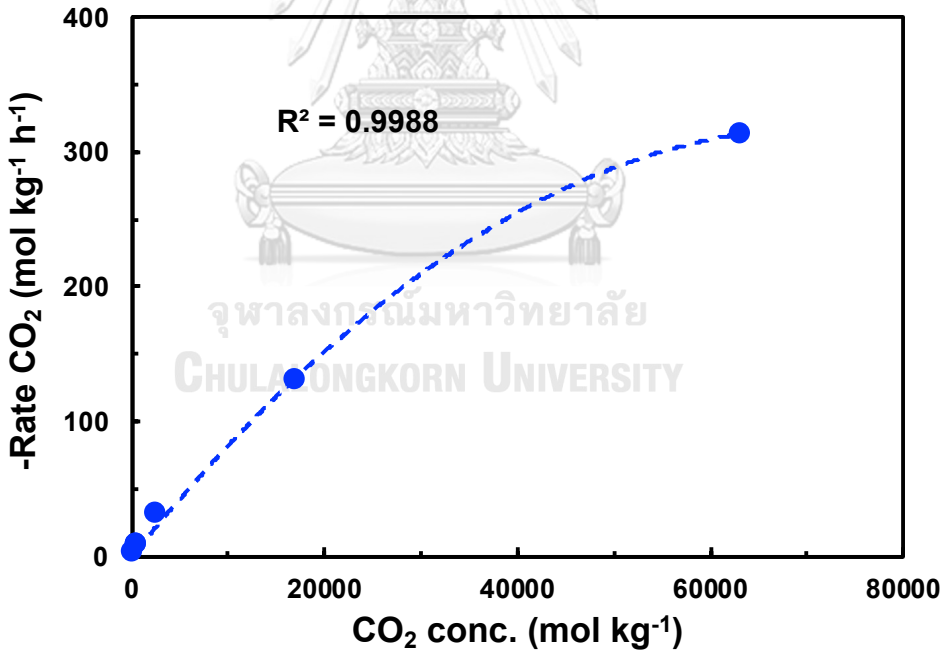

Figure H-1 Effects of inlet CO_2 concentration on the reaction rate for CO_2 hydrogenation over Fe-Cu(0.1)-K(0.1)-La(0.1)/TiO_2 catalyst at 573 K and 1.1 MPa.

Table H-1 The experimental data of CO_2 hydrogenation with Fe-Cu-La-K/TiO_2 catalyst for kinetics analysis.

Data	GHSV (L g^{-1} h^{-1})	$[CO_2]$ (mol kg^{-1})	$[H_2]$ (mol kg^{-1})	Rate of converted CO_2 (mol kg^{-1} h^{-1})	
				Experiment	Calculation
1	1.20	233	700	3.4	2.8
2	3.58	690	2071	8.3	8.2
3	3.62	693	2078	8.9	8.3
4	13.79	2660	7980	31.5	31.7
5	88.89	17144	51432	131.3	N/A
6	327.27	63121	189365	314.0	N/A

From Fig. H-1, the non-linear relationship was observed, which suggested that the surface reaction is a rate determining step (RDS) and the rate equation of Eq. H-1 could be proposed with the following assumptions.

$$CO_2 + H_2 \longrightarrow \text{Hydrocarbons} + H_2O \quad \text{(F-1)}$$

Assumptions:

1. The overall reaction is irreversible and the surface reaction is rate determining step (RDS).
2. Only CO_2 is adsorbed on catalyst site since the dissociative adsorption of H_2 is weak compared to CO_2 adsorption.
3. CO_2 is not dissociative adsorbed during the adsorption step.

The elementary reactions of CO_2 hydrogenation to hydrocarbons are written as adsorption step (Eq H-2) and surface reaction (Eq. H-3).

Adsorption:
$$CO_2 + * \overset{K_{CO_2}}{\longleftrightarrow} CO_2{}^{\bullet}{}^{*} \qquad \text{(H-2)}$$

Surface reaction:
$$CO_2{}^{\bullet}{}^{*} + H_2 \xrightarrow{k} \text{Hydrocarbons} + H_2O + * \quad \text{(RDS)} \qquad \text{(H-3)}$$

Hence, the rate equation of CO_2 hydrogenation can be written based on Langmuir-Hinshelwood model as follows [171];

$$Rate_{CO_2} = \frac{kK_{CO_2}[CO_2][H_2]}{\left(1 + K_{CO_2}[CO_2]\right)} \qquad \text{(H-4)}$$

$$Rate_{CO_2} = \frac{k'[CO_2][H_2]}{\left(1 + K_{CO_2}[CO_2]\right)} \qquad \text{(H-5)}$$

Where k' = the overall rate constant (kg mol^{-1} h^{-1})

K_{CO_2} = the adsorption constant of CO_2 (kg mol^{-1})

$[CO_2]$ = the concentration of CO_2 (mol kg^{-1})

$[H_2]$ = the concentration of H_2 (mol kg^{-1})

The kinetic parameters were estimated from non-linear regression of experiment data (GHSV = 1.2 – 13.8 L g^{-1} h^{-1}) as presented in Table. H-1. The rate equation could be expressed as follows;

$$Rate = \frac{1775\,[CO_2][H_2]}{\left(1 + 4.22 \times 10^5[CO_2]\right)} \qquad \text{(H-6)}$$

Figure H-2 shows the comparison of CO_2 conversion rate from the experimental data and calculation from rate equation (Eq. H-6) at various GHSV.

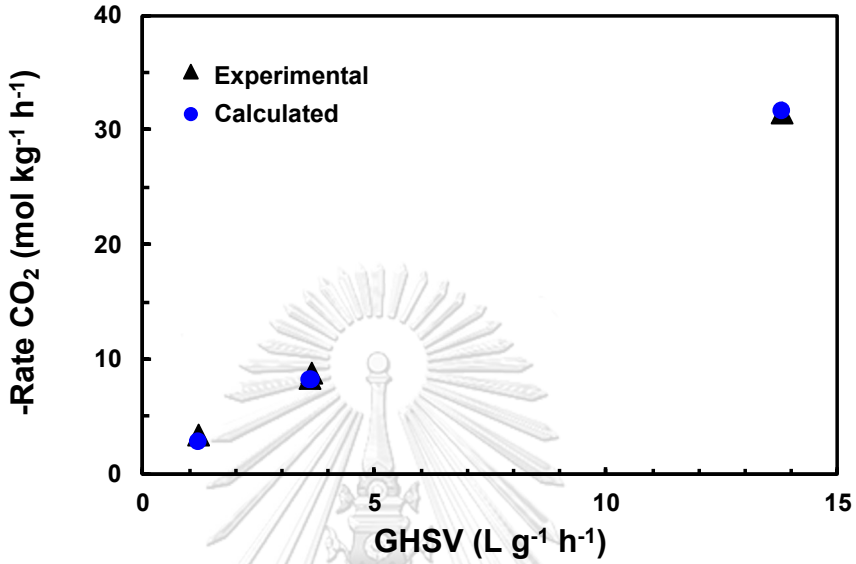

Figure H-2 The comparison of CO_2 conversion rate from experiment data and rate equation (calculation) of CO_2 hydrogenation with Fe-Cu-La-K/TiO_2 catalyst at various GHSV.

H-3 Simulation of CO_2 hydrogenation over Fe-Cu-K-La/TiO_2 catalyst

The simulation of the obtained experimental data was performed using ASPEN PLUS 8.6. The reactor model RPLUS was chosen, which provided a rigorous simulation of an ideal PFR. H_2 and CO_2 at the reactor inlet and carbon-containing components CO_2, CO, and C_3H_8 (represent hydrocarbons) at the reactor outlet. According to the main reaction pathway, CO_2 was first converted to CO *via* the reverse water-gas shift (RWGS) reaction (Eq. H-7) and subsequently converted to hydrocarbons *via* Fischer-Tropsch synthesis (FTS) (Eq. H-8). Both Eq. 6.7 and 6.8 were used as input reaction for the ideal PFR. The catalyst bed dimension used in simulation was 6 cm (diameter) x

36 cm (length) which was 1000 times the catalyst bed volume used in this experimental (6 mm (diameter) x 36 mm (length)). The summary of kinetic parameters from rate equation (Eq. H-6) and other necessary parameters used in the RPLUS reactor are tabulated in Table H-2.

$$CO_2 + H_2 \longleftrightarrow CO + H_2O \qquad \text{RWGS} \qquad \text{(H-7)}$$

$$3CO + 7H_2 \longleftrightarrow C_3H_8 + 3H_2O \qquad \text{FTS} \qquad \text{(H-8)}$$

Table H-2 The values of kinetic parameters and reactor parameter values used in the model.

Kinetic parameter		Reactor parameter	
k'	1775 kg mol^{-1} h^{-1}	Length	36 cm
K_{CO_2}	4.22 x 10^5 kg mol^{-1}	Diameter	6 cm
$E_{A,RWGS}$	55 kJ mol^{-1} [132]	Pressure	1.1 MPa
$E_{A,HYD}$	72 kJ mol^{-1} [132]	Temperature	573 K
		Bed voidage	0.5

From process flow diagram as shown in Fig. H-3, the simulation was performed to investigate the effect of GHSV on the CO_2 conversion of CO_2 hydrogenation in fixed-bed reactor. The GHSV (1.2 – 14 L g^{-1} h^{-1}) was varied by changing the catalyst weight (52 – 600 g) at constant volume feed flow rate (720 L h^{-1}) and reaction condition (573 K and 1.1 MPa). The mixed gas molar ratio of H_2/CO_2 was maintained constant at 3. The 2nd reactor with the same dimension was also added in series to investigate the reactor size scale-up as shown in Fig. H-4. From the simulation results, the CO_2

conversion and the product selectivity at various GHSV are shown in Fig. H-5 and Fig. H-6, respectively. The product distribution (stream flow rate) is also presented in the Table H-3 (1 PFR) and Table H-4 (2 PFR in series).

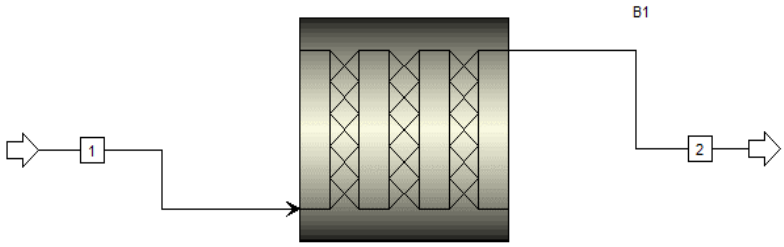

Figure H-3 Flow diagram of CO_2 hydrogenation in fixed bed reactor (1 PFR).

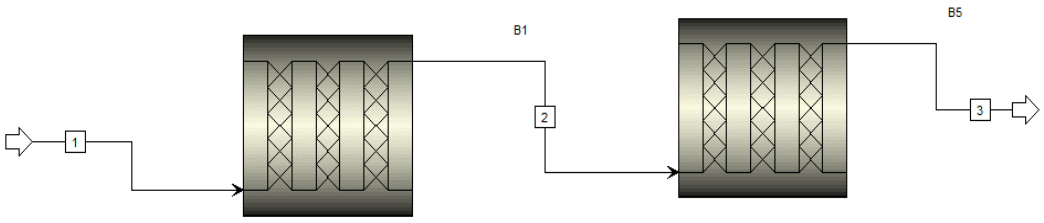

Figure H-4 Flow diagram of CO_2 hydrogenation in 2 PFR in series.

Table H-3 Stream table of CO_2 hydrogenation using 1 PFR simulation by ASPEN PLUS 8.6.

GHSV (L g^{-1} h^{-1})	1.2		3.6		7.0		10		14	
Catalyst weight (g)	600		200		103		72		52	
Stream	1	2	1	2	1	2	1	2	1	2
Temperature (°C)	300	300	300	300	300	300	300	300	300	300
Pressure (bar)	11	11	11	11	11	11	11	11	11	11
Vapor Frac	1	1	1	1	1	1	1	1	1	1
Mole Flow (kmol/h)	0.166	0.129	0.166	0.159	0.166	0.164	0.166	0.165	0.166	0.165
Mass Flow (kg/h)	2.074	2.074	2.074	2.074	2.074	2.074	2.074	2.074	2.074	2.074
Volume Flow (L/h)	720	558	720	692	720	712	720	716	720	718
Enthalpy (Gcal/h)	-0.004	-0.004	-0.004	-0.004	-0.004	-0.004	-0.004	-0.004	-0.004	-0.004
Mole Flow (kmol/h)										
CO_2	0.041	0.016	0.041	0.032	0.041	0.036	0.041	0.038	0.041	0.039
H_2	0.124	0.056	0.124	0107	0.124	0.117	0.124	0.12	0.124	0.121
C_3H_8	0.000	0.006	0.000	0.001	0.000	0.000	0.000	0.000	0.000	0.000
H_2O	0.000	0.043	0.000	0.013	0.000	0.006	0.000	0.004	0.000	0.003
CO	0.000	0.007	0.000	0.007	0.000	0.004	0.000	0.003	0.000	0.002

Table H- 4 Stream table of CO_2 hydrogenation using 2 PFR in series simulation by ASPEN PLUS 8.6.

GHSV (L g^{-1} h^{-1})	1.2			3.6			7.0		
Catalyst weight (g)	600			200			103		
Stream	1	2	3	1	2	3	1	2	3
Temperature (°C)	300	300	300	300	300	300	300	300	300
Pressure (bar)	11	11	1.1	11	11	1.1	11	11	1.1
Vapor Frac	1	1	1	1	1	1	1	1	1
Mole Flow (kmol/h)	0.166	0.129	0.125	0.166	0.159	0.158	0.166	0.164	0.163
Mass Flow (kg/h)	2.074	2.074	2.074	2.074	2.074	2.074	2.074	2.074	2.074
Volume Flow (L/h)	720	557	539	720	692	685	720	712	708
Enthalpy (Gcal/h)	-0.004	-0.004	-0.004	-0.004	-0.004	-0.004	-0.004	-0.004	-0.004
Mole Flow (kmol/h)									
CO_2	0.041	0.016	0.014	0.041	0.032	0.031	0.041	0.036	0.036
H_2	0.124	0.056	0.049	0.124	0.107	0.105	0.124	0.117	0.116
C_3H_8	0.000	0.006	0.007	0.000	0.001	0.001	0.000	0.000	0.000
H_2O	0.000	0.044	0.048	0.000	0.013	0.015	0.000	0.006	0.007
CO	0.000	0.007	0.006	0.000	0.007	0.007	0.000	0.004	0.005

Table H-4 Stream table of CO_2 hydrogenation using 2 PFR in series simulation by ASPEN PLUS 8.6 (cont.).

GHSV (L g^{-1} h^{-1})	10			14		
Catalyst weight (g)	72			52		
Stream	1	2	3	1	2	3
Temperature (°C)	300	300	300	300	300	300
Pressure (bar)	11	11	1.1	11	11	1.1
Vapor Frac	1	1	1	1	1	1
Mole Flow (kmol/h)	0.166	0.165	0.165	0.166	0.165	0.165
Mass Flow (kg/h)	2.074	2.074	2.074	2.074	2.074	2.074
Volume Flow (L/h)	720	716	713	720	718	715
Enthalpy (Gcal/h)	-0.004	-0.004	-0.004	-0.004	-0.004	-0.004
Mole Flow (kmol/h)						
CO_2	0.041	0.038	0.037	0.041	0.039	0.039
H_2	0.124	0.120	0.119	0.124	0.121	0.121
C_3H_8	0.000	0.000	0.000	0.000	0.000	0.000
H_2O	0.000	0.004	0.005	0.000	0.003	0.003
CO	0.000	0.003	0.003	0.000	0.002	0.003

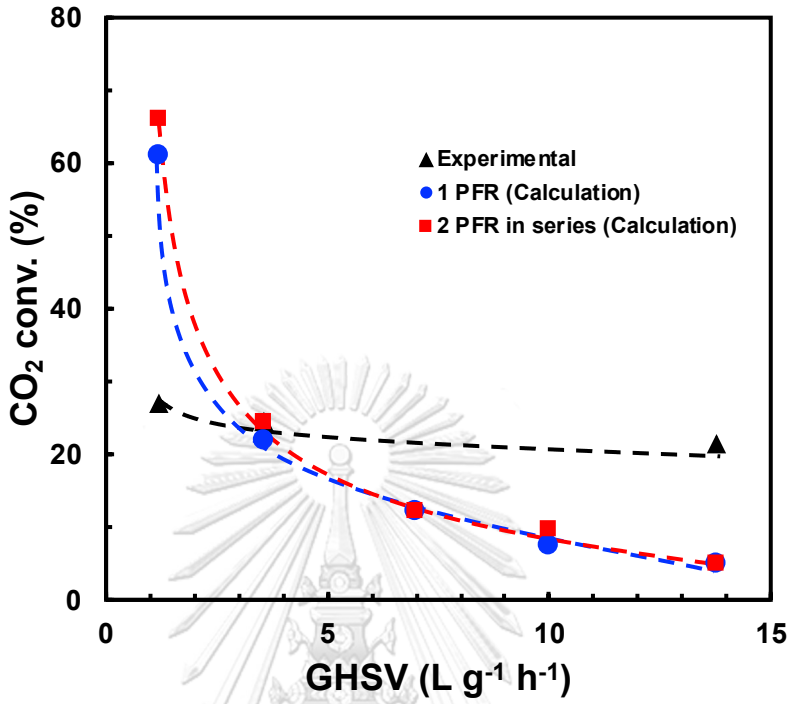

Figure H-5 CO_2 conversion of experimental data, 1 PFR (calculation) and 2 PFR in series (calculation) at various GHSV.

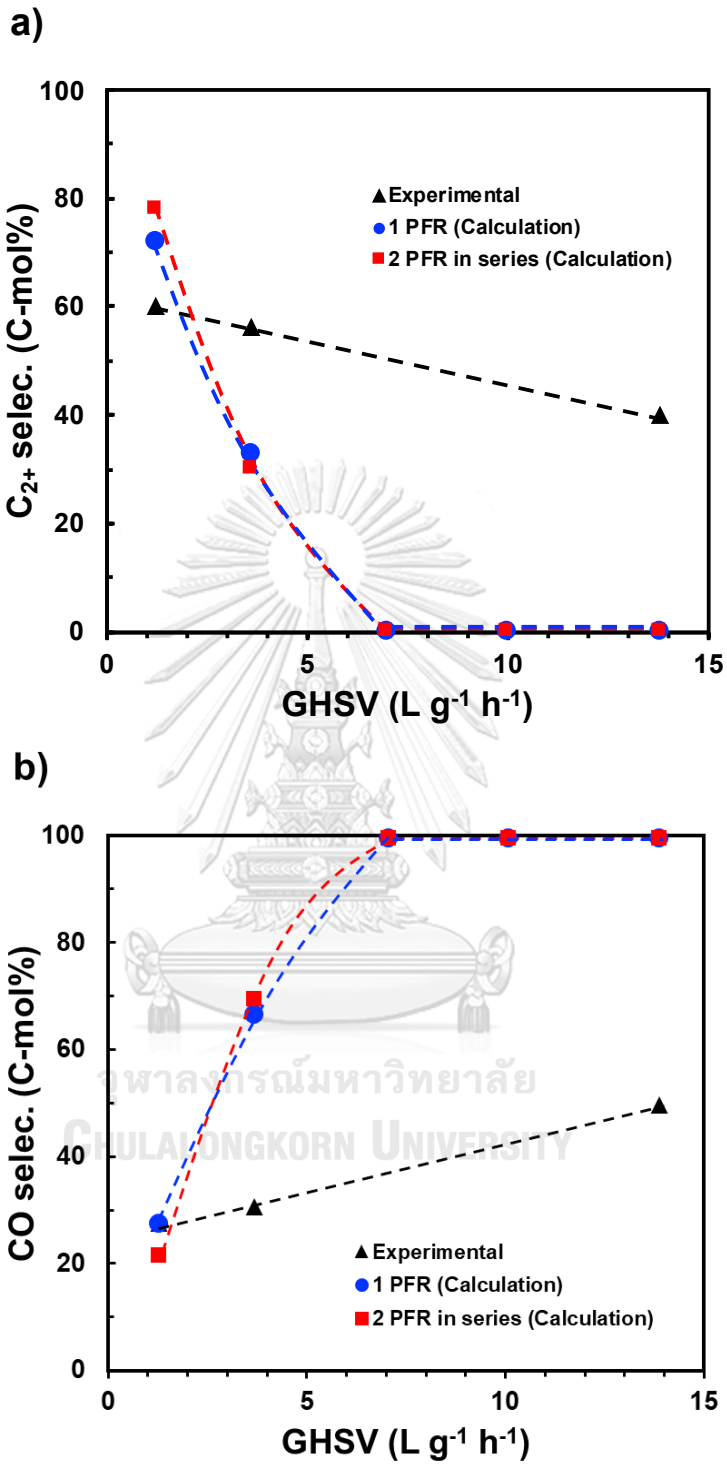

Figure H-6 (a) C_{2+} hydrocarbon and (b) CO selectivity of experimental data, 1 PFR (calculation) and 2 PFR in series (calculation) at various GHSV.

Table H-5 CO_2 conversion of experimental data, 1 PFR (calculation) and 2 PFR in series (calculation) at various GHSV.

	Experimental			**1 PFR**			**2 PFR in series**		
GHSV ($L\ g^{-1}\ h^{-1}$)	CO_2 conv. (%)	HCs selec. (%C-mol)	CO Selec. (%C-mol)	CO_2 conv. (%)	HCs selec. (%C-mol)	CO Selec. (%C-mol)	CO_2 conv. (%)	HCs selec. (%C-mol)	CO selec. (%C-mol)
1.2	26.9	60	28	61.0	72	28	65.9	78	22
3.6	24.4	56	31	22.0	33	67	24.4	30	70
7.0	N/A	N/A	N/A	12.2	0	100	12.2	0	100
10.0	N/A	N/A	N/A	7.3	0	100	9.8	0	100
14.0	21.3	40	50	4.9	0	100	4.9	0	100

According to the simulation result (Fig. H-5, Fig. H-6 and Table H-5), the CO_2 conversion of both processes could reach the maximum conversion (61 and 66%) at GHSV of 1.2 L g^{-1} h^{-1}. The process with two PFR in series gave slightly higher CO_2 conversion (up to 4% higher) than one PFR process, while the hydrocarbons product selectivity of 2 PFR in series was only 6% higher than that of 1 PFR. Therefore, it would be inappropriate to double up the reactor size since the GHSV of the process have more influence on the conversion than the reactor size. Surprisingly, when increased the GHSV up to 7.0 L g^{-1} h^{-1}, the hydrocarbon selectivity from the calculated hydrocarbon selectivity from the simulation approached 0% (no hydrocarbon was produced) suggesting that the residence time in the reactor was not enough for the hydrocarbon formation *via* FTS reaction. On the other hand, the CO could still be produced at high GHSV level (> 7 L g^{-1} h^{-1}) since RWGS is much faster than FTS reaction. The model prediction suggested that the FTS reaction is the rate-controlling step for the overall conversion of CO_2 to hydrocarbons.

However, when compared the CO_2 conversion from the simulation and the experimental value, the calculated CO_2 conversion (simulation under the assumptions) is much higher than those experimental data. It should be noted that the simulation would be further improved by more kinetic parameters, including equilibrium constant (K_{eq}) of RWGS, adsorption constant (K_i) of CO and other gas products estimated from more data of the realistic hydrocarbons formation. These kinetic parameters are the keys to developing the kinetic modeling which would be useful for the scale-up of CO_2 hydrogenation to commercial process in the future.

VITA

Nuttakorn Boreriboon was born on December 23, 1991 in Bangkok, Thailand. He received his B.Sc. (1st class honors) degree from Department of Chemical Technology, Chulalongkorn University in 2014. He continued pursuing Ph.D. in Chemical Technology under the supervision of Prof. Pattarapan Prasassarakich at Chulalongkorn University and received the Royal Golden Jubilee Scholarship (RGJ) from Thailand Research Fund. He has carried out his Ph.D. research for two years (2015-2017) at Clean Fuel and Catalysis Program (CFCP) at the EMS Energy Institute of the Pennsylvania State University (USA) under the guidance of Prof. Chunshan Song. He also served as a teaching assistant for undergraduate courses in "Chemical Engineering Thermodynamics", "Fuel Testing Lab" and "Unit Operation Lab II".

Journal Publication:

1. N. Boreriboon, X. Jiang, C. Song, P. Prasassarakich, Fe-based bimetallic catalysts supported on TiO2 for selective CO2 hydrogenation to hydrocarbons. J. CO2 Util. 25 (2018) 330-337.

2. N. Boreriboon, X. Jiang, C. Song, P. Prasassarakich, Higher hydrocarbons synthesis from CO2 hydrogenation over K- and La-promoted Fe-Cu/TiO2 catalysts. Top. Catal. (2018) (Accept with minor revision).

Conference Presentation (Oral presentation):

1. "Fe-based bimetallic catalysts supported on TiO2 for selective CO2 hydrogenation to higher hydrocarbons". 254th ACS National Meeting, August 20-24, 2017, Washington DC, USA.

2. "Selective CO2 hydrogenation to higher hydrocarbons over TiO2 supported Fe-based bimetallic catalysts". 2nd International Conference on Catalysis and Chemical Engineering, February 19-21, 2018, Paris, France.

3. "TiO2-supported Fe-based bimetallic catalysts for selective CO2 hydrogenation to higher hydrocarbons". RGJ – Ph.D. Congress 19, June 7-9, 2018, Chonburi, Thailand.

Award:

1. Outstanding oral presentation, RGJ – Ph.D. Congress 19, June 7-9, 2018, Chonburi, Thailand.